Silesian University of Technology

Faculty of Materials Engineering

Department of Materials Technologies

Goftila Gudeta Sirata Msc, Eng

# Influence of combined relaxation, creeping and low-cycle fatigue on the final durability and structure of material

*Dissertation*

Supervisor: dr hab. inż. Krzysztof Wacławiak

Assistant supervisor: dr inż. Grzegorz Junak

Katowice, 2024

# ABSTRACT

There is growing interest in developing more advanced materials that are cost-effective, lightweight, and durable, as conventional materials are unable to meet the demands of the automotive, aerospace, and military industries. Studying the mechanical properties of these materials is essential to enhance their suitability for demanding industries and ensure that they can withstand high stress under harsh environmental conditions. To meet the needs of these sectors, the use of advanced materials with superior properties is important. For this study, aluminium metal matrix composites (AMMCs) were chosen as they are promising advanced engineering materials with improved properties. AMMCs are notable in engineering applications due to their enhanced mechanical properties compared to conventional aluminium alloys. These advanced materials hold great promise for high-precision applications in various engineering industries. Aluminium metal matrix composites find essential applications in different technological fields. These materials have been developed to improve their strength, abrasion resistance, rigidity, creep resistance, and dimensional stability. Metal matrix composites (MMCs) using aluminium alloy as a base material have gained significant traction in the aerospace and automotive sectors due to their extensive and ubiquitous use.

However, the combination of complex loading and high temperatures significantly affects the durability of these materials. Creep and fatigue failures are more likely to occur when materials are subjected to cyclic load and elevated temperature. In this research work, experimental investigations were used to characterize the material behaviour of AMMC and its matrix alloy at elevated temperatures. Initially, uniaxial tensile tests were performed at room and elevated temperatures to assess the mechanical properties of the material. The hardness measurements were also conducted to evaluate the hardness of both composite and matrix alloy. Light microscopy and scanning electron microscopy were used to analyze the structure of the material.

The results of the microstructural analysis show that the SiC particles are uniformly distributed in the matrix. The results of the experimental tests indicate that the tensile properties and hardness of the Al-Si/SiCp composite are significantly higher than those of the unreinforced eutectic alloy. For Al-Si/SiCp composite, the tensile strength is 21%, the yield strength is 16%, the modulus of elasticity is 20%, and the hardness is 11% higher than the unreinforced matrix alloy. However, the

unreinforced EN AC-Al Si12CuNiMg alloy has a percentage elongation of 16% higher than the composite material. This shows that the Al-Si/SiCp composite has a lower ductility than the unreinforced EN AC-Al Si12CuNiMg alloy. The tensile specimens of the tested composite broke apart in a brittle manner with no discernible neck development, in contrast to the matrix specimens, which broke apart in a ductile manner with very little discernible neck formation.

The study reveals that the combination of fatigue and creep loading significantly reduces a material's fatigue life. The fatigue-creep loading sequence results in a 65% decrease in the number of cycles to failure compared to the full fatigue test. The material experiences more significant deformation during creep loading stages than during fatigue loading stages, especially when subjected to constant stress equal to the maximum cyclic stress level for an extended period. The combination of fatigue and creep loads accelerates material deterioration through mechanisms such as crack propagation and grain boundary degradation, resulting in a reduced service life. The fatigue-stress relaxation sequential loading test results show a 60% reduction in the material's durability due to the combined effect of fatigue and stress relaxation loading.

Fracture surface analysis of the Al-Si/SiCp composite shows fatigue fractures, primarily due to the debonding of the particle-matrix interfaces at elevated temperatures. The study examines the fracture behaviour of Al-Si/SiCp composite samples after creep loading at 250°C. The high temperature softens the Al-Si matrix, leading to microstructural changes that weaken the interface between SiC particles and the matrix, accelerating the degradation of the composite. SEM analysis reveals an intergranular fracture mode, cavities, and voids on the fracture surface, indicating localized deformation and stress accumulation. The composite has a combination of brittle and ductile properties, with ductile behaviour being dominant during the fracture process. Fatigue-creep loading leads to a higher degree of intergranular fracture and a higher density of secondary cracks, indicating a more complex failure mechanism. The material undergoes both ductile and brittle fracture processes under both fatigue creep and fatigue relaxation loading sequence. In general, the study presents the significant reduction of durability under fatigue-stress relaxation and fatigue-creep loading sequence.

## STRESZCZENIE

Rośnie zainteresowanie opracowywaniem udoskonalonych materiałów, które są opłacalne w produkcji, lekkie i trwałe, ponieważ konwencjonalne materiały nie są w stanie sprostać rosnącym wymaganiom przemysłu motoryzacyjnego, lotniczego i wojskowego. Aby zaspokoić potrzeby tych sektorów, ważne jest stosowanie zaawansowanych materiałów o doskonałych właściwościach. Badanie właściwości mechanicznych tych materiałów ma zasadnicze znaczenie dla zwiększenia ich przydatności w wymagających branżach i zapewnienia, że są one w stanie wytrzymać duże obciążenia w trudnych warunkach środowiskowych. W niniejszej pracy wybrano do badania kompozyt aluminium z osnową metalową (AMMC), ponieważ jest on obiecującym, zaawansowanym materiałem inżynierskim o ulepszonych właściwościach. AMMC są godne uwagi ze względu na ich ulepszone właściwości mechaniczne w porównaniu do konwencjonalnych stopów aluminium. Te zaawansowane materiały są bardzo obiecujące w zastosowaniach wymagających wysokiej precyzji w różnych branżach przemysłu. Aluminiowe kompozyty o osnowie metalowej znajdują ważne zastosowania w różnych dziedzinach przemysłu. Materiały te zostały opracowane w celu poprawy wytrzymałości, odporności na ścieranie, sztywności, odporności na pełzanie i stabilności wymiarowej. Kompozyty na osnowie metalowej (MMC) wykorzystujące stop aluminium jako materiał bazowy zyskały znaczną popularność w sektorze lotniczym i motoryzacyjnym ze względu na ich szerokie i wszechstronne zastosowanie.

Jednak występowanie złożonych obciążeń i wysokiej temperatury znacząco wpływa na trwałość tych materiałów. Pełzanie i uszkodzenia zmęczeniowe są bardziej prawdopodobne, gdy materiały są poddawane cyklicznym obciążeniom i podwyższonej temperaturze. W niniejszej pracy badawczej wykorzystano badania eksperymentalne w celu scharakteryzowania zachowania materiału AMMC i jego stopu bazowego w podwyższonej temperaturze. Początkowo przeprowadzono jednoosiowe próby rozciągania w temperaturze pokojowej i podwyższonej w celu oceny właściwości mechanicznych materiału. Przeprowadzono również pomiary twardości w celu oceny zarówno kompozytu, jak i stopu osnowy. Do analizy struktury materiału wykorzystano mikroskopię świetlną i skaningową mikroskopię elektronową.

Wyniki analizy mikrostrukturalnej pokazują, że cząstki SiC są równomiernie rozmieszczone w matrycy. Wyniki badań eksperymentalnych wskazują, że właściwości wytrzymałościowe na rozciąganie i twardość kompozytu Al-Si/SiCp są znacznie wyższe niż w przypadku niewzmocnionego stopu eutektycznego. W przypadku kompozytu Al-Si/SiCp przyrosty

właściwości wytrzymałościowych w stosunku do niewzmocnionego stopu matrycy są następujące: wytrzymałość na rozciąganie 21%, granica plastyczności 16%, moduł sprężystości 20%, i twardość 11%. Jednak niewzmocniony stop EN AC-Al Si12CuNiMg ma procentowe wydłużenie o 16% wyższe niż materiał kompozytowy. Pokazuje to, że kompozyt Al-Si/SiCp ma niższą ciągliwość niż niewzmocniony stop EN AC-Al Si12CuNiMg. Rozciągane próbki badanego kompozytu pękały w sposób kruchy bez widocznego rozwoju szyjki, w przeciwieństwie do próbek matrycy, które pękały się w sposób ciągliwy z bardzo mało widocznym tworzeniem się szyjki.

Badania wykazały, że połączenie obciążenia zmęczeniowego i pełzania znacznie zmniejsza trwałość zmęczeniową materiału. Sekwencja obciążenia zmęczeniowego i pełzania powoduje 65% spadek liczby cykli do zniszczenia w porównaniu z pełnym testem zmęczeniowym. Materiał doświadcza bardziej znaczącego odkształcenia podczas etapów obciążenia pełzającego niż podczas etapów obciążenia zmęczeniowego, zwłaszcza gdy jest poddawany stałemu naprężeniu równemu maksymalnemu cyklicznemu poziomowi naprężenia przez dłuższy czas. Połączenie obciążeń zmęczeniowych i pełzających przyspiesza degradację materiału poprzez mechanizmy takie jak propagacja pęknięć i degradacja granic ziaren, co skutkuje skróceniem żywotności. Wyniki testu sekwencyjnego obciążenia zmęczeniowo-relaksacyjnego wskazują na 60% redukcję trwałości materiału ze względu na połączony efekt obciążenia zmęczeniowego i relaksacyjnego.

Analiza powierzchni pęknięć kompozytu Al-Si/SiCp wykazuje pęknięcia zmęczeniowe, głównie z powodu utraty spójności na granicy cząstka-matryca w podwyższonych temperaturach. W pracy zbadano zachowanie się próbek kompozytowych Al-Si/SiCp po obciążeniu pełzaniem w temperaturze 250°C. Wysoka temperatura zmiękcza matrycę Al-Si, prowadząc do zmian mikrostrukturalnych, które osłabiają połączenie między cząstkami SiC a matrycą, przyspieszając degradację kompozytu. Analiza SEM ujawnia międzykrystaliczny tryb pękania, wgłębienia i puste przestrzenie na powierzchni pęknięcia, co wskazuje na miejscowe odkształcenie i akumulację naprężenia. Kompozyt ma kombinację właściwości kruchych i ciągliwych, przy czym zachowanie ciągliwe jest dominujące podczas procesu pękania. Obciążenie zmęczeniowe prowadzi do większego stopnia pękania międzykrystalicznego i większej gęstości pęknięć wtórnych, co wskazuje na bardziej złożony mechanizm zniszczenia. Materiał ulega zarówno ciągliwemu, jak i kruchemu procesowi pękania zarówno pod obciążeniem pełzania zmęczeniowego, jak i relaksacji zmęczeniowej.

# ACKNOWLEDGMENTS

Above all, I would like to thank Almighty God for his unconditional love and blessings that have helped me to reach this point in my academic journey. I would like to express my sincere gratitude to my main and co-supervisor, Professors Krzysztof Wacławiak and Grzegorz Junak, for their continuous guidance, encouragement, and patience throughout my research work. I am truly grateful for their commitment and expertise, which have had a lasting impact on my doctoral study.

I extend my gratitude to the Department of Materials Technologies of the Faculty of Materials Engineering for providing me with essential resources, including advanced laboratory facilities, research equipment, and valuable opportunities to conduct my research work. I also express my gratitude to the academic staff of the department, particularly Professors Anna Dolata and Maciej Dyzia, for their invaluable advice, unwavering support, and assistance in manufacturing and providing essential research materials.

I would like to thank the Zwick/Roell Company staff, Mr. Grzegorz Daniłko, for his assistance during technical problems encountered while conducting experiments using their testing machines. His expertise and quick response to our inquiries greatly contributed to the success of my research work.

I am grateful to my friends and colleagues for their constant encouragement and emotional support, which significantly influenced my perseverance during the challenging times of my research. Their unwavering support kept me motivated and inspired me to continue my studies.

I am also thankful to my family, my brothers and sisters, for their endless love and support. Their unwavering presence and encouragement were the pillars that supported me throughout this study. Their belief in me never wavered, and I am forever grateful for their unwavering support.

I would like to express heartfelt gratitude to all those whose names are not mentioned but who played a vital role during my doctoral study. Your support was instrumental in my success.

# Contents

# LIST OF FIGURES

# LIST OF TABLES

# NOMENCLATURES

| | |
|---|---|
| AMMC | Aluminum metal matrix composite,- |
| ASTM | American society for testing and materials,- |
| E | Young's modulus, GPa |
| HB | Brinell hardness,- |
| K' | Cyclic hardening coefficient,- |
| LM | Light microscopy,- |
| n' | Cyclic strain-hardening exponent,- |
| $N_f$ | Number of cycles to failure,- |
| R | Stress ratio,- |
| SEM | Scanning electron microscopy,- |
| SiC | silicon carbide,- |
| SiCp | silicon carbide particle,- |
| T | Temperature; k, °C |
| $T_m$ | Melting temperature; k, °C |
| UTS | Ultimate tensile strength; Pa |
| Wp | Cyclic plastic energy, $J/m^3$ |
| $W_{tot}$ | Total plastic energy, J |
| YS | Yield strength,- |
| $\Delta W_p l$ | Plastic strain energy per unit volume, $J/m^3$ |
| $\Delta \varepsilon$ | Strain range,- |
| $\Delta \sigma$ | Stress range, Pa |
| $\varepsilon$ | Strain,- |
| $\varepsilon_{max}$ | Maximum strain,- |
| $\varepsilon_{min}$ | Minimum strain,- |
| $\varepsilon_p$ | Plastic strain,- |
| $\sigma$ | Stress; Pa |
| $\sigma_a$ | Stress amplitude; Pa |
| $\sigma_{max}$ | Maximum stress; Pa |
| $\sigma_{min}$ | Minimum stress; Pa |

# 1. INTRODUCTION

The development of early civilizations, which are divided into the Stone Age, the Bronze Age, and the Iron Age, is a direct reflection of their progression in the production and exploitation of materials to satisfy the demands of society [1]. For example, during the Stone Age, early civilizations relied primarily on natural materials such as stone, wood, clay, and bone for their tools and weapons. However, with the advent of the Bronze Age, people began to use metal alloys such as bronze, which provided them with stronger and more durable tools. This was a significant advance in their ability to meet their needs and paved the way for further material development in later times. In the Iron Age, people were able to harness the power of iron, which revolutionized their ability to create tools and weapons. Iron was much stronger than bronze, which made it possible to develop even more efficient and effective tools. This advancement in metallurgy also led to the development of new industries, such as iron mining and blacksmithing, further contributing to the growth and complexity of civilizations. The progression from stone to bronze and afterwards shows the ingenuity and adaptability of early civilizations, which continually sought ways to improve their lives and shape the world around them [2].

Nowadays, there is a strong correlation between the availability of suitable materials and the progress of various technologies, significantly improving our daily lives. The lack of appropriate materials for life would seriously hinder the progress of technology. Throughout history, the progress of human civilization has always depended on the identification and effective use of appropriate materials. From the discovery of fire and the invention of the wheel to the development of complex machines and artificial intelligence, each technological breakthrough has relied on the existence of materials that possess the necessary properties. Without materials like metal alloys, plastics, or semiconductors, we would not have been able to create tools, infrastructure, or electronic devices. The availability of sustainable and environmentally friendly materials has become a pressing concern in today's world as we strive to mitigate the impact of technology on our planet. Therefore, as materials become more advanced, they enable the development of more advanced technologies, which in turn helps to create even more sustainable materials with low environmental impact.

## 1.1 Traditional and advanced materials

**Traditional materials**, such as wood, stone, metal, and glass, have been used for centuries. Traditional materials can be categorized into metals, ceramics, and polymers. Metals are known for their high strength and conductivity, making them ideal for construction and electrical wiring applications. They are characterized by metallic properties such as electrical conductivity, ductility, and high thermal conductivity. Ceramics are valued for their heat resistance and hardness, which makes them suitable for use in pottery and engineering components. They are generally composed of non-metallic elements. Ceramics include clay-based pottery, refractory bricks, and advanced ceramics for cutting tools and electrical insulators. Polymers, including plastics, rubber, and synthetic materials, are lightweight and flexible, making them widely used in everyday products such as bottles, packaging, and clothing. Each category has unique properties and applications, allowing various industrial uses.

**Advanced materials** are a class of materials that have been developed in recent years to meet the specific needs of demanding applications. These materials are often more expensive and more challenging to work with than traditional materials, but they offer superior properties such as high strength, lightness, and durability. Their production usually requires innovative production processes and specialized equipment. Despite the challenges, the use of advanced materials has revolutionized sectors such as aerospace, automotive, marine, and defense, enabling the development of cutting-edge products with unrivalled performance. As technology continues to advance, demand for advanced materials is growing. Advanced materials can be divided into: composites, nanomaterials, superconductors and smart materials. Each category offers unique properties and benefits that make them suitable for different applications.

Composites are materials made by combining two or more constituent materials with different properties. For instance, fibre-reinforced composites combine strong fibers (such as carbon or glass) with a matrix material (often a polymer or metal), resulting in high strength-to-weight ratios. These are used in aerospace, automotive, and sports equipment.

On the other hand, nanomaterials are materials with structures at the nanoscale, typically involving dimensions of less than 100 nanometers. Examples include carbon nanotubes and graphene, which

possess extraordinary electrical, mechanical, and thermal properties. These materials have applications in electronics, coatings, and medical devices.

The third one, superconductors, are materials that exhibit about zero electrical resistance at low temperatures. This property enables the development of highly efficient electrical and electronic systems, including magnetic resonance imaging (MRI) machines and particle accelerators.

The fourth type of advanced material is smart materials. Smart materials can respond to external stimuli, such as changes in temperature, pressure, or electric fields. Shape-memory alloys are a notable example. These materials have applications in industries like aerospace and healthcare.

## 1.2 Composite materials and metal matrix composites (MMCs)

Composite materials are those composed of two or more constituent materials, such as polymers and fibers that possess different physical or chemical properties. Through the combination of these properties, these constituent materials yield a material that exhibits enhanced properties that enable them to overcome the weakness of both materials. Composite materials can be classified based on the types of matrices, such as polymer, metal, or ceramic matrices, and reinforcements, such as fibers or particulates [3]. Figure 1 shows a flowchart illustrating the classification of composite materials based on the compositions of their matrix and reinforcement.
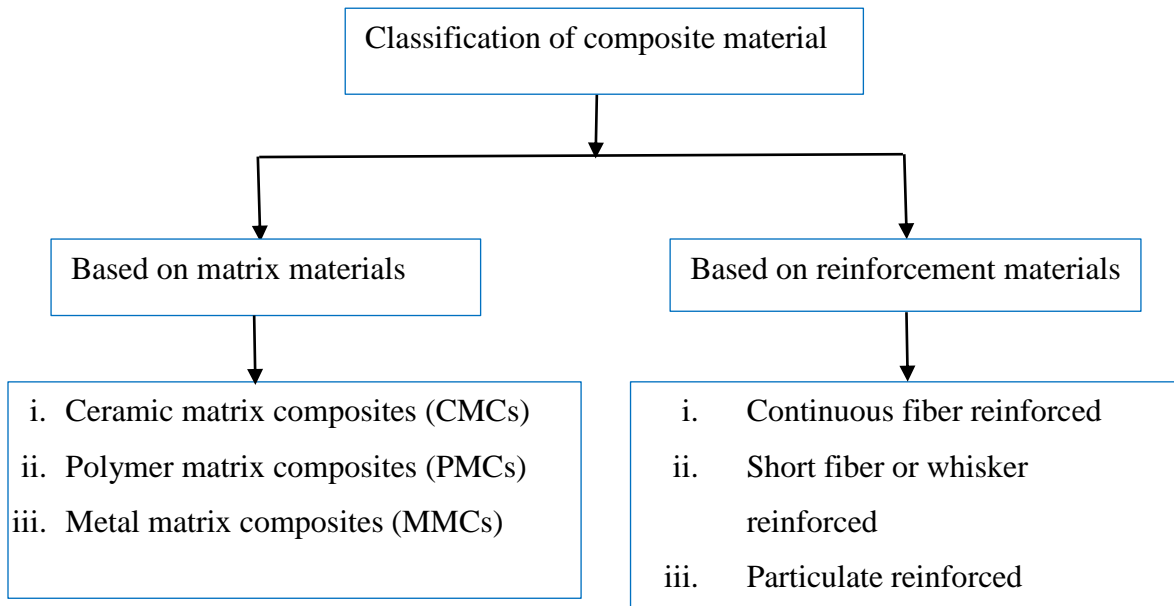
Figure 1. Composite material classification flowchart [4]

Ceramic Matrix Composites (CMCs) are nonmetallic composites that use ceramic as a matrix material, reinforced with fibres, whiskers, or ceramic particles. CMCs provide excellent high-temperature performance, including heat resistance, wear resistance, and stability. They are used in applications such as jet engine components, furnace linings, and heat exchangers [5,6].

Polymer matrix composites (PMCs) are the most common type of composite material. They use a polymer resin as a matrix, which binds the reinforcing fibers. Commonly used polymers in PMC include epoxy, polyester, vinyl ester, and nylon. The reinforcements can be fibers (glass, carbon, aramid), flakes (graphite) or particles (ceramic). PMCs are lightweight, strong and corrosion resistant, making them ideal for a wide range of applications in the aerospace, automotive, construction and sporting goods industries [7,8].

Metal matrix composites (MMCs) are a group of advanced materials made of a metal matrix and reinforcing materials such as ceramic particles, whiskers, fibres, etc. The metal matrix, such as aluminium or magnesium, is typically lightweight, while the reinforcement is usually hard ceramic, such as alumina or silicon carbide [9,10]. A combination of light metal matrix and reinforcing materials gives MMCs several advantages over traditional materials, including high strength and stiffness, high operating temperature, good wear resistance, and tailorable properties.

MMCs are produced using various techniques, including powder metallurgy, liquid metal infiltration, and stir casting. The processing technique depends on the type of reinforcement and desired properties of the material. MMCs are used in various applications, including aerospace, automotive, electronics, and biomedical. Figure 2 shows automotive components made of MMCs. Some fundamental advances in MMC technology include developing new reinforcement materials, improved processing techniques, and hybrid composites.

For metal-matrix composites (MMCs), the matrix is a ductile metal. These materials are used at higher service temperatures than their base metal counterparts. Various materials, including SiC, $Al_2O_3$, $B_4C$, $TiB_2$, $ZrO_2$, $SiO_2$, and graphite, are used as reinforcements to improve the mechanical properties of the AlSi alloy. The reinforcement can improve stiffness, strength, abrasion resistance, creep resistance, thermal conductivity, and dimensional stability. Super alloys and alloys of aluminum, magnesium, titanium, and copper are used as matrix materials. The reinforcement can be in particles, continuous and discontinuous fibers, and whiskers; concentrations typically range

Figure 2 Components made of MMCs [11]

from 10% to 60% by volume. Continuous fiber materials include carbon, silicon carbide, boron, aluminum oxide, and refractory metals.

On the other hand, the discontinuous reinforcements are mainly composed of silicon carbide barbs, staple fibers of aluminum and carbon monoxide, and silicon carbide and aluminum oxide particles. These reinforcements used to enhance the mechanical properties of the composite material, such as stiffness, strength, and durability.

**Composition and Structure of MMCs**

**1. Matrix material:** The matrix in MMCs is a metal such as aluminum, magnesium, or titanium. Metals are chosen for their excellent thermal conductivity, high strength, and good workability. These properties make them ideal for many engineering applications.

**2. Reinforcement material:** MMCs incorporate a secondary phase of reinforcement, which is often composed of ceramic materials like silicon carbide (SiC), aluminum oxide ($Al_2O_3$), or carbon fibers. The choice of reinforcement depends on the specific properties required for the application.

**3. Volume Fraction:** The properties of MMCs can be tailored by adjusting the volume fraction of the reinforcement material. Higher volume fractions typically enhance mechanical properties due to increased material density.

MMCs offer several advantages over traditional materials [12]. These advantageous properties are:

- **High strength and stiffness:** MMCs have a higher strength-to-weight ratio and stiffness-to-weight ratio than many other materials, making them ideal for applications where weight reduction is important.

- **High operating temperature:** MMCs can retain their strength and stiffness at elevated temperatures, making them well-suited for applications in hot environments.

- **Good wear resistance:** MMCs are typically more wear-resistant than traditional metals, making them ideal for applications where surfaces are subject to friction and abrasion.

- **Tailorable properties:** The properties of MMCs can be tailored to meet specific application requirements by varying the type, volume fraction, and distribution of the reinforcement.

Application area of MMCs

Due to their favorable properties, MMCs are employed in many industrial applications, such as aerospace, automotive, electronics, and biomedical [13].

- **Aerospace**: aircraft and spacecraft components, such as engine parts, structural components, and heat shields due to their lightweight, high strength, and resistance to high-temperature environments.

- **Automotive**: in applications like brake discs, engine components such as pistons and engine blocks, and lightweight structural parts, contributing to improved fuel efficiency and performance.

- **Electronics**: in electronic packaging applications to improve thermal conductivity and wear resistance.

- **Biomedical**: in implants, such as dental implants and artificial joints, due to their excellent biocompatibility and mechanical properties.

**Classification of MMCs**

Depending on the type of reinforcement, MMC can be classified into three main categories. The three main categories are:

**Particle reinforced MMCs:** These are the most popular types of MMC. They contain hard, dispersed particles, such as oxides (aluminium oxide, silicon carbide), carbides (boron carbide, titanium carbide) or intermetallic compounds in a softer metal matrix. Particle-reinforced MMCs provide improved wear resistance, strength, and stiffness compared to unreinforced matrices.

**Short fibers or whiskers reinforced MMCs:** These MMCs contain short (discontinuous) fibers as the reinforcing phase. Short fibers provide improved strength and wear resistance for the matrix.

**Continues fibers reinforced MMCs:** These long, unbroken fibers are embedded within the metal matrix, resulting in a composite material with superior properties compared to the unreinforced metal. Continuous fibers provide the greatest improvement in strength and stiffness. Figure 3 shows different classification MMCs based on their reinforcements.

Compared to traditional materials, MMCs offer superior performance and durability in harsh environments. In addition, their remarkable properties, such as high corrosion resistance, enhanced thermal conductivity, and improved wear resistance, make them a promising candidate for advanced engineering applications. For example, MMCs can be used in aerospace applications to manufacture aircraft components, such as turbine blades and engine components, which are typically subjected to harsh environments such as high temperatures, high mechanical loads, and corrosive environments.
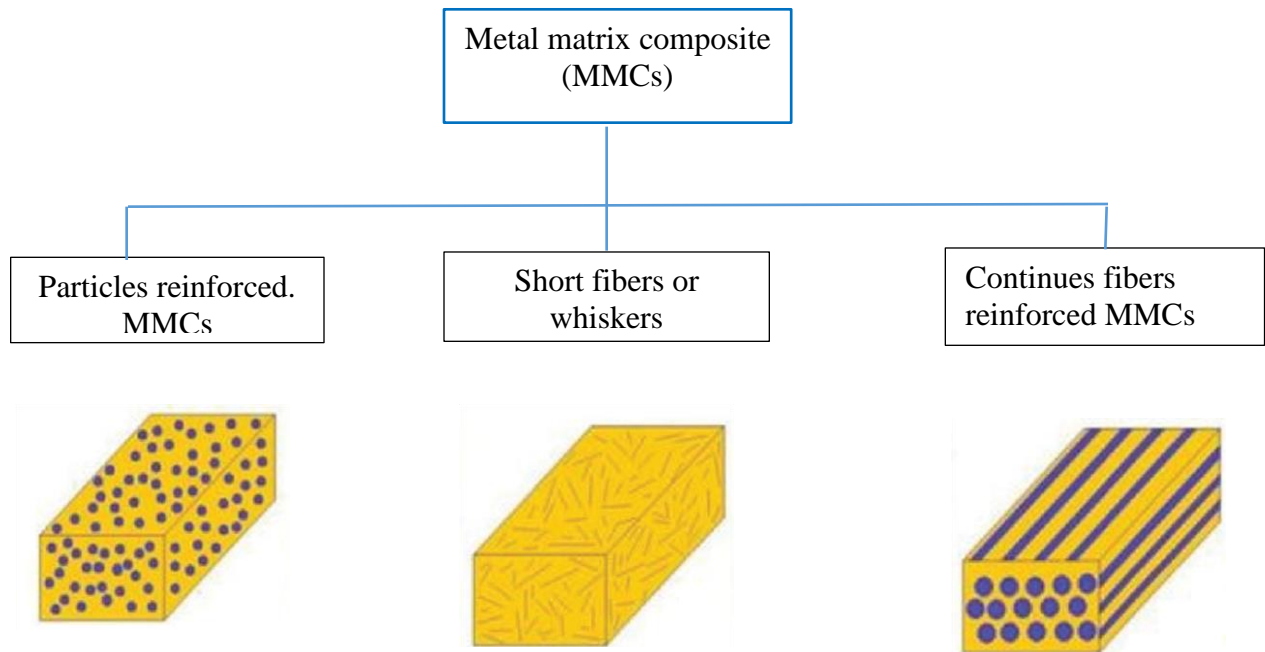
Figure 3. Classification of metal matrix composite [14]

Despite the remarkable mechanical properties of this material in harsh environments, its long-term exposure causes a time-dependent deformation. For example, their long-term performance when subjected to constant loads and cyclic loading sequences at high temperatures is a major concern as they fail over time. Therefore, it is important to consider the time deformation behavior of these materials to ensure their long-term performance is safe. Creep relaxation and deformation are time-dependent deformation behaviors of materials. Fatigue deformation is also a major concern for all materials, as these behave when subjected to cyclic stress. Selecting materials that are resistant to relaxation, creep, and fatigue by taking into account the operating temperature, stress levels, and loading conditions is essential to ensuring long-term performance and reliability.

**Relaxation phenomenon**

Relaxation is the time-dependent decrease in stress under a constant strain. The internal stress gradually diminishes, even though the strain remains constant. This occurs due to the gradual rearrangement of atoms within the material, primarily through the movement of dislocations (microscopic imperfections) in the metal matrix. Additionally, the interface between the reinforcement and matrix might experience debonding, further contributing to stress relaxation. The rate of relaxation is influenced by the temperature, applied stress, and microstructure of the MMC.

**Creep phenomenon**

Creep is the phenomenon of time-dependent plastic deformation that occurs under constant stress or loading conditions at elevated temperatures. It can occur at a stress level below a yield stress of the material due to a long-time exposure to constant stress [15]. Creep behavior in MMCs is often governed by mechanisms such as dislocation, grain boundary diffusion, and interface debonding between the matrix and reinforcement phases. Creep deformation has three stages: primary, secondary and tertiary. In the primary stages, creep deformation is initially slow and steady, as dislocations begin to build up and accumulate. In the secondary stage, the creep rate increases as dislocations accumulate further. The tertiary stage is characterized by the rapid acceleration of creep deformation, often leading to material failure. These three stages of creep are shown in Figure 4.
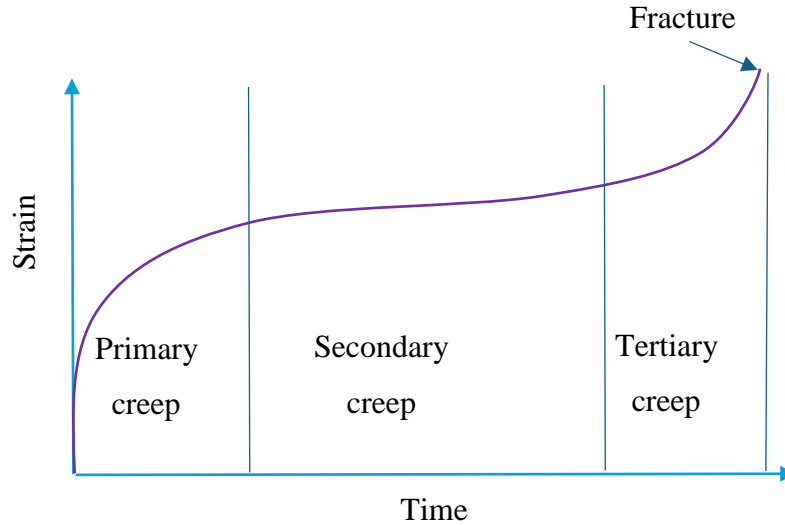
Figure 4. Creep deformation stages

**Fatigue phenomenon**

Fatigue is another critical phenomenon encountered in MMCs, characterized by the initiation and propagation of cracks under cyclic loading conditions. Several variables, including microstructure, stress amplitude, loading frequency, and the existence of discontinuities or flaws, affect how fatigue influences MMCs. Complex interactions between the matrix and reinforcement phases are frequently involved in fatigue in MMCs. These interactions can result in processes including fatigue crack initiation at matrix-reinforcement interfaces, fatigue crack propagation along interfaces, and ultimately, failure of the composite structure.

**Fatigue failure in AMMCs can result from:**

- **Crack initiation** occur at the interface between the matrix and the reinforcing particles. Stress concentration at these places is frequently induced by the disparity in mechanical properties between the two phases.

- **Matrix fatigue** causes microcracks to occur within the aluminium matrix. This can be worsened by the presence of hard and brittle reinforcing particles.

- **Debonding** at the interface, which can further accelerate crack growth under cyclic loading. Ultimately, this can lead to catastrophic failure of the material if not addressed. The combination of stress concentration, matrix fatigue, and debonding all contribute to the weakening of the material and the eventual propagation of cracks.

9

# 2. RESEARCH AIMS AND OBJECTIVES

**Objectives**

The main objective of this research is to investigate the effect of creep, relaxation, and fatigue on the durability of AlSi composites reinforced with SiC particles at elevated temperatures. Furthermore, the study aims to investigate the effects of individual loading and sequential loading of relaxation, creep, and fatigue on the structure of the composite material. Even though AlSi alloys and AlSi composite have good mechanical properties and are employed in manufacturing light mechanical structures, their mechanical properties deteriorate at elevated temperatures. As a result, the main task of this research is to assess the mechanical properties of AlSi alloy and its composite material under tension, creep-relaxation, and cyclic loads at elevated temperatures. The structural analysis of these materials, including metallography and fractography, is another study task. Investigating the microstructure of the composite material before and after being subjected to different loading conditions is also important to know the effect of the combined loading conditions on the structure of the material. Another aim of the study is to analyze the fracture modes of material under individual loading as well as combined loading conditions. Microstructural analysis is also performed to ensure the uniform distribution of the reinforcing particles.

Thus, this research focuses on the following specific objectives:

i. Conducting material characterization of the matrix alloy under both ambient and elevated temperatures.
ii. Investigating the stress-relaxation and creep behavior of the matrix alloy.
iii. Experimental investigation of the mechanical properties of composite material.
iv. Assessing the influence of loading sequences on the durability and structure of material

**Motivation**

A fatigue problem is the main cause of material failure in engineering applications. It causes gradual deterioration of the material over time due to cyclic loading. Creep is another common cause of material failure, especially in high-temperature conditions. Relaxation is yet another important issue that must be considered when designing engineering components. It refers to the tendency of a material to deform over time under constant stress. While there have been numerous

attempts to predict material durability under complex loading, these methods often fall short of accurately predicting durability under complex loading conditions. Fatigue, creep, and relaxation occur through different mechanisms and have different characteristics. They affect the material structure in different ways. Despite numerous attempts to assess material failure under complex loading, predicting the influence of complex loading on material durability remains a challenging task that requires additional research. This thesis studies the influence of the combined effects of low cyclic fatigue, creep, and relaxation on the final durability and structure of the material.

For this study, an AlSi composite reinforced with SiC particles was chosen as the research material. It is a modern and advanced material, along with its superior mechanical properties, that make it a suitable replacement for traditional alloys in various applications. The AlSi composite reinforced with SiC particles exhibits superior properties, including high strength, high fatigue resistance, and corrosion resistance, compared to traditional matrix alloys, making it ideal for various applications in automotive, aerospace, maritime, defense, etc. Studying the strength and durability of AlSi composites under complex loading conditions involving relaxation, creep, and fatigue is crucial to ensuring the safety and long-term performance of this material.

It is essential to understand how AlSi/SiC composites respond to low cyclic fatigue to predict their service life accurately and prevent failures. At elevated temperatures, materials can deform plastically over time under constant loads due to a phenomenon known as creep. This phenomenon can result in structural instability and component failure in high-temperature environments such as engines. Over time, internal stresses in a material can decrease even at constant strain, reducing the applied load required to maintain that strain; this phenomenon is known as relaxation.

**Scope of the research**

The scope of the study includes investigating the behavior of material under a sequence of loading, relaxation, creep, and fatigue. The study was carried out after selecting an AlSi composite reinforced with SiC particles as the research material. The composite specimens were prepared and then subjected to uniaxial tension, relaxation, creep, and fatigue tests.

Initially, uniaxial tensile tests were performed to determine the tensile properties of the base material and the composite material. Afterwards, the effect of combined stress relaxation, creep, and fatigue loading conditions (loading sequence) on the final durability and structure of the SiC particle-reinforced AlSi composite was investigated. The work also includes the microstructural characterization of the base material and the composite material. The structure analysis was conducted before and after the material was subjected to a combined sequential loading using scanning electron microscopy (SEM) and optical microscopy (LM).

**Structure of the thesis**

All of the work covered in this thesis is organized into seven chapters. Below is a brief description of the content of these chapters.

Chapter 1 presents an overview of traditional and advanced materials, classification composite materials and their filed of application, and the deformation mechanism of the AMMCs.

Chapter 2 discusses research aims and objectives. The motivation and scope of the study are also presented in this chapter.

Chapter 3 provides a detailed literature review related to aluminum alloys and aluminum metal matrix composites. The literature was presented to discuss the critical contributions made by various researchers to improve the mechanical properties of the aluminum alloys and AMMCs.

Chapter 4 focuses on the experimental techniques used to characterize the mechanical properties of the Al-12Si alloy. It discusses the manufacturing methods, experimental procedures, and detailed analysis of the alloy's microstructure and mechanical behavior. The experimental techniques used in this chapter include tensile and hardness tests, microstructural observation under an optical microscope, SEM analysis, etc. In addition, the relaxation and creep behavior of the alloy are presented in this section.

Chapter 5 presents the material characterization of AlSi composite reinforced with SiC particles. Similar to Chapter 4, this chapter also describes the detailed analysis of microstructure and mechanical behavior of AlSi/SiCp composite. It provides a comprehensive overview of the

material characterization of aluminum metal matrix composites. It also presents the comparison of mechanical properties and microstructure of Al-12Si alloy and AlSi/SiCp composite. The detailed analysis of microstructure of the matrix alloy and AlSi/SiCp composite were also discussed in this chapter.

Chapter 6 explores the effects of loading sequences on the final durability and structure of AlSi/SiCp composite. It focuses on how different loading sequences, particularly fatigue-creep loading, and fatigue-stress relaxation loading, can influence the durability and performance of AlSi/SiCp composite. It also explores how loading sequences can lead to premature failure. The results of the experimental studies were discussed in this chapter.

Chapter 7 presents a conclusion of the thesis. Key findings of the research carried out are summarized in this chapter. Recommendations for a future work are also presented in this chapter.

# 3. LITERATURE REVIEW

## 3.1 Aluminum alloys

Significant progress has been made in the provision of "improved" alloys, which offer a combination of favorable properties such as high strength, low density, and corrosion resistance. Aluminum is a light metal with a density of 2700 kg/m$^3$. High ductility, good electrical and thermal conductivity, and corrosion resistance are some of the characteristics of aluminum. However, in its pure state, aluminium has a low tensile strength of 80 MPa and a low Young's modulus (E) of 70 GPa when compared to iron, which has a tensile strength of 300 MPa and Young's modulus of 211 GPa. On the other hand, its specific modulus, which is calculated by dividing the modulus by the density of the material, is almost similar to that of magnesium, titanium, and iron [16].

Pure aluminum has limited applications due to its relatively low strength. However, its properties can be significantly improved by alloying it with elements such as copper, magnesium and silicon. Alloying elements significantly enhance the strength and durability of aluminium and make it much more suitable for a wide range of industrial applications. Commercial aluminum alloys with medium-to-high strengths are selected for various applications from a group of aluminum alloys such as 2xxx, 5xxx, 6xxx, and 7xxx alloys. Due to their strength and good corrosion resistance, 5*xxx* series (Al-Mg-based) and 6*xxx* series (Al-Mg-Si-based) alloys are commonly used in automotive applications [17,18]. For example, EN AC-Al Si12CUNiMg alloy is widely used to fabricate engine cylinder heads due to their relatively high strength-to-weight ratio, low manufacturing cost, and increase in operating parameters of internal combustion engines. Their manufacturing ease, low density, excellent corrosion resistance, and excellent weldability contribute to their popularity in the automotive industry [19].

## 3.2 Classification of aluminum alloys

Based on the processing methods, aluminum alloys are generally classified into two main groups: wrought aluminum alloys and cast aluminum alloys. A wrought aluminum alloy contains a lower percentage of alloying elements than a cast aluminum alloy. However, the tensile strength of the wrought aluminium alloy is generally higher than that of the cast aluminium alloy. This lower tensile strength is due to the difficulties in eliminating casting defects. Cast aluminum alloys may

have many internal and surface defects. Despite its low tensile strength, cast aluminium alloy is often preferred for applications requiring complex designs or shapes due to its ability to be easily cast into complex structures. Unlike forged aluminium, the increased alloying elements in cast aluminium alloy provide greater corrosion resistance, making it a popular choice for a variety of applications.

Both wrought and cast aluminum alloys have a designation system based on the chemical composition of the alloy, its properties, and its field of application. These include the Military Specification System (MIL-SPEC), the International Alloy Designation System (IADS), the Unified Numbering System (UNS), the Aluminium Association (AA) Designation System , and the European Standard Designation System (EN)   [20]. Among these systems, Aluminium Association (AA) Designation System is widely used for both wrought and cast aluminium alloys [21]. A designation system use four digits to designate the alloys. There are two designation systems for aluminium alloys under the European standards (EN designation system): one is based on a chemical symbol and the other depends on numbers. For wrought alloys, four digits are used, while cast alloys use five digits. In this case, EN stands for European standards followed by a space, A represents aluminium, W stands for wrought followed by a dash, and C stands for casting followed by a dash. EN AW-5754-O and EN AW-Al Mg3-O are examples of wrought aluminium alloys. The prefix "EN AC-" is used for casting alloys to differentiate casting aluminium alloys from wrought alloys. EN AC-42000KT6 is an example of a cast aluminium alloy.   Based on chemical symbols, the EN designation for cast aluminium alloys is similar to that of wrought aluminium alloys [22].

### 3.2.1   Wrought aluminum alloys

Wrought aluminum is produced by smelting pure aluminum ingots and adding the necessary amounts of alloying elements. The smolten alloy is then formed into billets or slabs that can be forged, rolled or extruded to achieve the final shape. Wrought aluminum is known for its strength, durability, and lightweight properties. These properties make the wrought aluminum alloy a popular choice for a wide range of applications in industries such as aerospace, automotive, and construction.

The Aluminium Association (AA) Designation System of wrought aluminum alloys have a unique identification system: a four-digit number. This number indicates the specific alloying elements present in aluminum alloy. Understanding the unique properties of each series helps with the selection of the most suitable alloy for different applications, ensuring that the final product meets the required specifications and standards.

- 1XXX Series: characterized by almost pure aluminium (over 99% Al): known for excellent formability and electrical conductivity.
- 2XXX Series: primarily made of copper, with small amounts of other elements. Copper provides high strength but lower corrosion resistance. This alloy is commonly used in aerospace applications due to its high strength-to-weight ratio. Additionally, the T351 temper provides improved stress corrosion cracking resistance, making it a popular choice for structural components in aircraft. The most common aircraft alloy is 2024. Alloy 2024-T351 alloy is also known for its good machinability, making it a versatile option for various aircraft components.
- 3XXX Series: contains manganese as the main alloying element, with small amounts of other elements. This type of series is known for its good weldability and formability. 303 alloy is one of this series alloys, which is workable and has a high strength.
- 4XXX Series: contains silicon as the main alloying element, with small amounts of other elements. Silicon provides good wear resistance and castability. The most common alloy from this series is 4043, which is known for its high fluidity and good resistance to hot cracking. Alloy 4047 is also popular for its excellent corrosion resistance and ability to effectively fill gaps in joints. These alloys are widely used in the automotive industry for welding applications.
- 5XXX Series: Magnesium is the principal alloying element. These alloys are known for their high strength, weldability, and corrosion resistance. This alloy series is often used for marine applications and making pressure vessels and storage tanks.
- 6XXX Series: Magnesium and silicon are added to this alloy, and it is known for its excellent strength and formability. It has been extensively used in the construction of truck and boat frames due to its ability to its strength.

- 7XXX Series: Zinc is the main alloying element of this series and provides the highest strength among wrought alloys. These alloys are commonly used in aerospace applications due to their superior strength-to-weight ratio and fatigue resistance. The common alloys of this series are 7050 and 7075, which are the most widely used for manufacturing aircraft components.

### 3.2.2 Cast aluminum alloys

Cast aluminum alloys are those manufactured through a casting process, which involves the process of melting in a furnace and then pouring into a mould to produce the final product. There are different casting processes used to produce cast aluminium alloys, including die casting [23], sand casting [24], permanent mould casting [25], centrifugal casting [26], investment casting [27], etc. Each of these casting processes has its advantages and limitations. Die casting involves injecting molten aluminium into the metal mould under pressure. Die casting is often used for high-volume production because of its fast cycle times, while sand casting is used for low-volume production [21]. In sand casting, the mould is made of sand. Sand is packed around a pattern. Molten aluminium is poured into the sand mould [28]. In permanent aluminium casting, the mould is made of metal. As a result, gravity pushes the molten aluminium into the mould at a relatively slow rate. The mould has a long life due to the durability of metal, which is why it is called a permanent mould. Casting aluminium in a permanent mould is expensive due to the machining expenses required for the mould [29,30]. Like die casting, permanent mould casting is used for high-volume production [23]. In centrifugal casting, the mould is made of metal, plaster, or graphite. The mould rotates on a centrifugal casting machine while molten aluminium is poured into the mould. The centrifugal force ensures that the molten aluminium alloy is evenly distributed throughout the mould [31,32]. Investment casting is also known as lost wax casting because the wax is injected into the mould to create the pattern of the finished product before the molten aluminium is poured into the mould [33–35].

Cast aluminum alloy offers various benefits such as high fluidity, which is demonstrated by its ability to flow smoothly in mould [36], a low melting point which enables efficient casting processes, a minimal tendency to hot cracking even under high temperatures, good surface finish for quality products, and excellent chemical stability [29].

Table 1. Characteristics of cast aluminum alloy series [21]

| Series | Alloys | Characteristics |
|--------|--------|-----------------|
| 1XX | >99.0% Al | Good electrical and thermal conductivity; excellent corrosion resistance |
| 2XX | Al-Cu | High strength but low corrosion resistance |
| 3XX | Al-Si-Mg, Al-Si-Cu, Al-Si-Cu-Mg | High strength and wear resistance; good corrosion resistance |
| 4XX | Al-Si | High ductility; good impact resistance; medium strength; |
| 5XX | Al-Mg | Moderate-to-high strength; high corrosion resistance; good machinability; attractive appearance |
| 7XX | Al-Zn | Good finish; good corrosion resistance; high strength through heat treatment |
| 8XX | Al-Sn | Low friction |

The Aluminium Association Designation System for cast aluminium alloys also based on the alloying elements. Similar to wrought aluminium alloys, the aluminium association designation system for cast aluminium alloys consists of four digits but with a decimal point. The first digit indicates the main alloying element. The second and third digits (xxx.x) are arbitrary numbers given to identify a specific alloy in the series. The final digit after the decimal point distinguishes whether the alloy is a casting (marked by '0') or an ingot (marked by '1') [37,38]. Characteristics of cast aluminum alloys are summarized in Table 1.

Like wrought aluminum alloy, the cast aluminum alloys are mainly made of aluminum, to which other alloying elements are added to improve their properties and performance [39]. The addition of alloying elements can improve the strength, corrosion resistance and machinability of cast aluminum alloys [40].

Factors associated with alloy preparation, such as casting and alloying [41], and those with the post-casting process, such as heat treatment [42], can affect the microstructure of the alloy, which in turn can affect the mechanical properties of the alloy. For example, the cooling rate during casting process can affect the formation of various phases within the alloy and ultimately influence

its strength and ductility [43,44]. Additionally, appropriate heat treatment after casting can further improve the mechanical properties of cast aluminum alloys. This implies the benefits of controlling the microstructure of cast aluminium alloys to achieve the desired mechanical properties.

All alloying elements are completely soluble in liquid aluminium when the temperature is high enough. On the other hand, the solubility of these elements in solid solutions is limited as none of the aluminium alloy systems exhibit continuous solid solubility. Aluminium-rich solid solutions are often formed and are called α-phase, α-Al phase, or α-Al solid solutions. Most of the phases that appear when α-Al is in equilibrium are of the hard type. Compounds such as $Al_2Cu$, $Al_8Mg_5$, $Al_6Mn$, $Al_3Fe$ and AlLi are examples of intermetallic elements or compounds that compose them [45]. These hard phases significantly improve the mechanical properties of the alloy, making it stronger and more durable. The presence of these phases also affects the general microstructure of the material, influencing its performance in different applications.

For example, in Al-Si alloy, the eutectic reaction occurs during solidification of the liquid alloy, leading to a formation of phase α and phase β. Phase α is the solid solution of silicon in aluminium, while phase beta is the eutectic mixture of silicon and aluminium. The eutectic reaction also plays a crucial role in determining the microstructure of the material, influencing its behavior under different conditions. It ensures a uniform distribution of these phases throughout the material, contributing to its consistency and stability of the material. The basic structure of most cast aluminium alloys is defined by the Al-Si phase diagram [46], as shown in Figure 5. The eutectic point can be reached with 12.5 wt% Si and a temperature of 577 °C. Adding or removing other alloying elements can affect the Si content of the eutectic, causing it to shift to different levels.

Eutectic microstructure forms during solidification and can be broadly classified as lamellar, coarse, or refined [47]. This eutectic microstructure is mainly affected by the alloying of elements with certain elements, favouring the formation of refined microstructures. Additionally, the cooling rate during solidification can also influence the final microstructure, and slower cooling rates generally result in a more refined eutectic. Lamellar and thick microstructures, on the other hand, are generally associated with lower mechanical properties due to their larger and less uniform structure. Only the refined microstructure is considered to have favourable mechanical properties; this is due to the delicate structure of the eutectic [48].

19
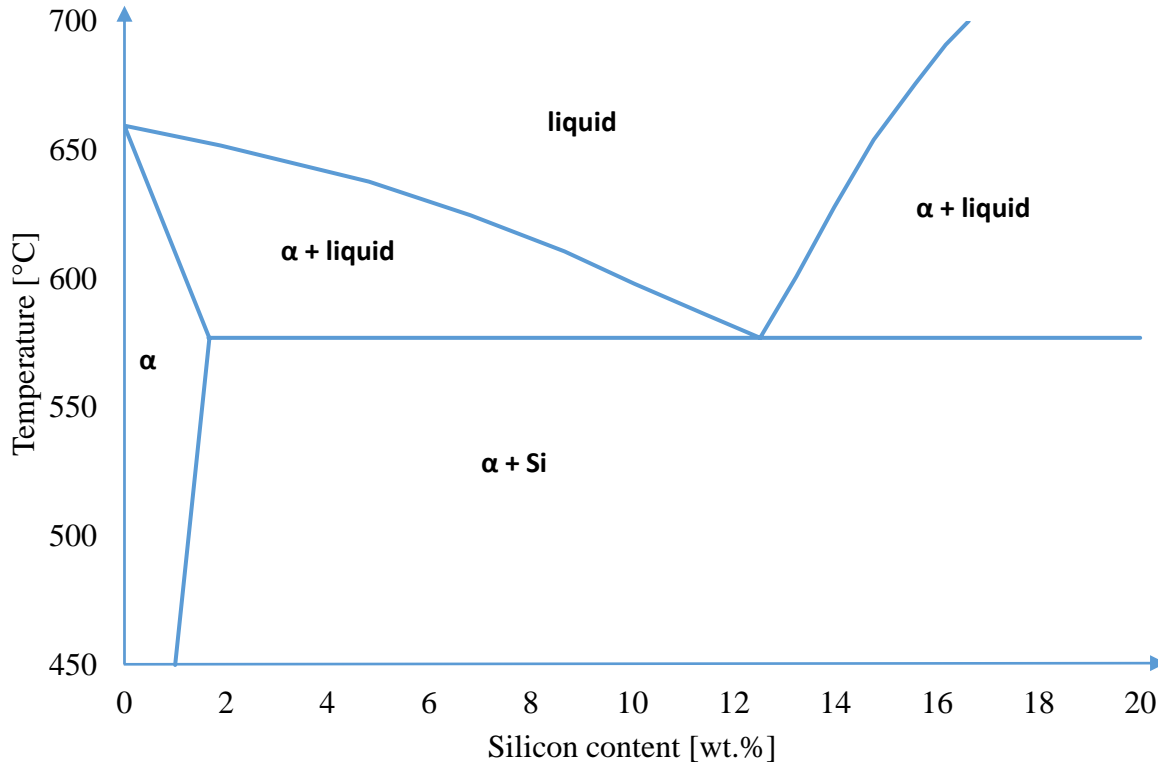
Figure 5. Al-Si phase diagram [46]

**Cast aluminum alloy elements**

**Silicon (Si)**:

Silicon contents of between 5 and 12 wt.% give the cast aluminium alloy better fluidity and also reduce shrinkage porosity of the cast alloy [47,49]. It promotes the formation of eutectic phases, which can lead to a more uniform distribution of elements in the material. This can lead to an improvement in its mechanical properties in the final casting. In addition, the presence of this element can also influence the nucleation of other phases during solidification, leading to a more refined microstructure with smaller grain sizes. However, a high silicon content can also lead to increased brittleness of the casting and make a crack initiation site in the material. Too low a silicon content can lead to a clustering of intermetallic compounds and an increase in porosity [50]. On the other hand, the dendrite arm spacing (DAS), which is the distance between the dendrite arms, can be reduced by increasing the Si volume [51,52], resulting in a more uniform and finer-grained structure. This reduction in DAS can also improve the strength and ductility of the alloy and make the material more resistant to deformation. Depending on the level of modification, the different forms of silicon can be identified as acicular needles, blocky plates, a lamellar structure, or a

20

refined fibrous structure [53,54]. Acicular and refined fibrous structures result in an increased strength and ductility of the material. In general, the addition of silicon to the aluminium alloy casting can affect the solidification process, leading to changes in the microstructure and ultimately impacting on the mechanical properties of the casting.

**Magnesium (Mg):**

Magnesium can enhance the mechanical properties of Al-Si-Cu alloys by refining the eutectic Si phase, increasing strength and hardness of cast aluminum alloys [55]. The addition of this alement mostly leads to the formation of an intermetallic phase, $Mg_2Si$, which precipitates and hardens the alloys. Magnesium also improves corrosion resistance, making it suitable for applications in harsh environments. Increased magnesium content up to 1 wt.% leads to enhanced strength, hardness, and mold filling behavior, however, it decreases ductility of the alloy [56]. However, higher magnesium content has detrimental effect on the oxidation behaviour and porosity of the alloys [57,58].

**Manganese (Mn):**

Manganese reduces the negative effects of iron, which is difficult to remove from aluminum alloys. It changes the morphology of phases containing Fe to a less harmful structure [59]. The morphology of the Fe-intermetallic compound can be changed from coarse platelets, enhancing the alloy's tensile strength. Mn also not only enhances tensile strength but also the low cycle fatigue resistance of the alloy [60]. The ratio of Fe to Mn should be approximately 2:1, and any excess of either element will result in a decrease in the amount of β-phase, an increase in the formation of the α-phase, and an increase in the number of unwanted intermetallic phases that contain Fe [61,62].

**Copper (Cu):**

The addition of Cu influences both the strength and hardness of aluminium alloys. Additionally, it improves the machinability of the alloy. Its limitations are that it reduces the corrosion resistance of the alloy [63]. Higher Cu content leads to the shift from Al-Si eutectic to a ternary Al-Si-Cu eutectic. In addtion, further increase of Cu content leads to a decrease in secondary dendritic arm spacing (SDAS) [64]. Secondary dendritic arm spacing (SDAS) is the distance between dendritic arms in a solidified alloy. This parameter significantly influences the microstructure and

mechanical properties of the material. The decrease in SDAS enhances the tensile strength, hardness, and creep resistance of the alloy [65]. Cu enhance the strength of the alloy by forming hardening precipitates during heat treatment. A decrease in the amount of copper can also lead to the initiation of cracks that are associated with the presence of silicon particles in the eutectic phase [50].

**Iron (Fe):**

In cast aluminium alloys, Fe is the most common impurity due to the formation of Fe containing intermetallic compounds. It negatively affects the mechanical properties of the alloy by increasing the porosity. During casting, it is difficult to completely remove it from the casting, but its presence can reduce the strength, ductility, and castability of the cast alloy [66,67]. However, there are several methods to minimize the detrimental effects of Fe in the cast aluminium alloy. The most common method is grain refinement, which reduces the size of Fe-containing intermetallic compounds formed during solidification. Furthermore, controlling casting parameters such as temperature and cooling rate can minimize the effect of Fe impurities on the mechanical properties of the cast alloy [68]. If the Fe content goes above 0.7 wt%, the Al5FeSi phase forms, which causes a substantial drop in the ductility of the alloy, which can be seen as a change from ductile to brittle fracture. Such phase formation significantly deteriorates the mechanical properties of the alloy, making it more vulnerable to crack formation and failure under stress [69–72].

**Enhancing mechanical properties of cast aluminum alloy**

To improve the mechanical properties of Al-Si alloy castings, two commonly used techniques are grain refinement and grain modification. Grain refinement is the process of adding a titanium-based grain refiner (Ti-B or Ti-C) into the melt to refine the grain size of the casting into a fine equiaxed structure. The modification process involves inoculation of the melt with a strontium-based modifier to change the morphology of the silicon from acicular flakes to fibrous, resulting in increased ductility and toughness [73].

Another way to improve the mechanical properties of Al-Si alloy casting is T6 heat-treatment process. The T6 heat treatment process consists of three steps. The first step is solution heat treatment, followed by the second step, quenching, and finally, the third step, artificial aging [74–76]. The heat treatment parameters used to determine the improvement of the mechanical properties of the treated materials in a given situation. The microstructure of cast aluminum alloys

22

is influenced by solution heat treatment, which improves the morphology of the eutectic silicon (fragmentation, spheroidisation, and coarsening) and ensures modification of the fracture zones [76,77]. After prolonged solution heat treatment, a spheroidal shape can be achieved in the Si phase, changing the properties of the aluminum alloy.

Heat treatment regulates the balance between the solid solution of alloying elements and their precipitates, which can be coherent or not coherent [61]. The movement of dislocations is significantly more difficult when coherent precipitates are present as compared to incoherent precipitates. Consequently, the ultimate tensile stress (UTS) of the alloy increases. Figure 6 shows a typical precipitation hardening heat treatment cycle.

Another method of enhancing mechanical properties is incorporating reinforcement into aluminium alloys. Reinforcement, such as silicon carbide (SiC) particles, can enhance the alloy's strength and stiffness. This type of reinforcement also helps to improve the alloy's fatigue and corrosion resistance. SiC particles are hard and act as barriers that prevent plastic deformation in the alloy, resulting in increased strength and durability.
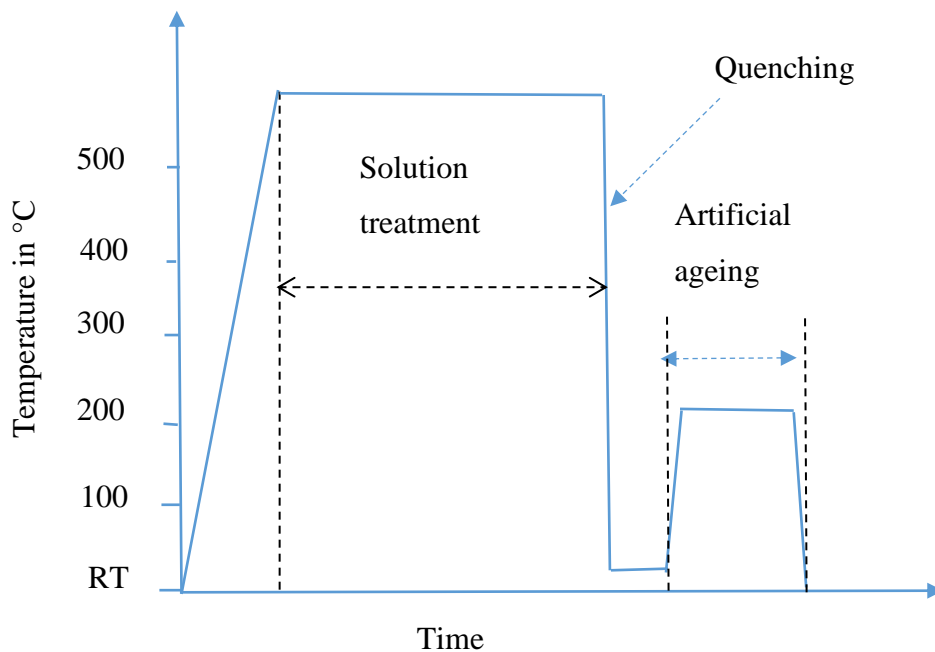


Figure 6. Heat treatment cycle of typical precipitation [61]

## 3.3    Aluminum metal matrix composites (AMMCs)

A metal matrix composite is a combination of the reinforcement and the aluminum matrix. When the metal matrix is aluminium, the combinations give an aluminium metal matrix composite. Because of their advantageous properties, including low density, high resistance to corrosion, abrasion and wear resistance, high thermal conductivity and high specific modulus, aluminium metal matrix composites are used in various industries, including automotive, aerospace, military and maritime [78]. In the automotive industry, aluminium metal matrix composites are used to manufacture lightweight and strong vehicle components [79]. In the aerospace industry, these composites are used to manufacture strong, durable parts for aircraft that are capable of withstanding extreme environmental conditions [80]. In the military, aluminium metal matrix composites are used to develop armour and protective equipment that offer superior protection and durability in combat situations [81,82]. In the maritime industry, aluminium matrix composites are extensively implemented to enhance manoeuvrability, fuel efficiency, ship speed, and access to low-drawing ports [83].

Aluminum metal matrix composites (AMMCs) offer many advantages. They offer superior characteristics to monolithic alloys. The aluminium matrix layer provides a porous surface in an aluminum alloy metal matrix composite (AMMC). Other materials embedded in this porous aluminum matrix layer act as reinforcement, often nonmetallic and ceramic, such as silicon carbide or aluminum oxide. The characteristics of AMMCs can be modified by changing the composition and volume fractions of their constituents.

**Fabrication processes of AMMCs**

The mechanical properties of AMMCs are highly dependent on the processing method. There are three commonly used AMMC manufacturing processes. These are the solid-state process, the liquid-state process, and the solid-liquid process [84]. In the solid-state process, the reinforcement particles are mixed mechanically into the aluminium matrix and then consolidated using methods like hot pressing or powder metallurgy [85,86]. In the liquid process, the reinforcement particles are mixed into the molten aluminium alloy, and then the mixture is solidified through methods like squeeze or stir casting [87,88]. The solid-liquid process incorporates parts of both processes. It involves partially melting the aluminium matrix before adding the reinforcement particles and solidifying the mixture using spray deposition or semi-solid processing [89]. Figure 7 shows the different fabrication processes of AMMCs.

**Stir casting**

The stir casting process is a economical, and simple technique used for the manufacturing of AMMCs [90]. It involves the addition of reinforcements to a molten liquid matrix and the subsequent solidification of the MMCs. Following the melting of the matrix, it is stirred vigorously for some time until a vortex is generated within the melt, and then reinforcement particles are added, as shown in Figure 8 [14].

Poor interfacial bonding and wettability issues between the matrix and reinforcing materials can be problems with stir casting. This can reduce the mechanical properties of AMMCs. In addition, the stir casting process can sometimes lead to an uneven distribution of reinforcement particles, resulting in inconsistent material properties throughout the final product. Despite these drawbacks, stir casting remains a popular choice for AMMC production due to its cost-effectiveness and simplicity in large-scale manufacturing processes.
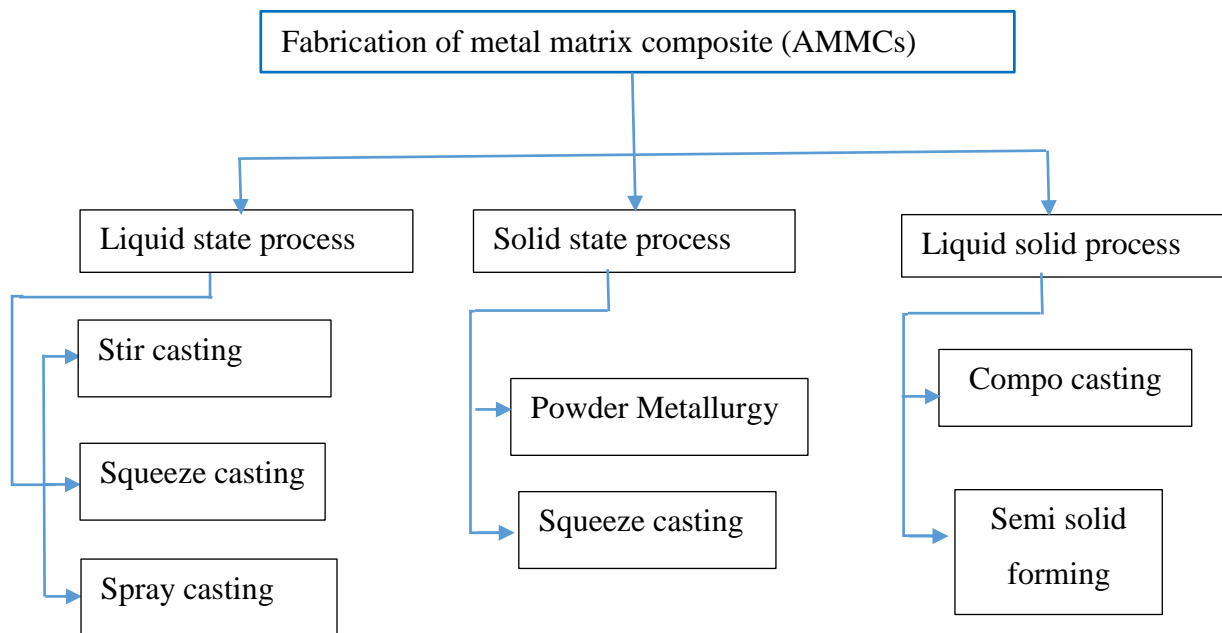
Figure 7. Fabrication methods of AMMCs [84]
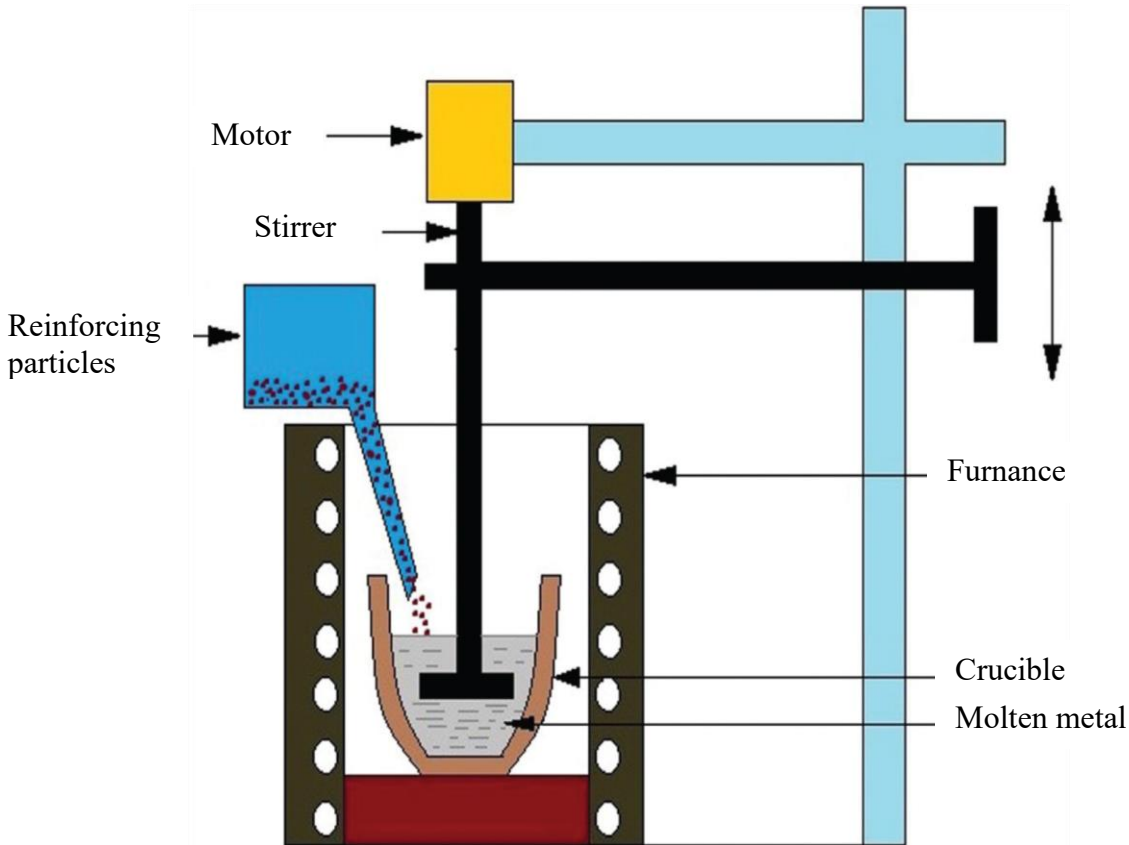
Figure 8. Schematic view of stir casting process [14]

## 3.4 Deformation behavior of aluminum alloys and its metal matrix composite

### 3.4.1 Stress relaxation

Stress relaxation is a material behaviour that occurs when a continuous load is applied while maintaining constant strain over time [91,92]. During the relaxation test, stress reduction is measured as a function of time. Over prolonged time, the elastic strain inside the material gradually transforms into plastic strain [93]. This process allows the material to reach a more stable and relaxed state by relieving the internal stresses caused by the initial applied load. Stress relaxation can affect the long-term performance and durability of materials under constant load.

Several studies [94–96] have reported that stress relaxation increases with the operating temperature. For instance, Authors of a paper [94] investigated the stress relaxation behavior of polycrystalline aluminum with varying grain sizes. The aluminum was annealed at 500°C and aged at room temperature for six months. The results clearly demonstrate that stress relaxation is influenced by aging time. A study described in a paper [95] illustrates the stress relaxation ageing

(SRA) behavior of AA7B04–P alloy. The study highlights that higher initial stress or temperature leads to increased stress relaxation. Authors of a paper [96] conducted stress relaxation tests on AA5182-O aluminum alloy sheet at 25°C, 100°C, 200°C, and 300°C to observe temperature and strain rate dependency. Results showed stress dropped more at 100°C during relaxation, and stress almost disappeared at 300°C. The results showed that the dominant relaxation mechanism is grain boundary slip due to the influence of temperature. Authors of a paper [97] investigated the stress relaxation behavior of AA7150-T7751 alloy under various temperatures, initial stress levels, and pre-strains. The results showed that temperature, initial stress levels, and pre-strains significantly influence the stress relaxation behaviour. The stress relaxation level increases with temperature. Similar to aluminium alloys, numerous researchers have examined the stress relaxation phenomenon in aluminium metal matrix composites (MMCs). Authors of a paper [98] investigated thermal stress relaxation in aluminium-based metal-matrix composites (MMCs) using mechanical loss and dynamic shear modulus measurements. Results indicate that a transient mechanical loss occurs due to dislocation generation and motion near the interfaces, which arises from the differential thermal contraction between the matrix and reinforcement. The authors of a paper [99] examined thermal stress relaxation mechanisms in Al 99.99% reinforced with SAFFIL alumina short fibres using mechanical spectroscopy. The study revealed that internal friction, elastic modulus, and zero point drift behaviours are highly sensitive to internal stresses, specifically related to dislocation generation or dislocation creep.

### 3.4.2 Creep loading

Creep is a time-dependent deformation that occurs under constant stress or loading conditions at high temperatures. When subjected to applied load or stress, any material will first deform elastically and then plastically after crossing the yield limit. In this case, the material deformation occurs due to creep loading even at stresses below the yield limit under the influence of constant stress and temperature over a long period of time [100].

Numerous experimental studies and theoretical models have been developed to characterize creep damage under a range of creep conditions. These studies have focused on the mechanisms of creep deformation and the factors that affect the creep life of the material. For example, the Larson-Miller model [101] is a widely used method for predicting the creep life of materials under high temperatures and constant stress levels. It considers the combined effects of time, temperature, and stress on creep deformation. However, the model has a limitation in its ability to accurately predict

creep conditions because some other factors, such as material composition, variable loads, and variable temperature that affect the creep life of the material, have not been considered. In a study by authors of a paper [102], the Larson-Miller parameter was modified to include factors like microstructure and alloy composition, improving the accuracy of predicting material creep life. Taking these factors into account, the modified model showed a stronger correlation between predicted and actual creep-life outcomes. This suggests that the original Larson-Miller model did not adequately account for these factors, highlighting a limitation in its accuracy.

Similarly, the authors of a paper [103] proposed a non-linear cumulative creep damage model that considers the damage history and loading effect to describe the creep deformation behaviour of metallic materials under variable stresses and temperatures. However, this model may not accurately predict the creep deformation of metallic materials with shorter lifespans under variable temperature conditions, mainly when high temperatures are initially applied under varying temperature conditions [104]. The author of a paper [105] proposed a non-linear model for creep damage accumulation that considers loading sequence damage and creep strain. However, contradictions were found in the model, making it difficult to establish a correct creep damage accumulation rule for the strain under the same loading conditions. A new creep damage assessment model based on Batsoulas' model was presented in a paper [106]. The model takes into account the loading process and the material's creep behaviour under different conditions. However, the proposed model lacks clear physical significance, which is essential for its practical implementation.

Like stress relaxation, the creep behaviour of aluminium alloys is also influenced by operating temperature. The two important creep parameters, creep strain and creep strain rate, tend to increase with temperature, as reported by the studies conducted by [107–109].

The authors of a paper [107] investigated the creep behaviour of 2A14 aluminium alloy at different temperatures by conducting a creep test, and the results show that the creep strain and creep strain rate increase with temperature. Other authors of a paper [108] suggested that the creep resistance of cast aluminium alloys decreases with increasing temperature, especially between 200°C and 300°C. The authors of a paper [109] examined the effects of temperature on the creep behaviour of the AlSi12CuNiMg aluminium alloy. They found that an increase in temperature resulted in a decrease in the creep lifetime and an increase in the minimum strain rate. The authors of a paper

[110] studied the creep behaviour of the Al-Cu-Mg alloy and constitutive models that describe the high-temperature creep behaviour of the alloy. They reported that the creep behavior of the Al-Cu-Mg alloy depends on temperature.

### 3.4.3   Fatigue loading

Fatigue is a phenomenon in which cyclic or fluctuating stresses, often below the material's yield strength, induce progressive and localized microstructural changes in a material, resulting in an accumulation of plastic strain that leads to a potential failure of the material [111]. Fatigue loading induces plastic strain, which leads to the formation of microcracks. These gradually grow and propagate under the effects of repetitive loading and unloading of the material. There are two typical fatigue failure modes: high-cycle fatigue and low-cycle fatigue. High cycle fatigue occurs when the material fails after a high number of stress cycles at a typically low stress level below its yield stress, while low-cycle fatigue occurs when a material fails after a smaller number of stress cycles, usually at a stress level exceeding its yield strength.

The two most commonly used approaches for modelling fatigue damage under cyclic loading are the stress-life approach and the strain-life approach. The stress-life approach is the graph of the stress versus number of cycles to failure, which is usually plotted. In strain-life approaches, the graph of strain versus the number of cycles to failure is plotted. Both approaches are useful for predicting the fatigue life of a material under cyclic loading conditions. The two most commonly used approaches for modelling fatigue damage under cyclic loading are the stress-life approach and the strain-life approach. The stress-life approach is the graph of the stress versus the number of cycles to failure, which is usually plotted. In strain-life approaches, the graph of strain versus the number of cycles to failure is plotted. Both approaches are useful for predicting the fatigue life of a material under cyclic loading conditions. The main drawback of these methods is that they only depend on a stress/strain criterion to determine fatigue life without involving loading or specimen geometry [112].

There are three phases of fatigue failure: crack initiation, crack growth (propagation), and ultimate failure. Crack initiation sites are mainly influenced by material defects due to stress concentration around the defects. The second phase is fatigue crack growth/propagation, where the crack begins to expand as the material is subjected to cyclic loading. The third phase is the ultimate failure,

where the crack has reached a critical size and the material can no longer withstand the applied external load, resulting in complete structural failure.

Low Cycle Fatigue (LCF) is defined as cyclic plastic deformation caused by irreversible microstructural changes occurring under cyclic loading. It can occur even when the effective stress is below the elastic limit of the material [61]. These microstructural changes accumulate around the stress concentration zone, causing progressive deformation of the material under loading and unloading, which ultimately leads to material failure.

Due to load reversals, dislocations tend to accumulate in ladder or cell structures [61]. In addition, dislocation movements tend to be concentrated in a limited number of slip bands. This leads to relatively thick sliding steps, which in turn lead to crack initiation. This crack initiation can eventually lead to the formation of cracks in the material, which can then propagate and lead to failure. The accumulation of dislocations in slip bands can also lead to localized plastic deformation, which can further contribute to fatigue failure. The continued accumulation of dislocations in slip bands can weaken the strength and durability of the material, ultimately making it more vulnerable to fatigue failure. Under certain circumstances, cracks caused by dislocation movements can often go undetected until catastrophic failure occurs. In reference [113], the processes that can cause fatigue of materials and components under cyclic loading and the corresponding dislocation behavior were deduced. Figure 9 shows a chronological overview of the damage processes that lead to failure.
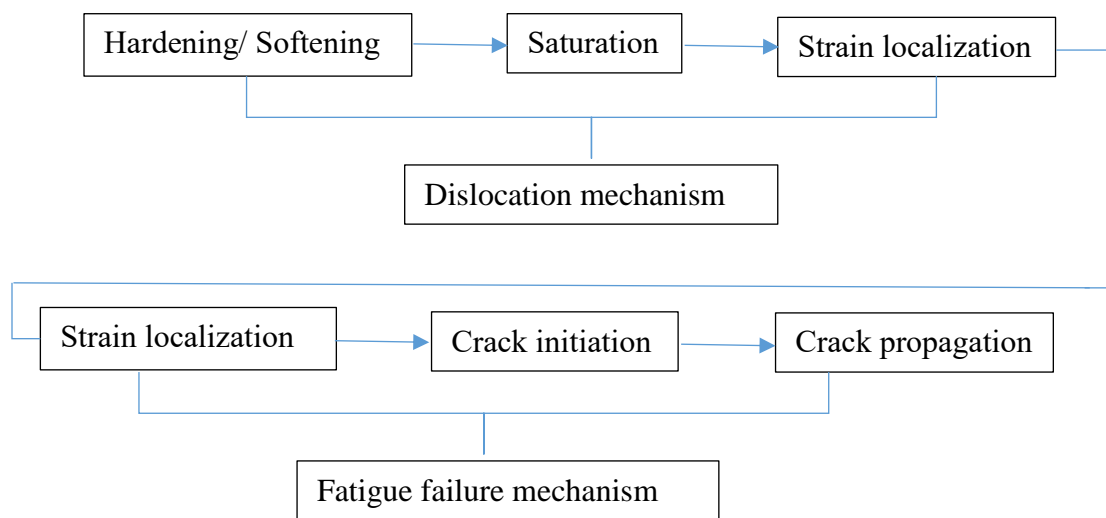


Figure 9. Summary of damage mechanisms leading to failure *(ada*pted from [61])

In low cycle fatigue, the applied strain has a significant plastic component and resultant lives fall up to $10^5$; on the contrary, in high cycle fatigue, the applied stress is primarily within the elastic range of material, and the resultant lives (cycles to failure-life) are high. The stress-life or S-N approach is standard for high cycle fatigue, whereas the strain-life approach is suitable for low cycle fatigue analysis. Basquin [114] observed that the stress-life data could be linearized on a log-log scale for steel and copper materials. This linearization led to the development of the Basquin equation, which relates the stress range to the number of cycles to failure. For low-cycle fatigue analysis, strain-life curves are typically plotted to describe the relationship between stress amplitude and the number of cycles to failure.

**Low cycle fatigue of aluminum alloys**

Authors of a paper [115] conducted low-cycle fatigue tests on two aluminium alloys, AA2024-T6 and AA7020-T6, under the same heat treatment. Results showed that strength and chemical composition significantly affect transition fatigue life. The compatibility and precipitation of zinc and copper on the parent metal led to higher fatigue properties in AA7020-T6. Different lifetime approaches were reported in reference [116] for fatigue analysis of aluminium engine components. The complex damage rate model of Neu/Sehitoglu was evaluated, and the Sehitoglu model provided the best accuracy in describing experimental lifetime results.

Other authors of a paper [117] investigate the effects of strain rate and mean strain on the cyclic behaviour and lifetime of aluminium-silicon alloys under thermo-mechanical and isothermal fatigue loadings. Low-cycle fatigue tests were performed on A356 and A357 alloys. Results show that HT-LCF lifetime and plastic strain energy are almost the same under TMF loadings, suggesting the use of lower-cost, lower-running time LCF tests for further research.

**Low cycle fatigue of metal matrix composites**

Several studies reported the fatigue behaviour of aluminium metal matrix composite. The author of a paper [118] investigated the fatigue behaviour of unreinforced and $Al_2O_3$-reinforced Al2014 alloy metal matrix composites. The study result showed that the $Al_2O_3$-reinforced Al2014 alloy metal matrix composites exhibited higher fatigue strength. The author of a paper [119] examined the fatigue properties of aluminium alloy (6061) metal matrix composites reinforced with different SiC particles. The study demonstrated that the uniform distribution of SiC particles primarily attributed to the improvement in the fatigue strength of the composite.

Other authors of a paper [120] examined the fatigue behaviour of a 20 vol. % SiCp reinforced A359 aluminium alloy matrix composite, analyzing its microstructure and thermo-mechanical properties. Various heat treatments were used, revealing a strong dependence on the treatment. The T6 composites showed better endurance limits but a 70% fatigue limit due to the enhanced cohesion and improved matrix-particulate interfacial properties. The HT1 condition had weak interfacial strength, resulting in de-bonding and compromising the fatigue performance of the composites. The T1 condition exhibited similar fatigue behavior but with reduced ductility, affecting its performance under cyclic loading.

The authors of a paper [121] examined the fatigue behavior of aluminium matrix-silicon carbide (SiC) particulate reinforced composite specimens compared to a matrix aluminium alloy with 12wt% Si. The results demonstrated that higher SiC particulate content led to a significant improvement in hardness and a notable enhancement in fatigue resistance. SiC particulates acted as barriers to cracks and decreased crack propagation rates, resulting in less fracture cycles.

Researchers of a paper [122] investigated the low cycle fatigue (LCF) resistance of 6061 Al/20 vol% alumina particulate metal matrix composites (MMCs) using reversed strain control testing. They reported three stages of composite response: initial fast hardening, gradual softening, and a rapid drop in stress-carrying capability.

Authors of a paper [123] examined crack-tip shielding mechanisms in metal matrix composites, focusing on crack bridging by uncracked ligaments. Simple analytical models are developed for bridging induced by overlapping cracks and coplanar ligaments in the wake of the crack tip. The predicted shielding degree is not large but consistent with experimental observations in high-strength P/M aluminum alloys reinforced with SiC particulate.

The study of metal matrix composites processed using powder metallurgy under strain control loading conditions was detailed in reference [124]. The study reported a direct correlation between the increase in SiCp content and the degradation of fatigue properties, as well as a significant alteration in stress-strain response due to varying strain ratio values. The increase in volume fraction and particle sizes directly correlates with the early initiation of cracks, highlighting the critical role of these factors in the structural integrity of the composites.

The study the fatigue behavior of a naturally aged powder metallurgy 2xxx series aluminum alloy and a composite with 15 vol pct SiCp are presented in a reference [125]. Results show that mean stress significantly influences fatigue life, with SiC reinforcement increasing it at low and intermediate stresses. However, composite materials have inferior fatigue resistance. Fatigue cracks initiate from various microstructural features or defect types.

The authors of a paper [126] investigated the effect of particle size, volume fraction, and matrix strength on the fatigue behavior and fracture probability of 2124 aluminum alloy reinforced with SiC particles. Results showed higher tensile and yield strengths and fatigue life in reinforced alloys. The frequency of particle fracture during crack propagation was dependent on matrix strength, particle size, volume fraction, and maximum crack tip stress intensity.

Authors of a paper [127] presents a microstructure-sensitive fatigue model for analyzing a discontinuously reinforced aluminum alloy metal matrix composite. The model reveals that the aluminum alloy's fatigue damage is strongly influenced by the volume fraction of the particulate reinforcement phase. The model accurately characterizes the evolution of fatigue damage into crack initiation and growth stages, highlighting the importance of particle size and volume fraction in determining fatigue lifetime.

### 3.4.4 Combination of stress relaxation, creep and fatigue loading

During the real application of AMMCs in various industries, including automotive, aerospace, marine, and military, there is a challenge from the combination of loading such as; a combination of relaxation and fatigue and/ or creep and fatigue especially at high temperature These combination of loadings are the main causes of premature failure of the material [128].

Deformation and failure mechanisms of AMMCs at high temperatures have become very complex and depend on material properties. The life assessment of such structures became a significant challenge for both the scientific and industrial communities [10]. There are several attempts made by researchers to find the failure criteria for MMCs. However, there are a lot of limitations to predict the failure characteristics of MMCs. Relaxation, creep, and fatigue are measured in different ways. The influences between these cognitive operations are not counted. According to the standards, MMCs failures are measured only for the dominant types of failure. In many

applications, where temperature operating conditions are high, this is creep or low cycle fatigue. Therefore, accepting loading history alone in finding the failures of MMCs has a lot of limitations.

Furthermore, the manufacturing process's effect on the durability of the MMC is not taken into account. It is well known that MMCs are better than other materials in resisting corrosion and wear, but this still affects the durability of MMCs. Therefore, environmental effects such as wear and corrosion must be taken into account when measuring MMC's durability.

This dissertation focuses on measuring the influence of combined relaxation, creep, and fatigue interaction on the durability of AMMCs, considering other factors that increase the damage of AMMC.

# 4. EXPERIMENTAL STUDIES OF EN AC-Al Si12CuNiMg ALLOY'S MECHANICAL PROPERTIES

A high strength-to-weight ratio and the ability to withstand high temperatures are typical requirements for the manufacture of various mechanical structures. Aluminium alloys possess a number of these distinctive properties that make them suitable for a wide range of applications, including the automotive, aerospace, and military industries [129–131]. For example, engine blocks, piston heads, steering boxes, inlet manifolds, rocker covers, deferential casings, brackets, and wheels are among the many components made from aluminium casting in the automotive industry [132]. Compared to other cast alloys, aluminium alloys offer excellent corrosion and oxidation resistance and favourable properties such as low density, wear resistance, high strength-to-weight ratio, and other good technological properties [133]. However, one of the main drawbacks of aluminium-silicon alloys is their propensity to produce coarse-grained structures, resulting in severe degradation of mechanical properties [134].

The most common alloying elements used in the production of aluminium alloys are Si, Mg, Cu, and Zn. Al-Si alloys have good casting properties and are widely used to manufacture automotive components that operate at ambient and moderately high temperatures [135,136]. Alloying elements have an impact on both microstructural and mechanical properties [137]. Al-Mg, Al-Cu, and Al-Zn alloys have better mechanical properties than Al-Si alloys, but their casting properties are often poor. The silicon content of standardized commercial cast aluminum alloys ranges from 5 to 23 % by weight. Adding Si to aluminium alloys improves the fluidity and casting properties of the aluminium alloys, while Mg enhances corrosion resistance [138]. Typically, Cu is added to Al-Si alloys to improve machinability. Increasing the Cu and Mg content of an alloy enhances strength while decreasing ductility. Similarly, increasing the Fe content of an alloy decreases the ductility of the alloy [139]. On the other hand, Na in cast Al-Si alloys significantly improves mechanical properties, especially ductility [140]. A small amount of Ni is added to aluminum-silicon alloys to improve hardness and strength at high temperatures [141].

The presence of Cu, Mg, Ni, and Fe in the Al-Si alloy causes the formation of various intermetallic compounds such as: $Al_2Cu$, $Mg_2Si$, $\alpha$-$Al_{12}(Fe, Mn)_3Si_2$, and $\beta$-$Al_5FeSi$ in the microstructure [142]. The presence of the intermetallic phases influences the physical properties of the alloy such

as ductility, thermal expansion, and hardness. In addition, the physical properties of individual constituents, such as the relative distribution of Al matrix and Si crystals, their volume percentage in the mixture, and morphological distribution, size, and shape, determine the mechanical properties of these alloys [143,144].

Several studies reported that various factors, such as: superheating of the melt, holding duration, and solidification rate, affect the microstructure of the cast aluminium-silicon alloy [145–147]. Superheating Al-Si alloys produces a shift in the eutectic reaction toward higher levels of silicon, accompanying with the appearance of dendrites in the hypo-eutectic and eutectic Al-Si alloys [148,149]. The solidification rate determines the coarseness of the microstructure, the formation of dendrites and defects [150,151]. The microstructural coarseness includes the percentage, size, shape, and distribution of intermetallic phases and the segregation profiles of solute in the α-Al phase.

Aluminum-silicon alloys are composed of the aluminium phase (α -phase) and the silicon phase (β -phase). It should be noted that the aluminum phase has excellent ductility characteristics, while the silicon phase has brittle characteristics and mostly needle-like structure [152].

Despite the importance of the Al-Si alloy and its wide range of applications, its functionality is limited to low and moderate temperatures because its strength decreases significantly when exposed to high temperatures. The ability of an aluminum alloy to retain its desirable properties at elevated temperatures is critical in several applications where it is widely used. Therefore, to ensure structural stability and determine the temperature range in which components made of this alloy can operate, mechanical characterization of Al-Si alloys at various temperatures is essential.

## 4.1 Tensile specimen preparation

The academic staff of the Department of Materials Technologies at the Silesian University of Technology prepared the specimens in accordance with the following procedures: Initially, a 2.5 kg ingot was cut and then melted in the resistance furnace at 720°C. After melting, the molten metal (charge) was kept at the same temperature for 15 minutes to ensure a uniform material composition (homogenization). Throughout the heating process, argon gas was continuously fed into the furnace chamber at a rate of 0.5 $l_N$/min to create an inert atmosphere and prevent the alloy from oxidizing. Before casting, the oxide layer, which can negatively affect the casting quality, was removed with a trowel.

The castings were prepared using the MetalHealth system, a system known for maintaining a stable mold heating temperature throughout the casting process. The mold feeding system was based on the KALPUR-POURING SLEEVES system, known for its efficient metal flow control, along with Foseco's SVX 0R X 22/10 filter, which ensures precise filtration of impurities. Following the casting process, the required specimen parts were sectioned out of the casting. Both ends of these specimens were then threaded to the required M16 dimensions using a threading machine. A total of 27 tensile specimens with a length of 60 mm and a diameter of 10 mm were prepared. The prepared tensile specimens are shown in Figure 10. The chemical composition of the investigated alloy, which is presented in Table 2, was measured by optical emission spectroscopy (OES).

Table 2. The measured chemical composition of EN AC-Al Si12CuNiMg (weight percentage)

| Fe | Si | Cu | Mg | Zn | Mn | Ti | Ni |
|------|------|------|------|------|------|------|------|
| 0.4 | 11.4 | 1.27 | 1.24 | 0.18 | 0.18 | 0.04 | 1.48 |



Figure 10. Tensile specimens

## 4.2 Uniaxial tensile test

In accordance with ISO 6892-1, uniaxial tensile tests were performed on these specimens in their as-cast condition on the Zwick/Roel Z100 universal testing machine. The testing machine was fitted with a furnace and universal 3-zone furnace controller. A 3-zone universal furnace controller is used to control the furnace temperature and specimen surface temperature via six thermocouples. The tests were conducted at room temperature and elevated temperatures of 150, 250, 300, and 350°C. Figure 11 a) and b) illustrate the experimental setup of the uniaxial tensile tests, showing

the configuration at both room temperature and elevated temperatures. At each temperature, the tensile tests were repeated five times. A high temperature extensometer with ceramic sensor arms was used to record load elongation data in the elastic zone. Figure 12 shows a Maytec high temperature extensometer with ceramic sensor arms. For the elevated temperature tensile test, the heating furnace on the Z100 universal testing machine was used to heat the specimens. The strain rate of $6.7 \times 10^{-3}$ $s^{-1}$ was employed in all tensile tests. The specimens were loaded under a uniaxial tensile load until a fracture occurred. The Zwick testXpert software was used to monitor and control the load application and temperature through a digital closed-loop control system. The recorded load-extension data was used to plot the stress-strain curves, which were then used to determine the tensile properties of the as-cast specimens, such as their yield strength, ultimate tensile strength, Young's modulus, and percentage of elongation. Subsequently, the impact of temperature on the tensile properties of the alloy was investigated.
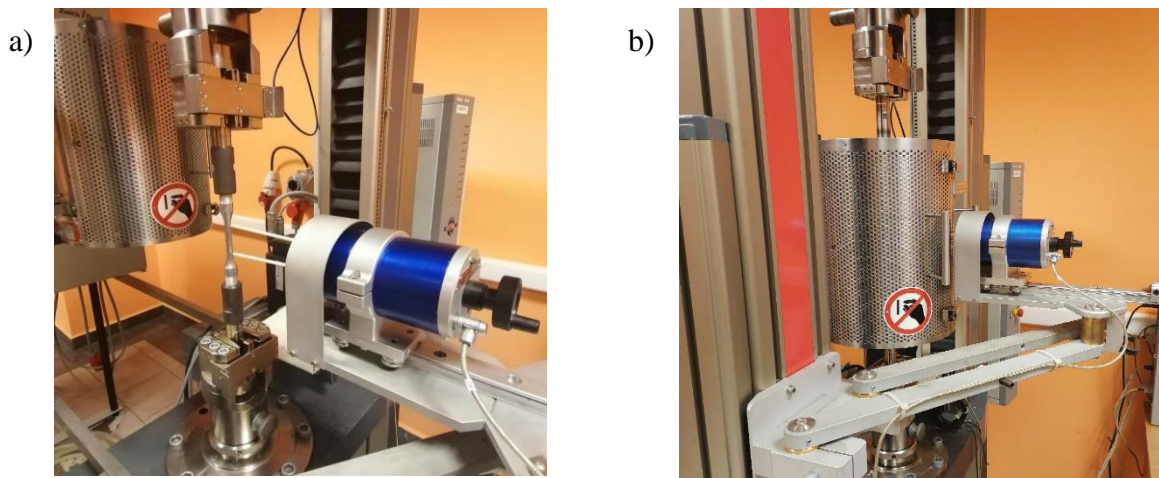


Figure 11. Specimen clamped in a testing machine at: a) normal b) elevated temperature
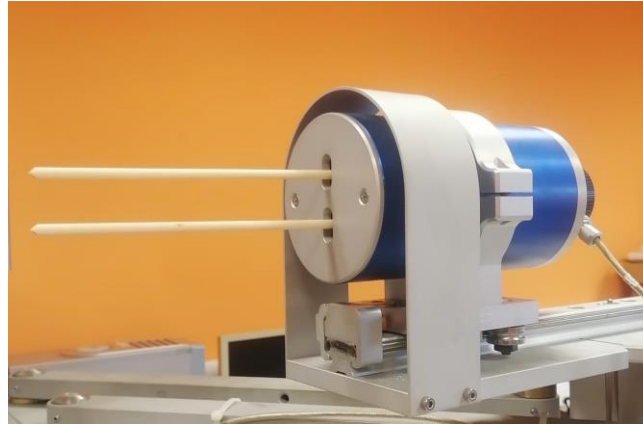
Figure 12. Extensometer with ceramic sensor arms

## Uniaxial tensile test results

### Stress-strain curves

The stress-strain curve is used to describe the tensile properties of materials, such as yield strength, tensile strength, Young's modulus, and fracture strain. Figure 13 shows the engineering stress-strain curve of the investigated alloys at room temperature. Figure 14 shows stress-strain curves at various temperatures. As the temperature increases, the percentage of elongation increases. At room temperature, the material tends to exhibit brittle failure behaviour. However, it tends towards ductile fracture behaviour at elevated temperatures, despite the absence of a cup shape and cone at the fracture site. Therefore, the fracture behaviour of this material changes in response to temperature changes.
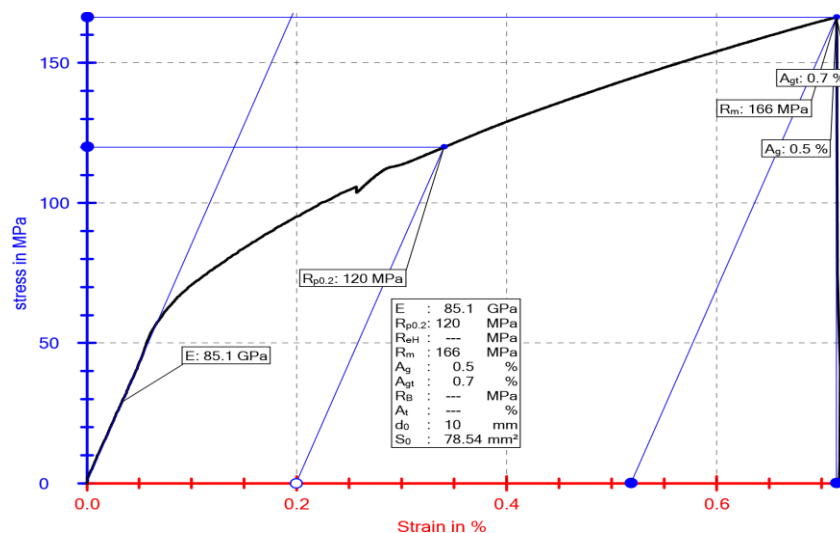


Figure 13. Stress-strain curve of EN AC-Al Si12CuNiMg at room temperature

39
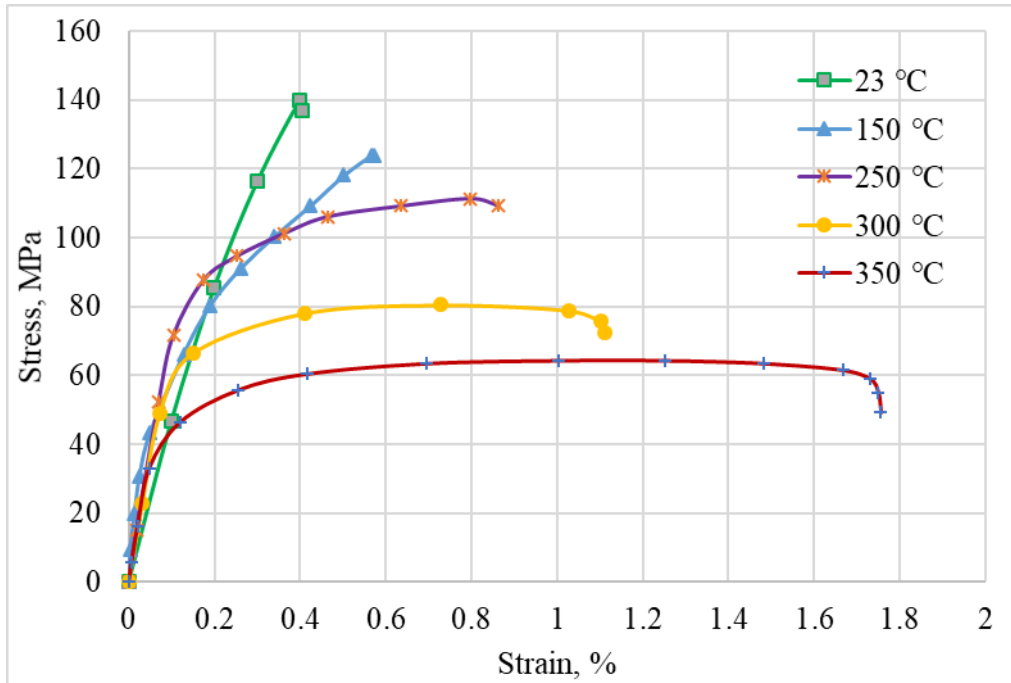
Figure 14. . Stress-strain curve of EN AC-Al Si12CuNiMg at various temperatures

The tensile strength is the maximum stress value on the stress-strain curve. Figure 15 shows the tensile strength of EN AC-Al Si12CuNiMg alloys as a function of temperatures. The values shown are the average of five test results compared with the result presented in a paper [153]. The figure clearly shows the decrease in tensile strength with increasing temperature. For example, at room temperature, the tensile strength of this alloy is 140 MPa, but at 150°C and 250°C, the tensile strength is 125 MPa and 112 MPa, respectively. Therefore, the tensile strength decreases by 5% to 15% from room temperature to 150°C and 250°C, respectively. On the other hand, temperatures between 250°C and 350°C led to a 40-50% reduction in the tensile strength of the alloy. This indicates that the decrease in tensile strength is very small at low and moderate temperatures, but when the temperature exceeds 250°C, the tensile strength dramatically degrades.

The low tensile strength of this investigated alloy results from various casting conditions and the nature of microstructures compared to those in the literature [153]. The coarse-grained microstructures of these alloys have a detrimental effect on their mechanical properties at low and high temperatures.
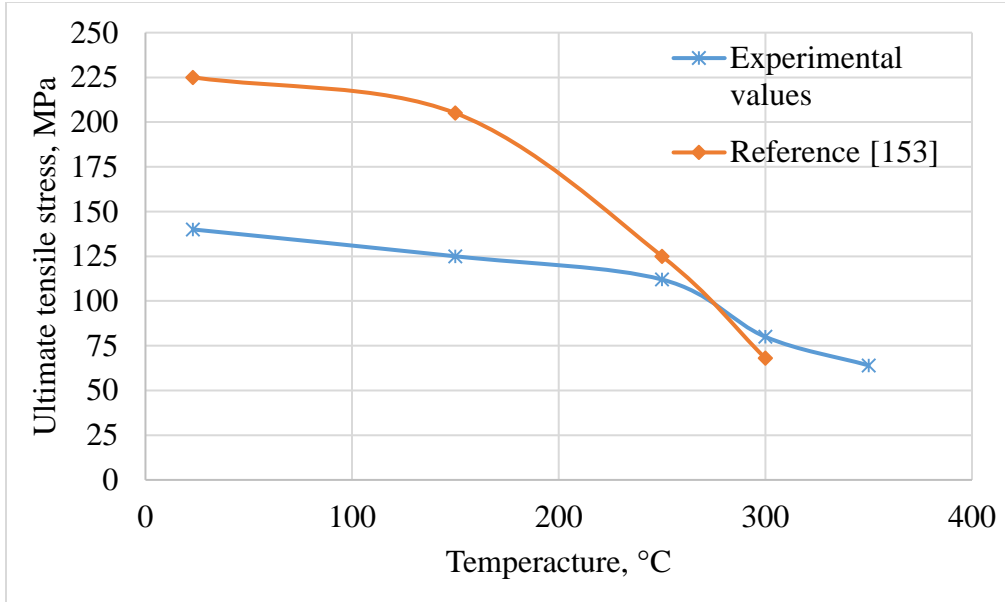
Figure 15. Ultimate tensile stress of the alloy at various temperatures

Figure 16 shows the yield strength and fracture strain of the alloy plot against temperature. The average values of the five test results are presented in this graph. Unlike the 10% drop of the yield strength observed in the temperature range from room temperature to 250°C, a rapid decline of the yield strength is observed at temperatures above 250°C. In other ways, the fracture strain of the specimen at low testing temperature is extremely low compared to the fracture strain at high temperature. Therefore, the relationship between fracture strain and test temperature is contrary to yield strength. For temperatures above 250°C, the deformation of the fracture increases significantly with increasing temperature. The fracture strain determines the ductility of the materials. Therefore, the ductility of the alloy increases with increasing temperature.
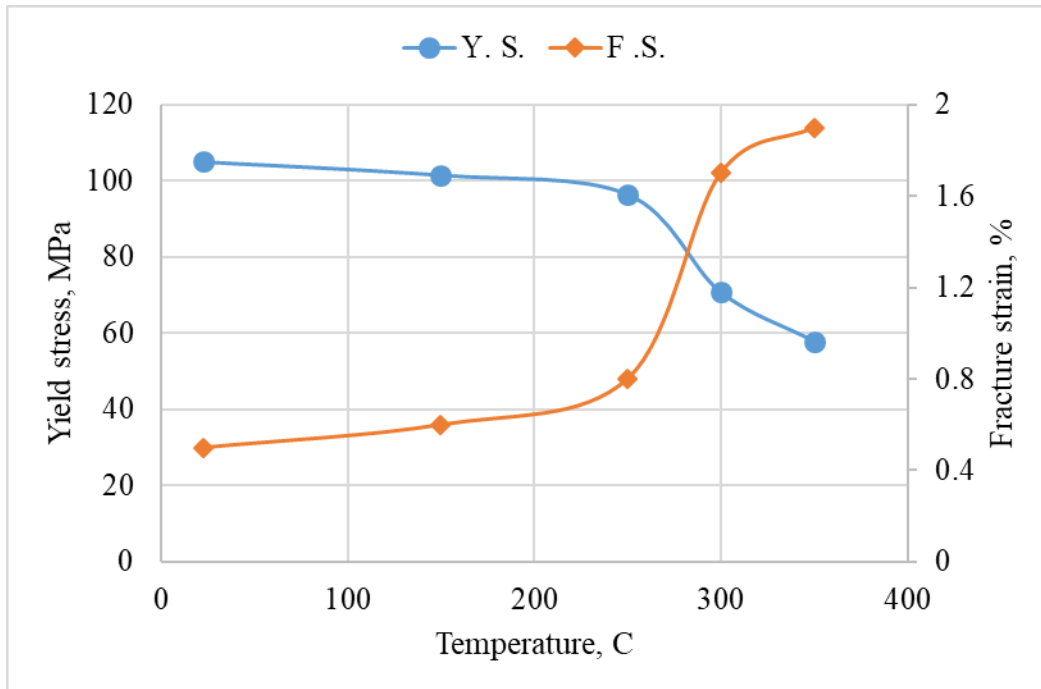
Figure 16. Yield strength and fracture strain of EN AC-Al Si12CuNiMg alloy at various temperatures

Young's modulus measures the resistance of a material to elastic deformation. Its value is obtained by measuring the slope of the axial stress-strain curve in the elastic region. The temperature of the test affects Young's modulus of materials. Figure 17 shows the effect of temperature on Young's modulus of this alloy. The average Young's modulus of the five test results was plotted against temperature. The test result reveals that Young's modulus of EN AC-Al Si12CuNiMg alloys increases in the low temperature up to about 150°C and then decreases with the increase of temperature.
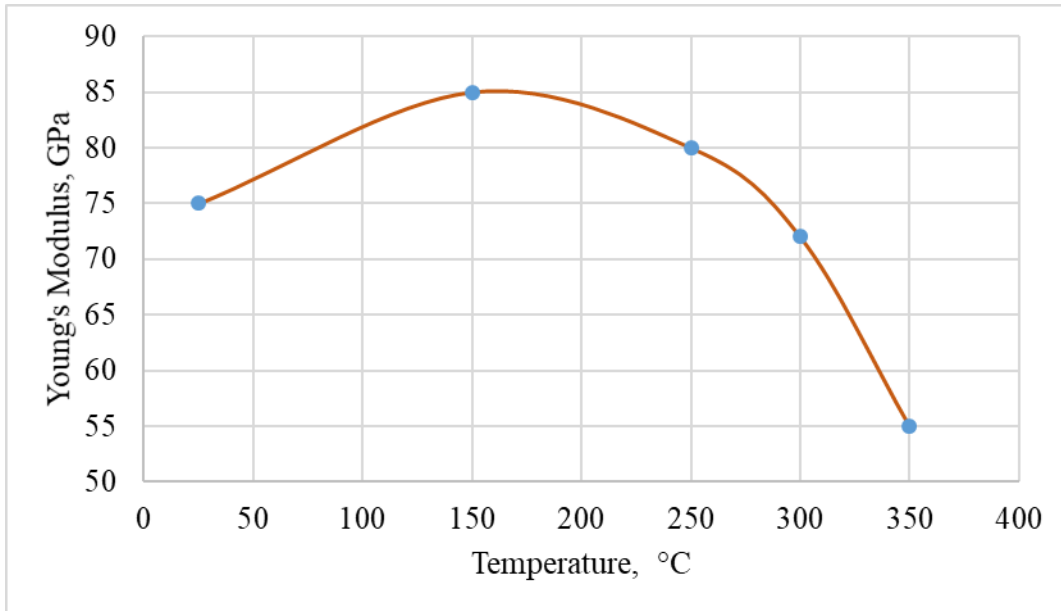
Figure 17. Young's modulus versus temperature of EN AC-Al Si12CuNiMg alloy

## 4.3 Hardness measurement

An axial load of 2450 N was applied for 15 seconds using a Brinell hardness tester to measure the macrohardness of the aluminum alloy as well as EN AC-Al Si12CuNiMg with 10 wt.% SiC composite. In accordance with the ASTM: E8/E8 M-11 standard, tensile specimens were cut from each of the cast composites and alloy EN AC-Al Si12CuNiMg. Figure 18 shows the specimens of the alloy for hardness measurement.



Figure 18. Specimens EN AC-Al Si12CuNiMg of the alloy for the hardness test
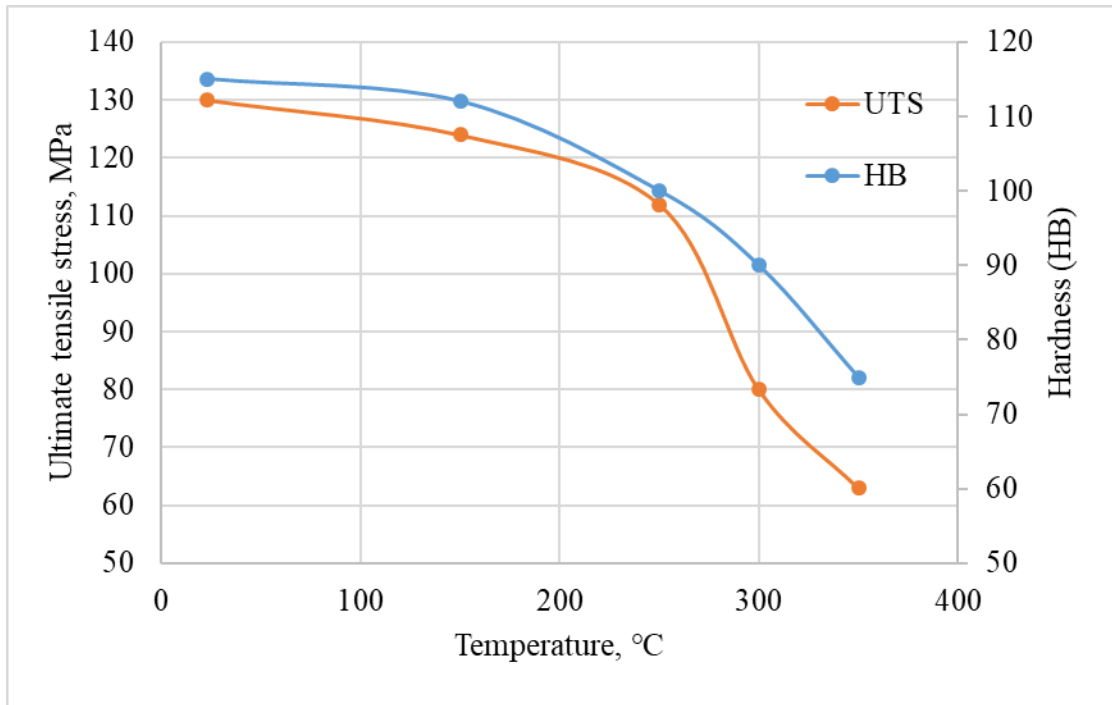
Figure 19. Brinell hardness measurement and ultimate tensile stress versus temperature

The ultimate tensile stress and Brinell hardness value of the alloy for various temperatures are shown in Figure 19. As the temperature was increased over 150°C, both tensile strength and the Brinell hardness of the alloy declined considerably.

## 4.4 Experimental procedures of stress relaxation and creep test

The stress relaxation and creep tests were performed on the same testing machine used for the tensile tests. These tests were carried out at temperatures of 150, 250, and 350°C. To study the effect of these temperatures on the stress and creep properties of the alloy, an initial stress level equivalent to 50% of the alloy's yield strength was used. The mechanical properties of the alloy at each temperature are described in Section 4.2 and have also been published in a paper [154].

Initially, the specimen was installed and aligned in the center of a furnace, then heated for about one hour until steady state temperature was reached. Throughout the entire process, heat transfer was controlled using a 3-D universal furnace controller through thermocouples. Once the target temperature was attained, 50 N of preload was applied to ensure that no slippage occurs during the testing process.

The relaxation tests were conducted in accordance with ASTM E328-21 [155]. During the relaxation test, the load was applied at a strain rate of $2 \times 10^{-4}$ s$^{-1}$ until initial stress was imposed.

Once the initial stress level was reached, the strain was kept constant while the stress was dropping until the end of the test. Throughout the process, the load was monitored as a function of time, and the test was generally continued for about 24 hours.

During the creep test, the load was applied until the initial stress was reached, at which point the stress was kept constant for about 45 hours. The extensometer was used to measure the elongation of the specimen.

## 4.5  Rheological model of stress relaxation and creep behavior

The Standard Linear Solid Model (SLSM) is a constitutive model commonly used to analyze the relaxation and creep behavior of materials [156,157]. This model assumes that the material is a linear combination of a spring element and a dashpot element, the spring element representing the elastic response of the material and the dashpot element representing the viscous response of the material. It is usually represented by two different forms: Maxwell and Kelvin forms. Figure 20 show the Maxwell and Kelvin forms of the standard linear solid model. For this study, the Kelvin form of the SLSM was used.
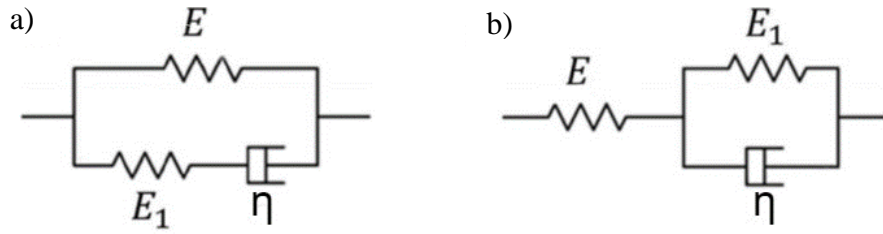


Figure 20. The three parametric standard linear solid model: a) the Maxwell and b) the Kelvin form

Based on a standard linear solid model, the stress relaxation behavior of the material can be described using either Equation (1) or Equation (2):

$$\sigma(t) = E\varepsilon_1 \left( \frac{E_1}{E_1 + E} + \frac{E}{E_1 + E} \exp\left( -\left( \frac{E_1 + E}{\eta} \right) t \right) \right) \tag{1}$$

$$\sigma(t) = E\varepsilon_1 \left( \frac{H}{E} + \left( 1 - \frac{H}{E} \right) \exp\left( \frac{-t}{n} \right) \right) \tag{2}$$

Where, $\varepsilon_1$ stands for the constant strain during relaxation, E =$E_e$ stands for the relaxation modulus at the beginning of stress relaxation, $E_1$ stands for the relaxed modulus that describes how much

the relaxation modulus drops from the beginning of stress relaxation to the end, $\eta$, stands for viscosity which describes the material's ability to flow under applied stress, and H stands for the relaxation modulus as time approaches to infinity $(t \to \infty)$ and n is a time constant. The model parameters of Equation (1) can be related to the model parameters of Equation (2), which can be described by Equations (3) and (4).

$$\frac{1}{H} = \frac{1}{E} + \frac{1}{E_1} \tag{3}$$

$$n = \frac{\eta}{(E + E_1)} \tag{4}$$

The creep strain, as per the SLSM model, can be described as a function of time by using either Equation (5) or (6).

$$\varepsilon(t) = \frac{\sigma_1}{E}\left[\frac{E}{H} + \left(1 - \frac{E}{H}\right)\exp\left(-\frac{H}{nE}t\right)\right] \tag{5}$$

$$\varepsilon(t) = \frac{\sigma_1}{E}\left(1 - \frac{E}{H}\right)\left[1 - \exp\left(-\frac{H}{nE}t\right)\right]\exp\left(-\frac{H}{nE}t\right) \tag{6}$$

where $\sigma_0$ is the constant stress during the creep test. The other quantities are the same as the relaxation parameters.

**Stress relaxation curves**

Relaxation curves indicate a good agreement between experimentally obtained results and the SLSM curve fits with coefficients of determination $(R^2)$ values more than 0.99. The value of stress is expressed as a function of time. Figure 21 shows the stress relaxation curves obtained at various temperatures and the fitted curves achieved through the SLSM of Equation (1). The initial stress level used at this temperature was about 50% of the yield stress (50, 45, and 30 MPa) at each corresponding temperature. As clearly indicated in Figure 21, the amount of relaxed stress increases with increasing temperatures. For example, at 150°C, the relaxed stresses are 23 MPa, indicating that the material release 46% of its initial stress. As the temperature increases to 250°C, the relaxed stresses increase to 33 MPa, with a stress level drop of 73%. Finally, at 350°C, the relaxed stresses reach 27 MPa, with a stress level drop of about 90%. The most significant drop in the stress level occurs within approximately 2 hours of loading. Depending on the level of stress relief, the entire relaxation process can be categorized into three distinct stages. In the initial phase,

stress exhibits rapid relaxation; however, in the subsequent phase, stress demonstrates a slower relaxation rate. After a long period of relaxation, the stress eventually approaches a steady state where the relaxation rate becomes almost constant in the third phase. In the first stage of relaxation, the relaxation behavior is nonlinear and decreases with the duration of the test as it progresses. In the second stage of stress relaxation, the material develops compressive stress, and the stress relaxation rate decreases significantly. Finally, in the third stage, the rate of stress relaxation becomes almost constant.
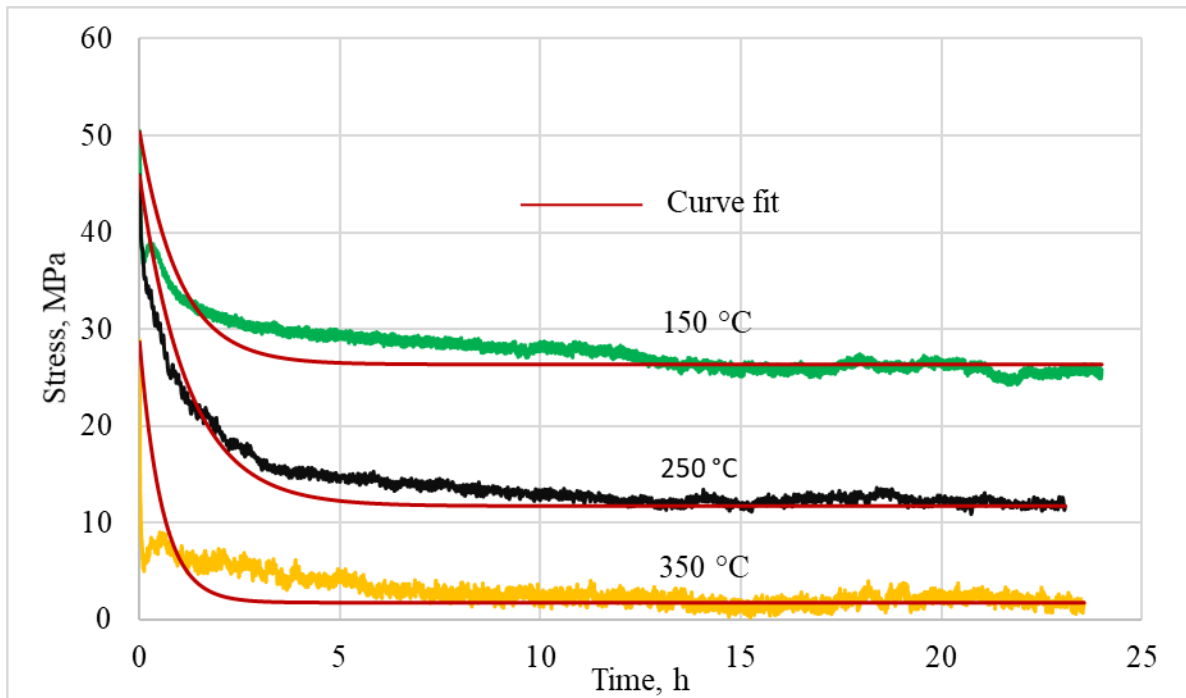


Figure 21. Experimental stress relaxation curves and fitted curves at various temperatures

**Creep curves**

Figure 22 shows the obtained creep-strain curves of the investigated alloy. These curves were obtained at various temperatures of 150, 250, and 350°C with the corresponding 50% of the yield stress of the material, 50, 45, and 30 MPa. As clearly shown in Figure 22, the creep strain increases as the temperature increases. For example, at a time of 10 hours and a temperature of 150°C, 250°C, and 350°C, the creep strain values are 0.09%, 0.19%, and 0.48%, respectively. This indicates the significant effect of temperature on the creep behavior of the investigated alloy. It also shows that at higher temperatures, the material is more vulnerable to creep deformation. There are similarities between the plotted creep curves and typical creep curves defined by two stages: the primary stage where the creep rate decreases and the secondary phase where the creep rate

47

becomes constant [158,159]. As stated in reference [160,161], the creep rate in the primary creep stage is initially high due to the initial formation and movement of dislocations and is followed by a rapid decrease as the dislocations continue to accumulate and their mobility decreases. As shown in Figure 23, the creep strain curve corresponding to a temperature of 350°C shows higher creep rates than the creep rate associated with temperatures of 250°C and 150°C. This suggests that a higher creep temperature results in higher creep strain.
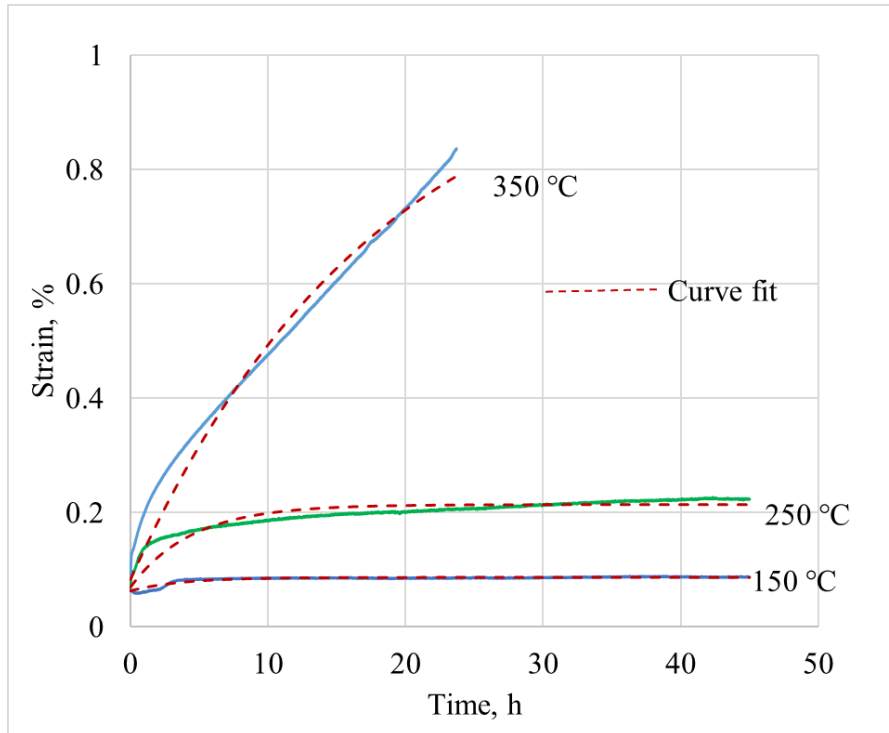


Figure 22. Creep curves at various temperatures
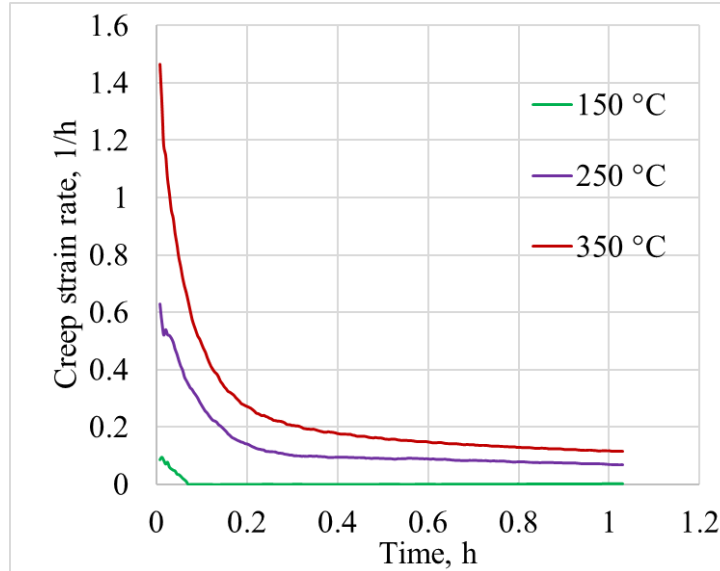
Figure 23. Creep rate curves of the primary stage at various temperatures

**The standard linear model of solids (SLSM) parameters determination**

The test result indicates that all parameters of the SLSM relaxation model vary significantly with temperature. For example, the relaxation modulus at the beginning of relaxation (E) decreases as the temperature increases. When the temperature increased from 150°C to 250°C, it decreased by about 7%. However, a significant reduction was observed when the temperature increased from 150 to 350°C, with its value reduced by approximately 32%. For the relaxation modulus $E_1$, there is no significant change in temperature from 150°C to 250°C. However, when the temperature increases from 150 to 350°C, it decreases by 45%. Additionally, the viscosity decreases significantly as the temperature increases. The values of viscosity decreased by 30 to 70% as the temperature increased from 150 to 250°C and 350°C. This shows that temperature significantly affects the relaxation model parameters of the investigated alloy. The chart in Figure 24, which displays the relaxation model parameter values as a function of temperature, clearly illustrates the trend of decreasing values as the temperature increases.
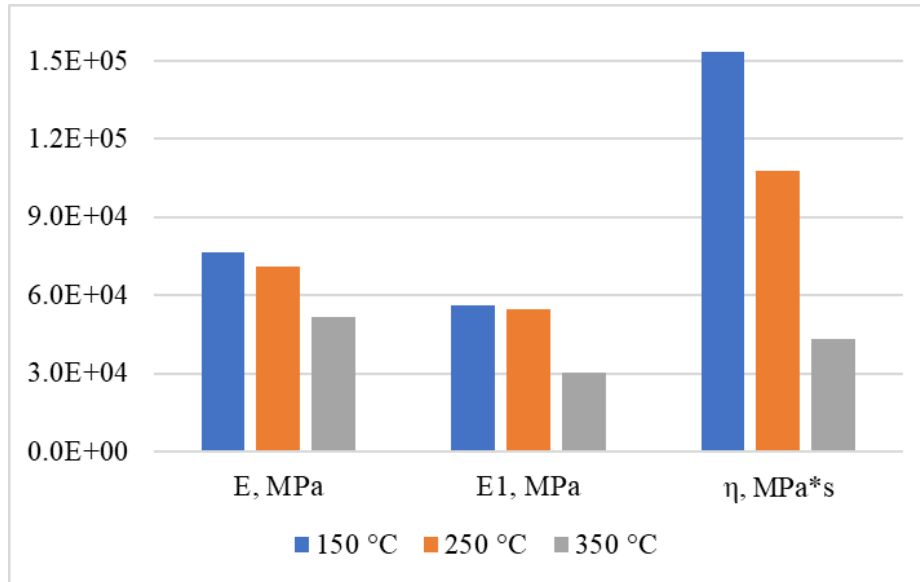
Figure 24. Relaxation model parameters of the investigated alloy at various temperatures

The creep model parameters of the studied alloy are influenced by temperature. Figure 25 illustrates how these parameters change with temperatures. The three standard model parameters ($E$, $E_1$, and $\eta$) all decrease with increasing temperature, with $E_1$ experiencing a more significant reduction compared to the other parameters. Specifically, as the temperature increased from 150°C to 250°C, the value of $E_1$ decreased by approximately 85%. This reduction becomes even more noticeable as the temperature increases from 150°C to 350°C, with $E_1$ decreasing by approximately 95%. Since $E_1$ measures the material's resistance to creep deformation, these substantial decreases in this parameter indicate that the alloy's ability to resist creep deformation decreases at elevated temperatures. This means that at elevated temperatures the alloy may experience more plastic deformation and structural changes. As the temperature increases, the thermal energy within the material increases and promotes the mobility of dislocations and the diffusion of atoms [161]. The enhanced mobility of dislocation and diffusion of atoms are likely attributed to these changes in creep behavior.

In both stress relaxation and creep, both model parameters ($E$ and $\eta$) decrease as temperature increases by almost the same values. However, $E_1$ drops significantly as the temperature increases from 150 to 350°C during creep rather than during stress relaxation. This indicates that the increase in temperature has a greater impact on $E_1$ during creep compared to stress relaxation.
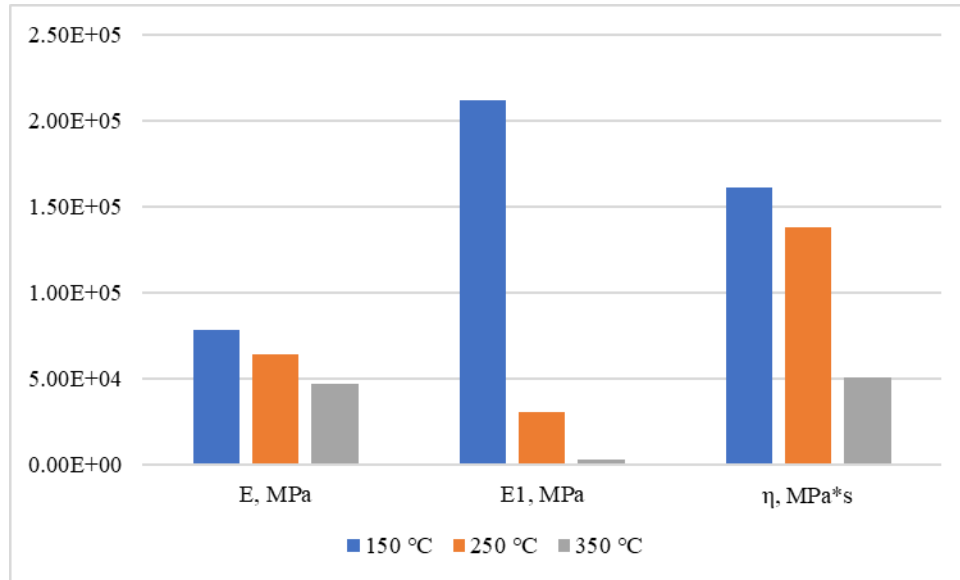
Figure 25. Creep model parameters of investigated alloy at various temperatures

## 4.6 Metallographic specimen preparation

Metallographic samples were prepared using standard metallographic preparation processes such as grinding and polishing. Waterproof SiC emery papers with grit sizes up to 2000 were used to polish the surface of the specimens. Then, polishing was continued using a 3 and 1 µm diamond suspension on a disc polisher until a mirror-like surface was obtained. This was done to allow for better microstructural observation. The polished surface of the specimens allowed for clear and detailed observation of the microstructures present in the samples. Figure 26 shows the prepared metallographic specimens. After preparing the metallographic samples, the microstructures were examined using a light microscope (LM).



Figure 26. Metallographic specimens

## 4.7 Microstructural surface analysis

The microstructures of the investigated alloy were observed, and their micrographs are presented in Figures 27. The micrographs observation shows the presence of α-Al matrix, eutectic Si particles, and other intermetallic particles in the microstructure of the alloy. Gray silicon plates and other intermetallic particles are embedded in a large white α-Al matrix. In all specimens, microstructural observation reveals dendrites of α-Al as the main constituent and with an elongated needle-like structure (flakes) of silicon. The aluminium dendrite arms are visible in the framework, indicating that the cast samples have not solidified under equilibrium conditions. In Figure 27, the aluminum dendrite arms are clearly visible. Non-equilibrium solidification of the cast produces non-homogeneity in the microstructural of the the alloy. This non-homogeneity includes micro and macro-segregation of eutectic Si solute in the α-Al phase. The dark semi-circular shape shown in the microstructure is a shrinkage pore. The formation of shrinkage porosity is related to the parameters used in the crystallization and casting processes. In general, the shrinkage porosity and segregation of the solute components resulting from non-equilibrium solidification are detrimental to the mechanical properties of the alloy. For example, the segregation of Si solute atoms in the composition of that alloys affects the mechanical properties of these alloys by reducing the ductility [151].
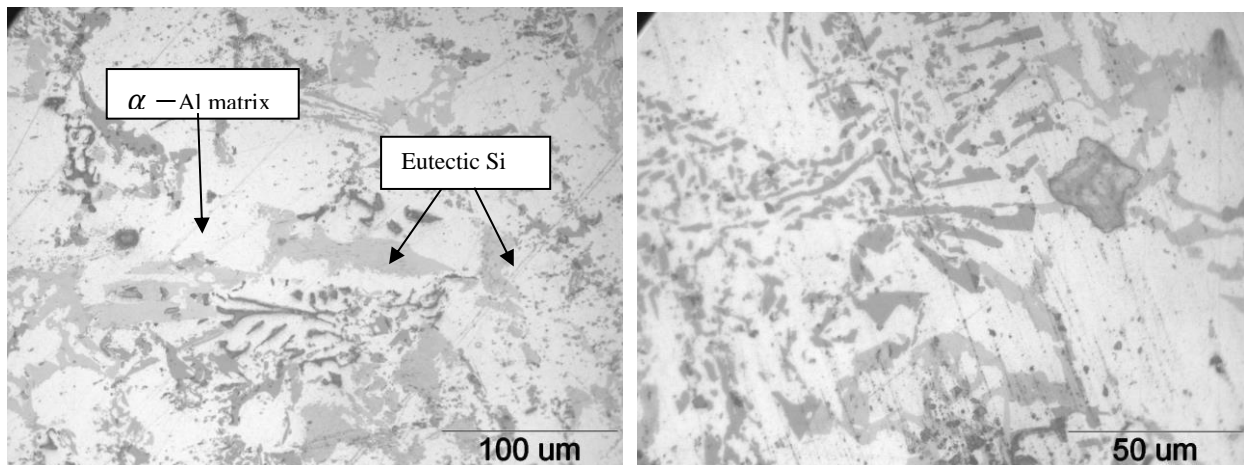


Figure 27. Microstructure of as-cast EN AC-Al Si12CuNiMg alloy

## 4.8 Fracture surface analysis

Fractographic analysis of all the samples reveals that they have a similar appearance. A transcrystalline fracture was observed in all samples. In addition, the dimpled fracture surface of the specimens, despite the absence of typical ductile cup cone fracture, suggests ductile fracture of

cast aluminum alloys when subjected to high-temperature tensile loads. Figures 28 show the fracture morphology of EN AC-Al Si12CuNiMg alloys samples after room temperature tensile test. On the fracture surface of this sample, intergranular-like fractures, as well as tiny cleavage-like brittle cracks, can be seen. Additionally, a few fracture planes and a few dimples can be seen on the morphology of these fracture surfaces. However, the dimples' size is tiny, exhibiting a semi-brittle behavior.

Figure 29 shows the fracture surfaces of the EN AC-Al Si12CuNiMg alloys after a tensile test at 350 ℃ temperature. Like the sample tested at room temperature, the cleavage-like brittleness is observed but very low. In addition, the observation demonstrates the presence of a large and more extensive dimple size, suggesting ductile fracture [162]. The larger the dimple size and depth, the greater the fracture strain. In general, particle dislocation due to high temperature, high stresses at specific locations, or plastic deformation around inhomogeneous inclusions or other defects are factors that contribute to the formation of micro-cracks.
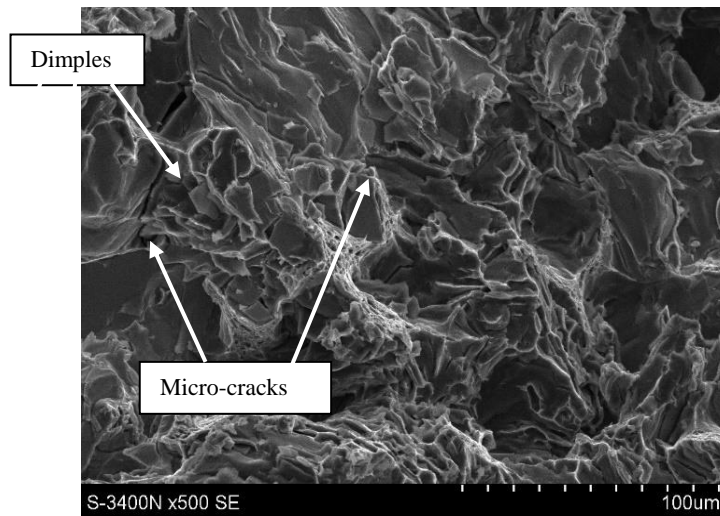


Figure 28. Fractography of the specimen broken at room temperature tensile load
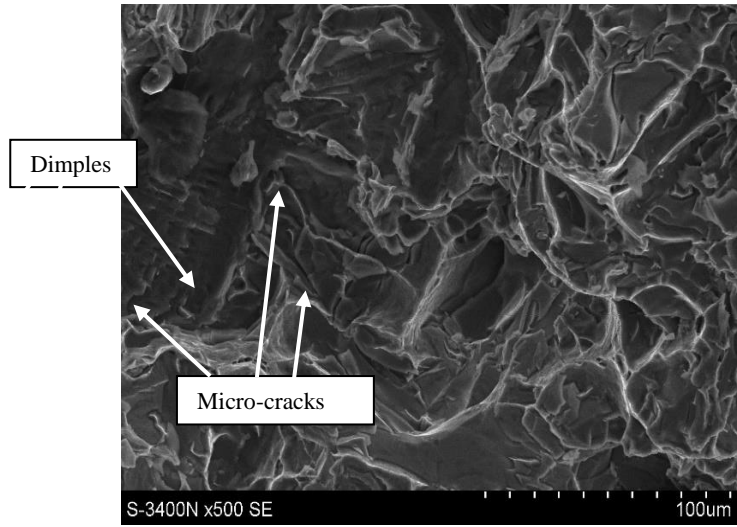
Figure 29. Fractography of the specimen broken at 350°C temperature tensile load

# 5. EXPERIMENTAL STUDIES OF MECHANICAL PROPERTIES OF ALUMINUM SILICON COMPOSITE REINFORCED WITH SILICON CARBIDE PARTICLES

Aluminum alloys enhanced with SiC particles (SiCp) can withstand high temperature operating conditions and exhibit high strength, stiffness, wear and abrasive resistance capability, creep resistance behavior, and lower thermal expansion compared to other conventional aluminum alloys [163,164]. Because aluminum alloy matrix composites reinforced with SiC or $Al_2O_3$ particles are lightweight and resistant to wear and thermal deformation, they are widely used in the automotive and aerospace industries. For example, engine components, including pistons, cylinder heads, connecting rods, and other applications where operating temperature is critical, are made from this composite material. In the aerospace industry, advanced aluminium metal matrix composites, and boron fibres are used to reinforce the space shuttle orbiter and continuous graphite fibres for the Hubble telescope [137,165].

At elevated temperatures, the mechanical properties of the Al-Si alloy deteriorate and reduce the performance of the structure [166,167]. Therefore, it is essential to enhance the mechanical properties of Al-Si alloy and increase its resistance to temperature and load variation for this type of application. Reinforcing the alloy with a suitable reinforcement material is one way to enhance the material's mechanical properties. It provides additional strength and stability to the alloy, making it more resistant to temperature and stress variations.

Silicon carbide (SiC) and aluminum oxide ($Al_2O_3$) are inexpensive reinforcement materials commonly used to reinforce aluminum alloys. Other ceramic particles such as silicon oxide ($SiO_2$), titanium carbide (TiC), titanium diboride ($TiB_2$), aluminum nitride (AlN), zirconium diboride ($ZrB_2$), and silicon nitride ($Si_3N_4$) are also used to reinforce the aluminum alloy [168–170]. These ceramic phases are very durable and hard. Due to their low density and strong specific mechanical properties, aluminum matrix composites (AMCs) reinforced with SiC particles are among the most favorable materials for lightweight applications. Compared to unreinforced aluminum alloys, SiC-reinforced aluminum matrix composites exhibit higher strength, stiffness, creep resistance, and wear resistance [171–175]. Due to their favourable properties, SiC-reinforced aluminium matrix

composites are gradually replacing traditional aluminium alloys in many applications involving operation under complex and harsh conditions [170,176].

Numerous studies have incorporated silicon carbide (SiC) particles as a reinforcing material within an aluminum matrix composite. Tamer Ozbenet et al. [177] investigated the mechanical and machining properties of an aluminum matrix composite (Al-MMC) fabricated with silicon carbide (SiC) particles. The AMC material showed an improvement in tensile strength, hardness, and density with an increasing reinforcement ratio. However, a corresponding drop in impact toughness was observed in their study. In their study, Ozden et al. [178] examined the impact behavior of particle-reinforced aluminum matrix composites (AMC) made of aluminum (Al) and silicon carbide (SiC) at different temperatures. The particle clustering, particle cracking, and poor bonding between matrix and reinforcement significantly influence the impact behavior of the composites. These results imply that temperature variations do not significantly affect the impact behavior of aluminum matrix composites.

Shuvho et al. [179] studied the mechanical behavior of an aluminum matrix composite reinforced with SiC, Al2O3, and TiO2. Their study revealed that the reinforced aluminum matrix composite exhibits higher hardness, tensile strength, and yield strength than the base alloy. Zhang Peng et al. [180] investigated the impact of particle clustering on the mechanical response of aluminum matrix composites. The authors suggest that elastic deformation is less sensitive to clustering than plastic deformation and that early clustering promotes interface disconnection and void formation.

Pawar et al. [181] studied the mechanical properties of aluminum matrix composites reinforced with silicon carbide (AMC) particles to fabricate power transmission elements, such as gears, which are subjected to a continuous load. The authors used two manufacturing methods, i.e., casting and powder metallurgy. They presented that powder metallurgy is better for achieving uniform distribution of reinforcement particles but is not as economical as the casting method.

Studying the mechanical properties of AMMC at elevated temperatures is essential to understanding its behavior under various operational conditions during its use [182]. However, few studies have been reported on the tensile properties of AlSi12/10SiCp composites at elevated temperatures. In this work, the tensile properties of EN AC-Al Si12CuNiMg alloy and AlSi12CuNiMg/10SiCp composite were investigated at room temperature and elevated

56

temperatures ranging from 150 °C to 350 °C. The effect of temperature on tensile properties was described.

## 5.1 Specimen preparation and uniaxial tensile test

**Tensile specimen preparation**

In this study, eutectic EN AC-AlSi12CuNiMg aluminum alloy was used as the matrix material and 10 wt.% SiC particles was used as the reinforcement. Stir casting was used to manufacture AlSi/ SiCp composites because of its low cost and ease of manufacture. The EN AC-Al Si12CuNiMg ingot was initially melted in the resistance furnace. When the desired temperature was reached, a constant volumetric flow of argon was used to prevent the aluminum alloy from chemically interacting with the oxygen and nitrogen in the air. A trowel was used to gently remove the slag. The SiC reinforcement particles were then weighed according to the specifications of the experiment and preheated in a preheating chamber. Preheating was carried out to ensure proper mixing of the reinforcement, to remove moisture and air trapped between the reinforcement particles, to reduce the temperature gradient between the reinforcement particles and the molten alloy, and to remove impurities from the reinforcement particles.

Once the aluminum alloy was completely melted, the stirring device was adjusted to stir the melt. Using the speed control, the stirrer speed was set and the melt was stirred to create a vortex to allow the reinforcements to mix evenly into the melt. At this point, the preheated reinforcements were carefully added, and the mixture was stirred for an additional time before being poured into the mold. The entire melting process was carried out under the supply of argon. In addition, the mold was preheated to ensure uniform solidification. The melt was then poured into the preheated mold. The melt was cooled in the mold and finally, the specimens were removed from the mold.

**A uniaxial tensile test**

A uniaxial tensile test was performed to determine the basic mechanical properties of the fabricated composite specimens. These specimens had the same dimensions as the alloy specimens described in Section 4.1. The tensile testing procedure described in Section 4.2 was followed for the composite specimens. The tests were repeated five times at each temperature, and the average of the five results was considered the final tensile test result. The prepared tensile specimens are shown in Figure 30.

Figure 30. Tensile specimens of composite material

## 5.2 Microstructural characterization

**Microstructural characterization of EN AC-AlSi12CuNiMg alloy**

Both the matrix alloy and the composite were subjected to microstructure studies. Metallographic samples were taken from the cast aluminum alloy and the composite. A standard metallographic procedure was used to polish the samples. Waterproof SiC emery papers with grit sizes up to 2000 were used to polish the surface of the samples. Then, polishing was continued using a 3 µm and 1 µm diamond suspension on a disc polisher until a mirror-like surface was obtained. This was done to allow for better microstructural observation. A light microscope (LM) and a scanning electron microscope (SEM) working with an X-ray spectrometer were used to perform microstructural analysis.

The LM and SEM micrographs of the investigated cast EN AC-AlSi12CuNiMg alloy are shown in Figures 31 and 32 respectively. As can be seen, the microstructure of the base EN AC-Al Si12CuNiMg eutectic alloy consists mainly of the primary phase (α-Al), needle-like α(Al)+β(Si) eutectic mixture (its amount depends on the Si content in the Al alloy), and plate-like Si primary crystals in the shape of polyhedrons. The presence of the Cu, Mg, Ni, Mn, and Fe elements results in the formation of various intermetallic compounds correlated with the chemical composition of the eutectic Al-Si alloy. The $Al_2Cu$ and $Mg_2Si$ phases and more complex compounds in different systems like Al-Ni-Cu, Al-Fe-Si Al-Fe-Mn-Si, were identified in the microstructure. The morphology of Si phases can change after modification and heat treatment. In addition, the cooling rate influences the microstructural composition's size, morphology, and distribution, including intermetallic phases.
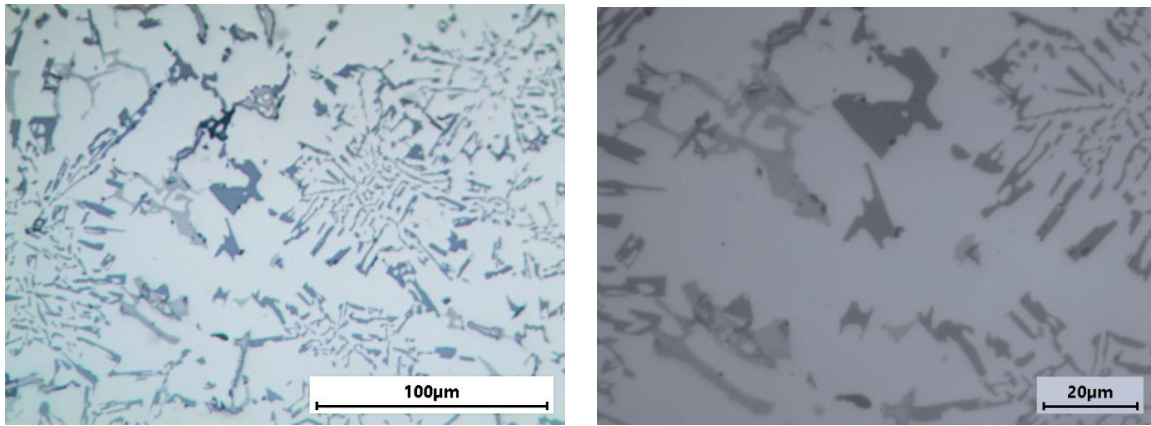
Figure 31. LM images of the EN AC-Al Si12CuNiMg alloy at different magnification
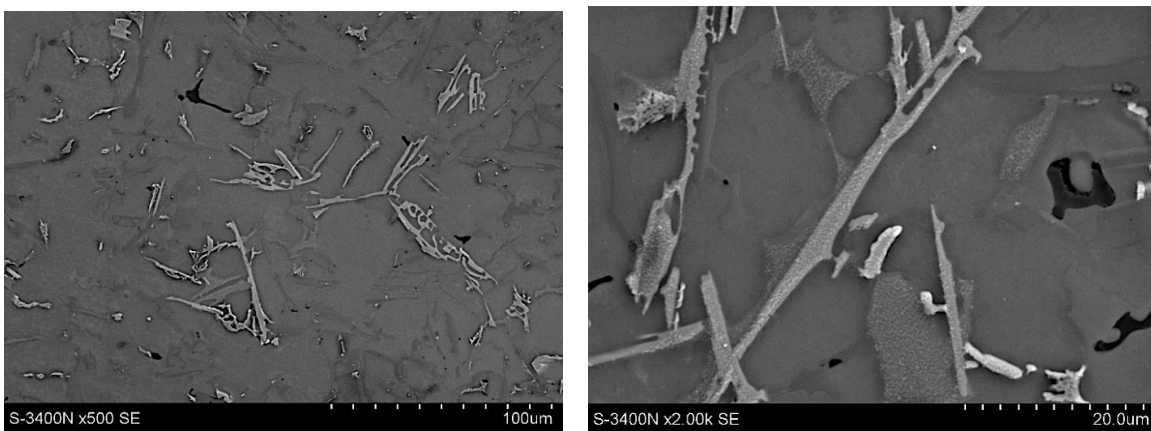


Figure 32. SEM micrographs of the EN AC-Al Si12CuNiMg alloy at different magnification

**Microstructure of the AlSi composite reinforced with 10 wt.% SiC**

The micrographs of the AlSi composites reinforced with SiC particles are shown in Figures 33 and 34. The microstructure of the AlSi composite consisted of several phases, including matrix-Al, Si and intermetallic phases. The intermetallic phases were formed by the combination of Mg, Ni, Fe, Cu, and Al, which significantly improved the base alloy's high-temperature properties [183,184]. The SiC particles appear as dark spots and are uniformly dispersed throughout the aluminum matrix. Some porosity could be observed around the structures of reinforcement particles. The eutectic Si phase was heterogeneously nucleated in the form of needles on the surface of the reinforcement, as shown in Figures 33 and 34 and mentioned in [176]. Due to the formation of intermetallic compounds at the interface, the SiC particles are also observed to have a strong bond with the aluminum matrix, as stated in the literature [185]. The added SiC particles significantly

affect the grain refinement of the base alloy. This is because the grain size of the (Al) + (Si) eutectics is noticeably finer than that of the base alloy
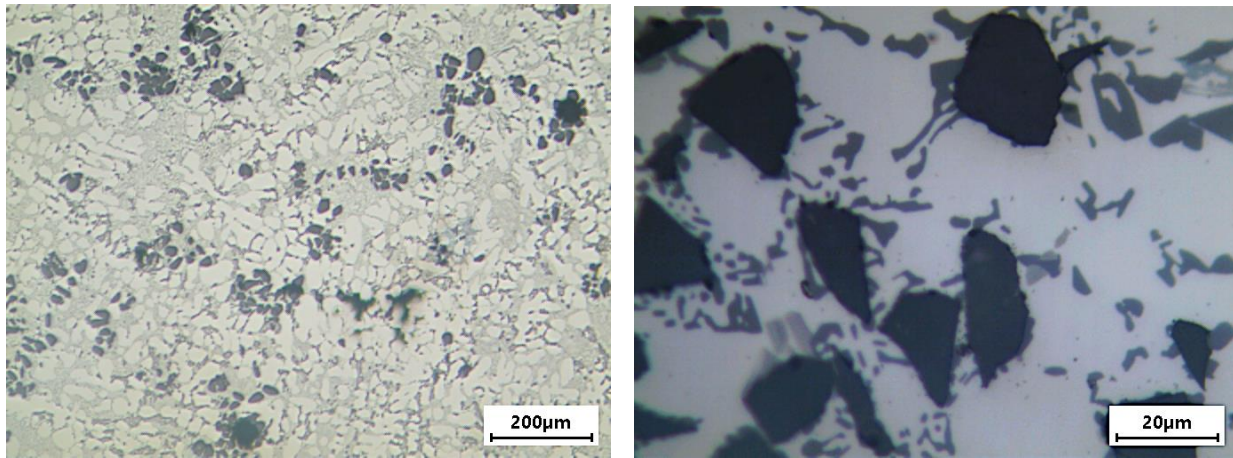


Figure 33. LM images of the AlSi composite at different magnification
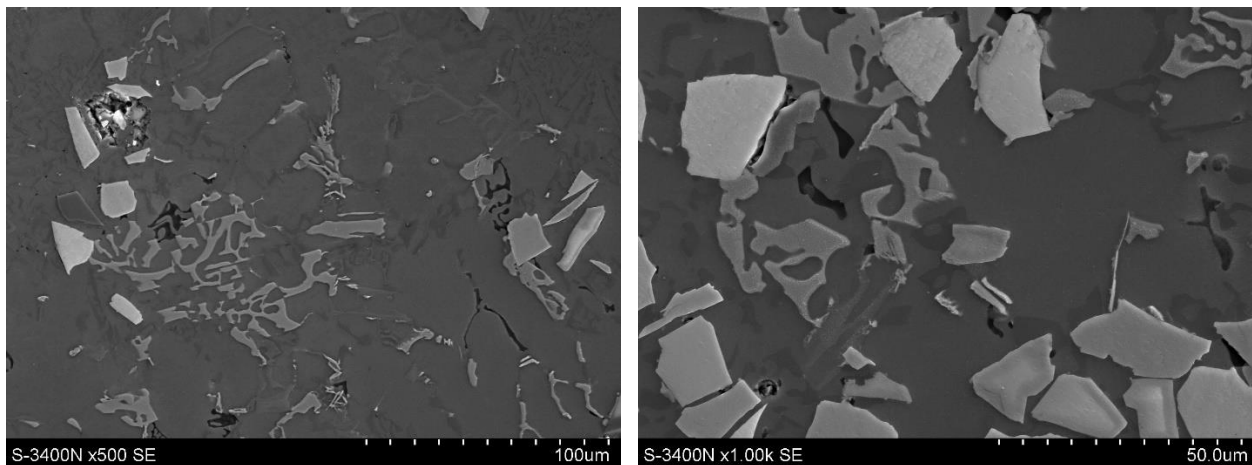


Figure 34. SEM micrographs of the AlSi composite at different magnification

## 5.3 Tensile and hardness test results of matrix alloy and composite

**Tensile properties**

The addition of 10 wt.% of SiC particles have a substantial impact on the tensile properties of the produced composites. Therefore, it is important to test materials at room and elevated temperatures. Table 3 shows the test results of the EN AC-Al Si12CuNiMg alloy and SiC-reinforced composite at room temperature. The room temperature tensile test results show that SiC-reinforced composite has a higher base tensile strength than non-reinforced alloys. The yield

strength, ultimate tensile strength, and modulus of elasticity of SiC-reinforced composites are 17%, 20%, and 6% higher than those of the unreinforced alloy.

Table 3. The determined tensile properties of EN AC-Al Si12CuNiMg alloy and AlSi composite at room temperature

| Materials | Yield Strength (MPa) | Tensile Strength (MPa) | Young's Modulus (GPa) | Elongation (%) |
|---|---|---|---|---|
| EN AC-Al Si12CuNiMg | $120 \pm 6$ | $140 \pm 12$ | $73 \pm 5$ | $0.57 \pm 0.1$ |
| AMMC | $145 \pm 8$ | $175 \pm 8$ | $78 \pm 4$ | $0.5 \pm 0.12$ |
| Relative change (%) | $> +17$ | $> +20$ | $> +6$ | $< -20$ |

The excellent interfacial bonding between the matrix and the reinforcement could be a reason to improve the tensile properties of the composites. On the other hand, the EN AC-Al Si12CuNiMg alloy showed a 20% higher percentage elongation. This implies that the SiC-reinforced composite has a low ductility compared to the matrix alloy.

Figure 35 shows the ultimate tensile strength of both the EN AC-Al Si12CuNiMg alloy and its composite at various temperatures. The values presented are the average of three test results with their error bars. The graph clearly shows the decrease in ultimate tensile strength with increasing temperature. For example, the ultimate tensile strength of EN AC-Al Si12CuNiMg alloy at room temperature is 140 MPa, but at 150°C and 200°C, it decreases to 125 MPa and 120 MPa, respectively. From room temperature to 150°C and 200°C, it decreases by about 5% and 15%, respectively. In addition, the ultimate tensile strength of the matrix alloy decreases by 20-50% for the temperature between 250 and 350°C. In the case of the composite material, the ultimate tensile strength decreased by about 3-6% for the temperature range of 150-200°C compared to the result at room temperature. However, for the temperature range between 150 and 350°C, the ultimate tensile strength of the composite was reduced by about 17% to 50%. This shows that the decrease in ultimate tensile strength at low and moderate temperatures is negligible; however, when the temperature exceeds 250°C, both materials' tensile strength deteriorates significantly.

Figure 36 shows a plot of the yield strength and fracture strain of the SiC-reinforced composite and the unreinforced alloy versus temperature. The average values of the three test results are shown in this graph. The yield stress was reduced by 8% from room temperature to 200°C in the case of the EN AC-Al Si12CuNiMg alloy. At 350°C, however, it dropped by about 50%. In the case of EN AC-Al Si12CuNiMg/10%SiC composite, it was dropped by 4% from its room temperature to 200°C. But it dropped by about 40% at 350°C. This implies a rapid decrease in the yield strength of both the matrix alloy and composite at temperatures above 200°C.

On the other hand, the fracture strain of the EN AC-Al Si12CuNiMg alloy increases rapidly for temperatures above 200°C, while the fracture strain of the composite increases slowly. This relates to the ductility properties of the EN AC-Al Si12CuNiMg alloy and the composite. The unreinforced alloy has a higher fracture strain at both low and elevated temperatures. The ductility of both the unreinforced alloy and the composite increases with temperature.
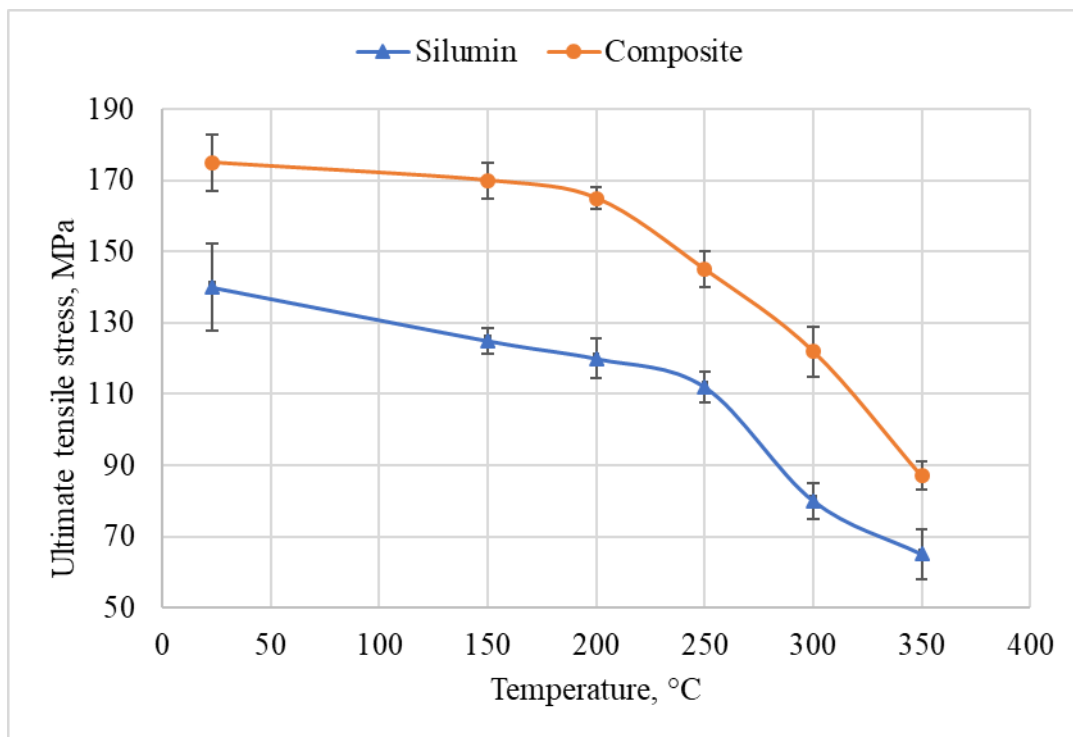


Figure 35. Ultimate tensile stress of EN AC-Al Si12CuNiMg alloy and composite at various temperatures
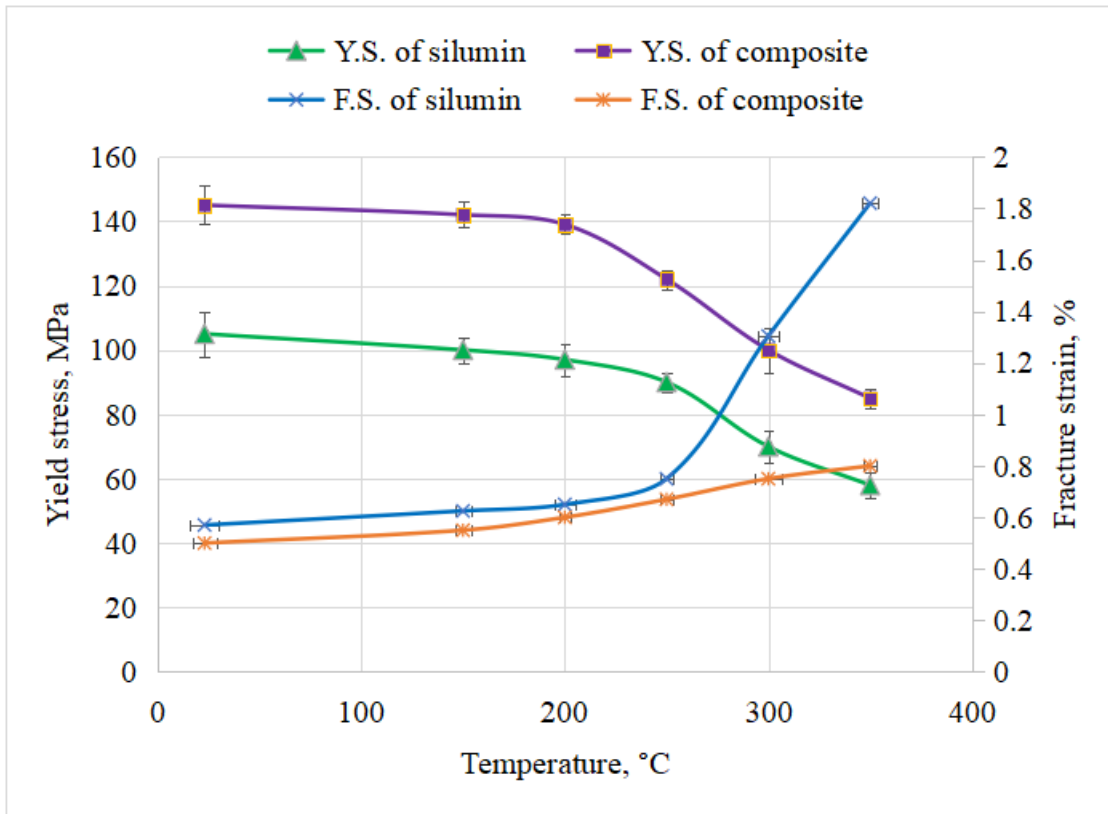
Figure 36. Yield strength and fracture strain of EN AC-Al Si12CuNiMg alloy at various temperatures
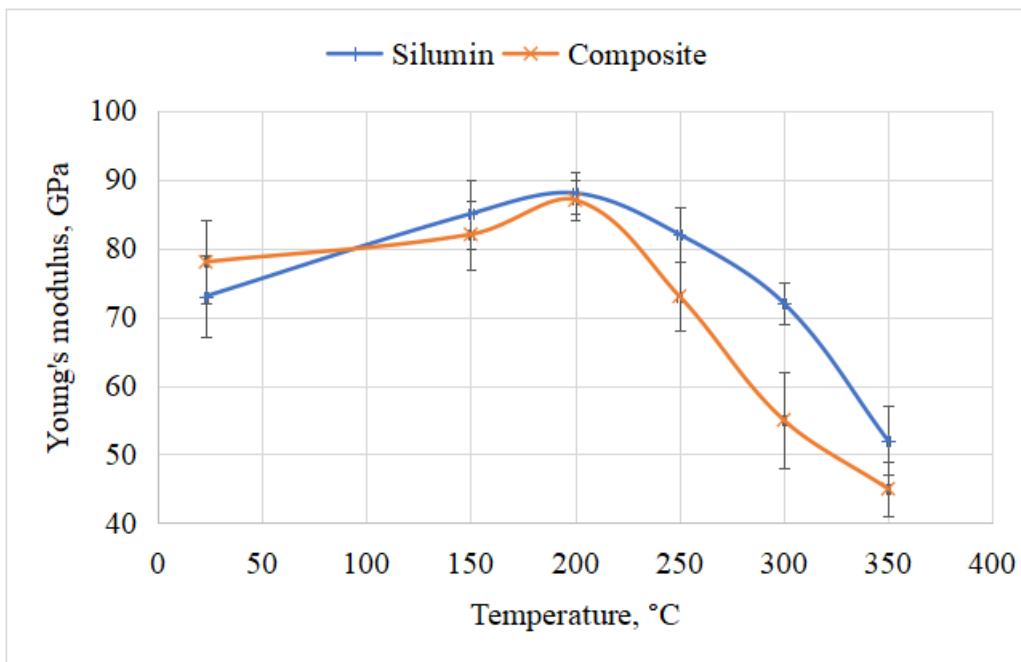


Figure 37. Young's modulus of EN AC-Al Si12CuNiMg alloy and composite at various temperatures

63

Young's modulus is used to measure the resistance of materials to axial deformation. The operating temperature of materials can have an impact on Young's modulus. Figure 37 shows how temperature affects the Young's modulus of the matrix alloy and the SiC-reinforced composite. The average Young's modulus of the three test results was plotted against temperature. The study shows that Young's modulus of the EN AC-Al Si12CuNiMg alloys increases from room temperature up to about 200 ℃ and then starts to decrease as the temperature increases. The same pattern was observed for the SiC-reinforced composite. The SiC-reinforced composite exhibited a more significant decrease in Young's modulus over a higher temperature range than the EN AC-Al Si12CuNiMg alloy.

**Hardness measurement**

Following the standard test method ISO 6506-1, an axial load of 2450 N was applied for 15 seconds using a Brinell hardness tester to measure the hardness of both the aluminum alloy and the prepared composite specimens. Figure 38 illustrates the prepared composite specimens for hardness measurement. An average hardness value of the five test results for the EN AC-Al Si12CuNiMg alloy was about 120 HB ± 5, while for the composite it was around 140 HB ± 8, each with their respective deviations. This implies a remarkable improvement in the hardness of the composite when compared with EN AC-Al Si12CuNiMg alloy. An improvement of 15% is observed in the hardness of the composite when compared with the unreinforced alloy. The strong bond between the matrix material (AlSi12CuNiMg) and the silicon carbide (SiC) particles could be the reason for the increased surface hardness value of the composite specimens. SiC, a hard reinforcement, renders the inherent property of hardness to the matrix material, thereby enhancing its resistance to deformation. It is an experimentally proven fact that the hardness of the matrix material can be improved significantly by adding hard reinforcement into a soft ductile matrix material like aluminum alloy [186]. The hardness behavior of composite is also affected by grain refinement of matrix alloy and fine and even distribution of reinforced particles. Reduction in grain size always enhances the hardness of the composites. The smaller the grain size, the higher the obstructions for dislocation motion, thereby improving the resistance to plastic deformation, resulting in increased hardness [187]. This characteristic of SiC could be the cause of the increased hardness of the composite specimens.

Figure 38. Hardness test specimens of the composite material

## 5.4 Tensile fractography

Fractographic analysis of the matrix alloy and composite material was carried out for tensile fracture tested at various elevated temperatures. Figure 39 shows the EN AC-Al Si12CuNiMg alloy fractographies at various temperatures. The result showed that the test temperature directly influenced the fracture behavior of the matrix alloy and composite material. The room temperature tensile fracture of the matrix alloy shows small dimples and a few cleavage planes, indicating the semi-brittle behavior of the matrix alloy. However, as the temperature increases from room temperature to 150, 250, and 350°C, the size of the dimples increases, and the fracture surface of the matrix alloys changes from semi-brittle to ductile. The presence of larger dimples on the fracture surface indicates larger plastic deformation during fracture.

On the other hand, the fracture properties of the composite material depend on the properties of the reinforcement, matrix, and interface, as well as on the test temperature. Figure 40 shows the fractography of the composite at various temperatures. Fractographic observation shows that the composite material exhibits a brittle fracture mode at room temperature, with a fracture surface characterized by cleavage planes. This is due to the presence of the SiC particle reinforcement, which is very hard and brittle. Since the alloy is semi-ductile at room temperature, the crack can initiate at the interface between the matrix and the reinforcement and propagate through the reinforcement. As the temperature rises from room temperature to 150, 250, and 350°C, the fracture mode becomes semi-ductile. This is because the matrix alloy becomes more ductile at higher temperatures, allowing cracks to propagate more slowly. The degree of plastic deformation of the composite material also increases with temperature.
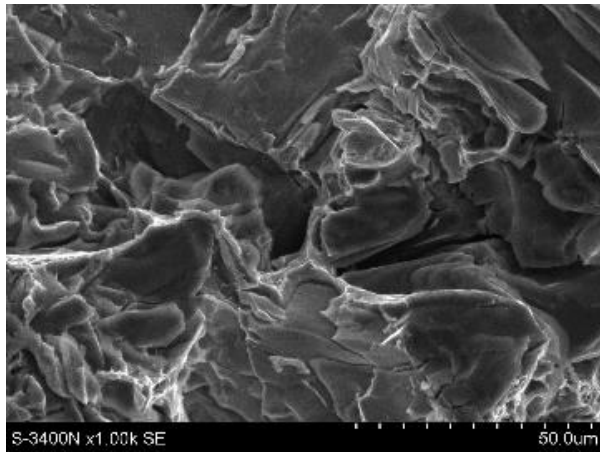
(a)
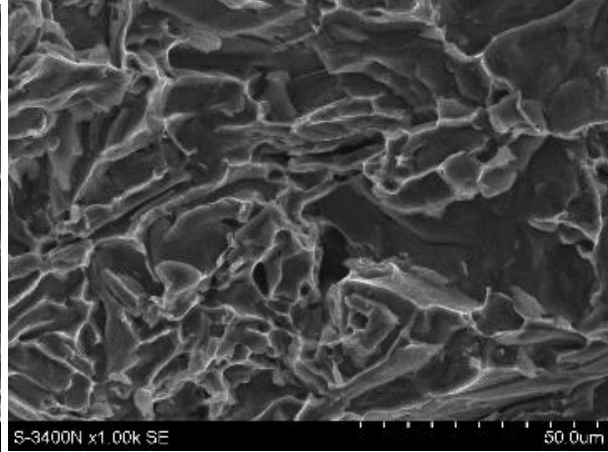


(b)
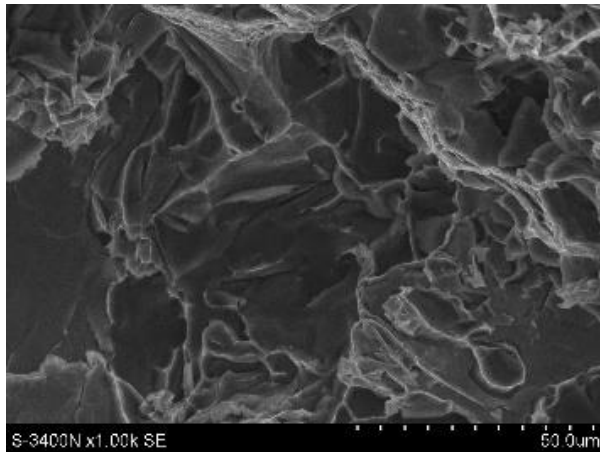


(c)
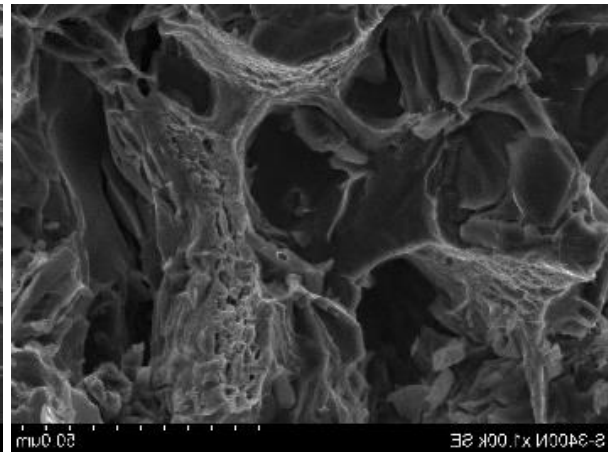


(d)

Figure 39. Fractography of matrix alloy specimens broken at various temperatures: (a) room temperature, (b) 150°C, (c) 250°C, and (d) 350°C
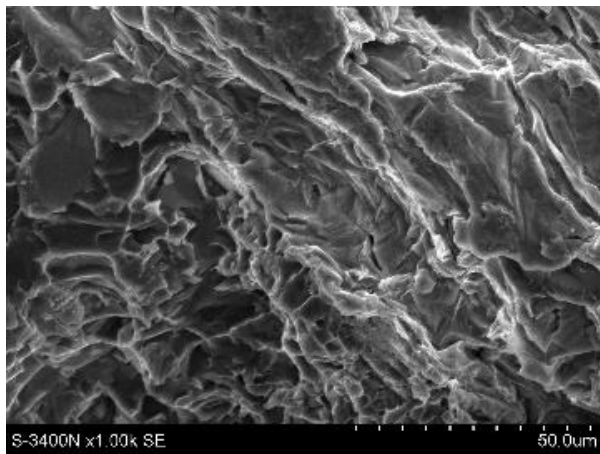


a
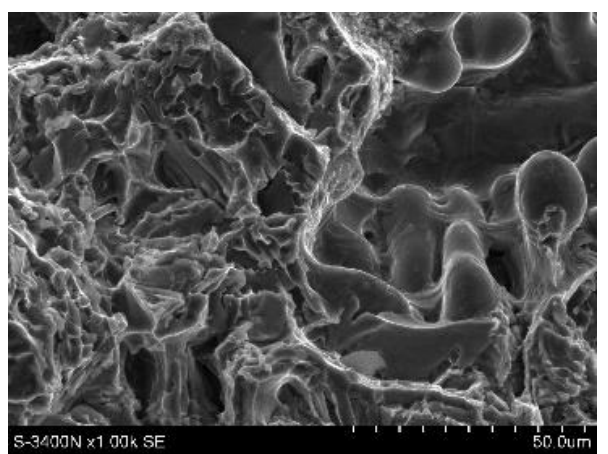


b
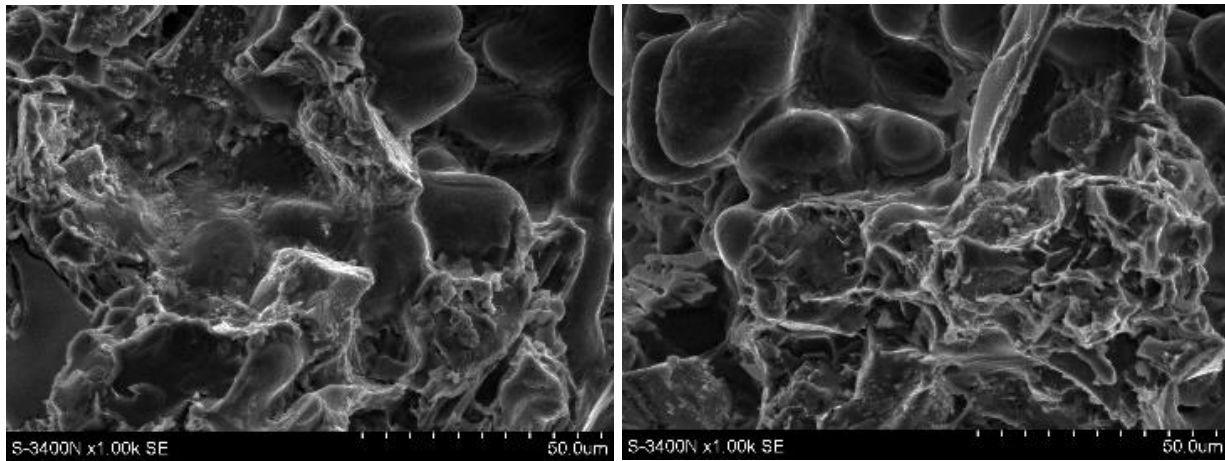
c                                                    d

Figure 40. Fractography of the composite specimens tested at various temperatures: a) room temperature, b) 150°C, c) 250°C, and d) 350°C

# 6. STUDY OF LOADING SEQUENCE ON THE STRUCTURE AND DURABILITY OF THE AlSi COMPOSITE REINFORCED WITH SiC PARTICLES

In this chapter, the effect of sequential loading (fatigue-relaxation and fatigue creep) on the durability of the AlSi composite reinforced with SiC particles is described. Several applications of AlSi composite, such as aerospace components like turbine blades and automotive components like engine pistons, are subjected to fatigue, creep, and relaxation loading conditions. Therefore, it is important to investigate the behavior of the AlSi composite under these loading conditions to ensure the long-term performance of the material. Fatigue is the phenomenon of deterioration of the mechanical properties of the material under cyclic loading, leading to failure. Creep is the gradual deformation behavior of a material under constant stress, which typically prevails at elevated temperature ($T > 0.4*T_m$, where $T_m$ is the melting point of the material in Kelvin). Relaxation is the phenomenon of the gradual decrease in stress in a material over time under constant strain.

## 6.1   Damage mechanism of the composite under sequential loading

AlSi composite is an advanced material with favourable properties such as a high strength-to-weight ratio, low density, and corrosion resistance. AlSi composites have several applications in various industries like aerospace, automotive, and defence industries that require lightweight, high-performance materials [188–190]. In such applications, AlSi composites are often subjected to a combination of several types of loading, such as fatigue, creep, and relaxation, which can affect their durability and structure. For example, fatigue loading can cause microstructural defects that serve as nucleation sites for creep deformation. On the other hand, creep loads can cause plastic deformation, which, in turn, can alter the microstructure of the material and make the subsequent fatigue loading worse.

Incorporating reinforcements, such as SiC particles, into matrix alloys enhances the mechanical properties and fatigue resistance of the composite compared to an unreinforced matrix alloy. They prevent dislocation movements, enhance crack deflection by acting as barriers, and significantly improve the resistance of the composite to crack propagation. Research studies [191] have shown

68

that the dispersed phases of SiC effectively enhance the fatigue resistance of the unreinforced alloy. However, the composite may also show inferior fatigue resistance compared to unreinforced alloy, this is related to the ductility of the compared to the matrix alloy. In addition, the size, shape, and distribution of the reinforcement, as well as the interfacial bonding between the matrix and the reinforcement, play an important role in determining the fatigue resistance of the composite material. For example, a higher volume fraction of SiC particles may lead to a lower fatigue strength [126]. Finer and more uniformly distributed SiC particles can enhance the fatigue resistance of the material. A strong interfacial bond prevents cracks from initiating at the reinforcement and matrix interface.

Several types of damage that can occur to AlSi composites include matrix cracking, interfacial debonding, microvoid formation, and reinforcing particle cracking [192–194]. These types of damage start to show up early in the fatigue life of composites [195]. Fatigue can cause the formation of voids and microcracks, while creep contributes to plastic deformation, leading to the degradation of the mechanical properties of AlSi composites. Relaxation leads to dislocation movement that changes the microstructure of composites. The microstructural changes, such as interfacial debonding and microcrack formation, can reduce the durability of the composite under sequential loading, leading to premature failure.

To predict the durability of AlSi composites under loading sequences accurately, it is important to know the deformation mechanisms induced by each type of loading and the effect of their combination. Under fatigue loading, AlSi composite can be affected by factors such as crack initiation at the interfaces between the matrix and reinforcement particles. When AlSi composites undergo creep loading for a prolonged time, the interfacial bonding between the particles and matrix may weaken, leading to gradual deformation of the material. When AlSi composite is subjected to stress relaxation, the internal stresses within the material will slowly decrease over time as the atoms rearrange themselves to reach a more stable state. This can result in a reduction in the strength and stiffness of the material.

Stress- and strain-based descriptions are still widely used in measuring the fatigue life of the material. However, energy-based approaches are now becoming popular for describing material behavior during cyclic loading [196,197]. Unlike traditional stress or strain-based methods for predicting fatigue life, the energy-based approach considers factors such as loading frequency and

material properties including strength, ductility, and work-hardening behavior [198]. Considering loading frequencies in fatigue life prediction is important as a higher frequency can accelerate deformation even at low stress, strain amplitudes. The strain energy dissipation is often the basis of energy descriptions of the fatigue process [199].

The aim of this study is to investigate the effect of loading sequences, specifically fatigue-creep and fatigue relaxation loading sequences on the durability and microstructure of AlSi composites reinforced with SiC particles. The study was conducted by analyzing individual effects of fatigue, creep, and relaxation on the durability of the composite, followed by analyzing their sequential effects. Furthermore, the study focuses on the influence of loading sequence on the microstructure of the composite. Using scanning electron microscopy (SEM), the effect of the loading sequence on the microstructure of the composite was analyzed.

## 6.2 Plastic strain energy under uniaxial cyclic loading

Energy is dissipated during cyclic loading due to plastic deformations. Some of the energy is dissipated in the form of heat, and certain parts are converted into others that are unrecoverable during each cycle of loading due to the absorption of energy. This phenomenon leads to irreversible plastic deformation, which accumulates gradually and leads to material failure. The dissipation of plastic strain energy depends on the material properties and loading conditions.

The hysteresis loop represents the amount of plastic strain energy dissipated during each cycle of loading and unloading. The larger the area of the hysteresis loop, the more energy dissipates, and the higher the material damage, which is known as hysteresis [200,201]. Figure 41 shows a scheme of energy dissipation during one cycle.
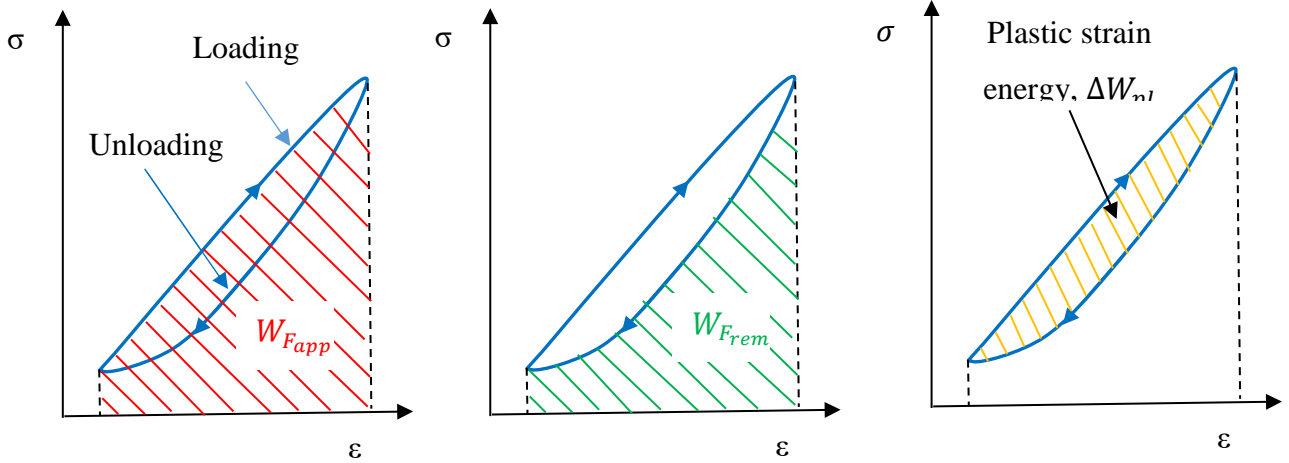
Figure 41. Scheme of strain energy dissipation under uniaxial cyclic load

The energy-based fatigue life approach uses the relationship between stress σ and strain ε to describe the characteristics of the hysteresis loop. The most commonly used method to describe the relationship between cyclic stress and strain is the Ramberg–Osgood model [202], which defined by Equation (7). The equation could be fitted by the least-squares method [199].

$$\frac{\Delta\varepsilon}{2} = \frac{\Delta\sigma}{2E} + \left(\frac{\Delta\sigma}{2K'}\right)^{\frac{1}{n'}} \tag{7}$$

Where $\Delta\varepsilon$ is the total strain range; $\Delta\sigma$ is the stress range; E is Young's modulus of the material, which could be determined from the monotonic tensile test; $K'$ is a cyclic hardening coefficient, and $n'$ is a cyclic strain-hardening exponent.

The equation describing the ascending branch of a hysteresis loop can be obtained from equation (7) by multiplying with 2. Once n' and K' parameters are determined from a stress-strain relationship of the Ramberg–Osgood model, plastic strain energy $\Delta W_{pl}$, of one hysteresis loop can be obtained for any level of $\Delta\sigma$ and $\Delta\varepsilon$.
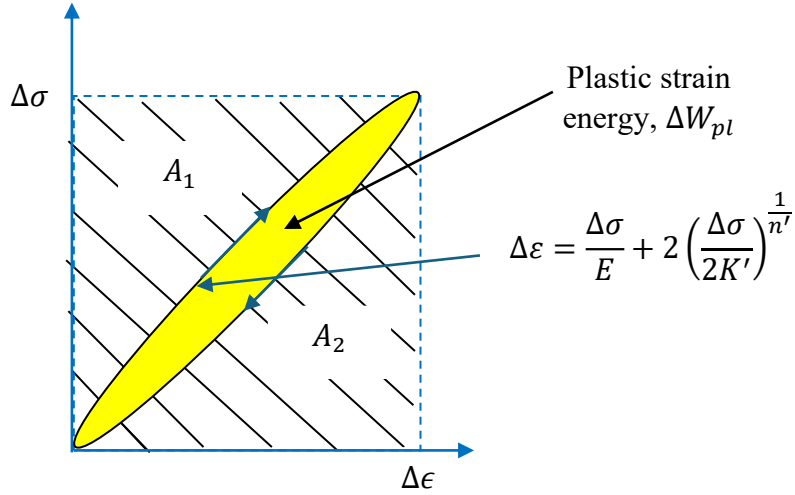
Figure 42. Scheme of plastic strain energy determination procedures

Figure 42 shows the procedures of plastic energy determination based on the Ramberg–Osgood equation. Assuming A1=A2=A, a plastic strain energy ($\Delta W_{pl}$), can be calculated as:

$$\Delta W_{pl} = \Delta\sigma \cdot \Delta\varepsilon - 2A = \Delta\sigma \cdot \Delta\varepsilon - 2\int_0^{\Delta\sigma}\left(\frac{\Delta\sigma}{E} + 2\left(\frac{\Delta\sigma}{2K'}\right)^{\frac{1}{n'}}\right)d\sigma \tag{8}$$

This Equation (8) can be rewritten as equation (9) as its detail is described in the literature [203]

$$\Delta W_{pl} = \Delta\sigma \cdot \Delta\varepsilon - \frac{\Delta\sigma^2}{E} - 4\frac{\Delta\sigma^{\frac{1}{n'}+1}}{\left((2K')^{\frac{1}{n'}}\right)\cdot\left(\frac{1}{n'}+1\right)} \tag{9}$$

## 6.3  Fatigue life prediction using strain energy density (SED) approach

**Strain energy density** can be used to estimate the fatigue life of the material. It can be used for both stress control, in which $\sigma_a$ is constant and strain control, in which $\varepsilon_a$ is constant. Dissipated energy accumulated in the fatigue test until the sample failure, $\sum\Delta W_{pl}$, is calculated as the sum of the areas of all the hysteresis loops:

$$\sum\Delta W_{pl} = \sum_{i=1}^{N_f} \Delta W_{pl(i)} \tag{10}$$

72

When calculating the total energy ($\sum\Delta W_{pl}$) dissipated under constant stress amplitude, it is usually assumed that the area of each hysteresis loop is equal, i.e., the same amount of energy is dissipated during each cycle. Consequently, the total amount of energy dissipated in the material to failure can be determined by multiplying the energy of a single loop ($\Delta W_{pl(i)}$), corresponding to the material's stabilization period by the number of cycles to failure. If no stabilization period is observed during the cyclic loading, the energy of a single loop at half the fatigue life $\frac{1}{2}N_f$ is multiplied by the number of cycles to failure [204].

$$\sum\Delta W_{pl} = N_f \cdot \Delta W_{pl(i=0,5N_f)}$$ (11)

## 6.4 Experimental procedures

The material used in this study was AlSi composite reinforced with SiC particles of about 20 μm size. The weight fraction of the SiC reinforcement was 10%. Test specimens were manufactured using a stir-casting method, as described in Section 5.1. Figure 43 shows the prepared specimens to test the effect of fatigue, creep and relaxation sequential loading on the durability of the material. Each specimen had 60 mm of gauge length and 10 mm of diameter. The microstructure of the specimens was characterized using scanning electron microscopy (SEM) after sequential loading test to analysis the loading effect on the structure of the material. Metallographic samples were taken from the part of broken specimens then prepared by grinding and polishing.



Figure 43. The prepared fatigue, relaxation, and creep test specimens

### 6.4.1 Fatigue test

Before fatigue testing, a static tensile test was performed on the Zick/Roel Z100 universal testing machine (shown in Figure 44), to determine the ultimate stress of the material. The ultimate tensile strength of the composite material corresponding to 250°C was obtained to be 140 MPa. After the static tensile test, a fatigue test was performed on the same machine at a temperature of 250°C and a stress ratio of 0.1. The maximum stress for the cyclic loading test was decided to be 50% of its ultimate tensile strength. The test was conducted at a strain rate of $1 \times 10^{-3}$ $s^{-1}$. The aim of the test was to evaluate the behaviour of the materials under cyclic loading and determine the number of cycles to failure ($N_f$). Load versus elongation was recorded and used to analyze the stress-strain response of the material.



Figure 44. Fatigue, relaxation, and creep test set-up

### 6.4.2 Creep and stress relaxation tests

Creep is a time-dependent deformation phenomenon that can adversely affect the material's performance over a prolonged period. Engineering components, especially those that operate under high-temperature conditions and even below their yield strength for prolonged periods, are more susceptible to creep deformation. A creep test is typically performed at constant stress levels at elevated temperatures over an extended period. Figure 45 shows a schematic representation of creep loading. Several factors, such as stress level, temperature, and exposure time, can affect the creep behaviour of the material [205]. As the stress level, temperature, and exposure time increase, the creep behaviour of materials deteriorates, and material failure accelerates.
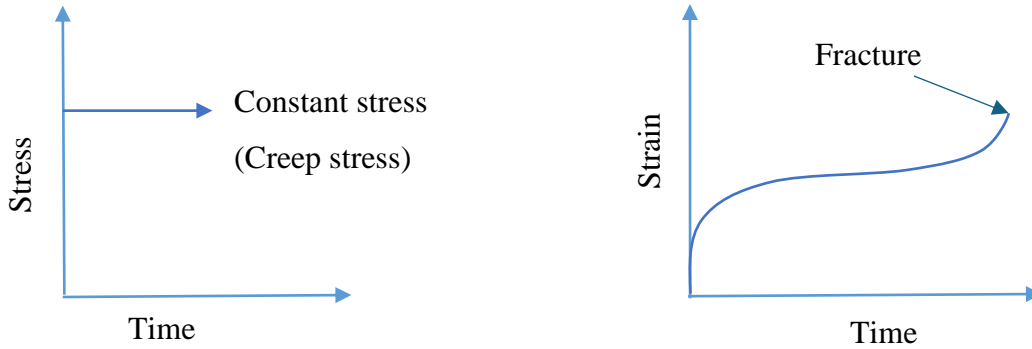
Figure 45. A schematic representation of creep loading

For this study, the creep behavior of SiC-reinforced aluminum matrix composite was performed at a temperature of 250°C. To perform the test, 50% of the ultimate tensile stress of the composite was used as a constant stress. 50% of the ultimate tensile strength corresponding to a temperature of 250C is 70MPa. During the test, a strain response of the material versus time was recorded.

Like creep test, the initial stress imposed on the specimen for the relaxation test was 50% of the composite ultimate tensile stress. Then, the strain was held constant once this initial stress was imposed. As the test continued, the stress began to decrease. The amount of this stress drop was then recorded. A schematic representation of relaxation test is shown in Figure 46. The graph shows a relaxation curve under constant strain. The initial stress ($\sigma_o$) gradually decreases over time (t) until reaching a steady-state stress level ($\sigma_\infty$).
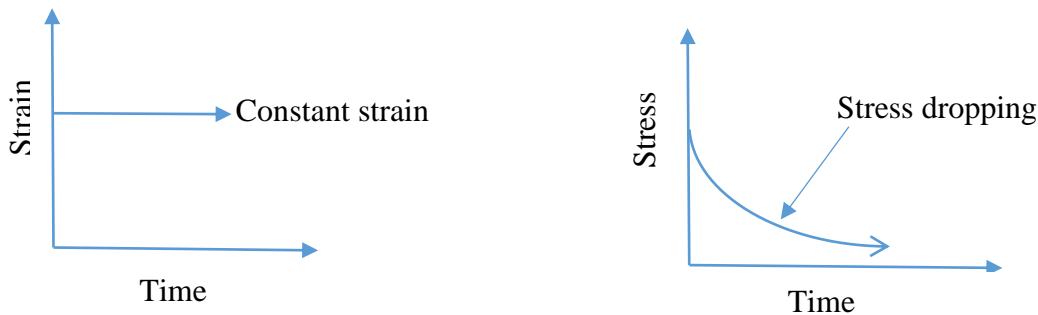


Figure 46. A schematic representation of relaxation loading

## 6.5 Fatigue and creep sequential loading conditions

Two types of loading were applied in sequence, as illustrated in Figure 47: fatigue and creep loading. In the fatigue loading stage (FLS), constant stress amplitude was used so that the upper and lower stresses of the cycles were kept constant. Following the fatigue loading stage, creep

loading was applied. During the creep loading stages (CLS), a constant stress equivalent to the maximum stress level of the fatigue stage was used. The creep duration was the same for all creep stages during a loading sequence.

During the uniaxial fatigue test, the total number of cycles to failure ($N_f$) for the composite specimens at 250°C was determined as described in Section 6.4.1. This total number ($N_f$) was then divided into 10 stages for the fatigue-creep sequential loading test, with the division being arbitrary for this experimental design. During each fatigue loading stage, the specimen was subjected to repetitive loading and unloading cycles for 10% of $N_f$ at a stress ratio of 0.1. The test was conducted at a strain rate of $1.0 \times 10^{-3}$ s$^{-1}$.
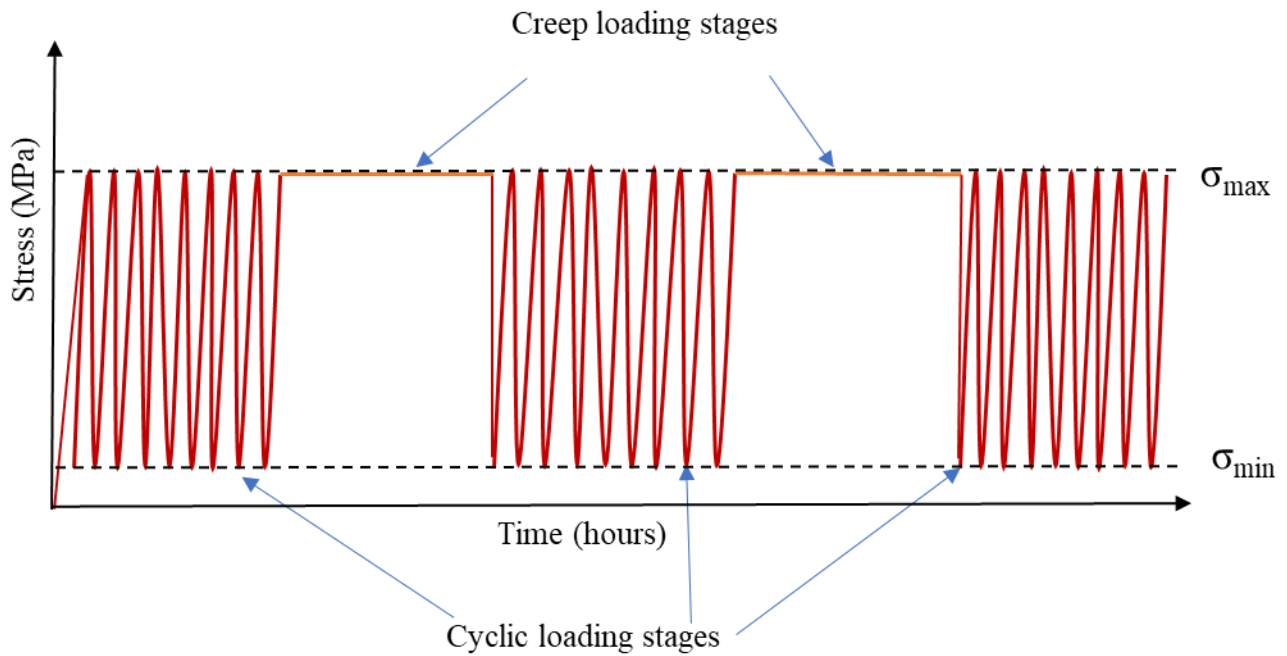


Figure 47. A sequence of creep and cyclic loading stages

The total creep life of the material at 250°C, which was determined in Section 6.4.2, was divided into 10. Therefore, the first fatigue loading stage of the sequential load test was set at 10% of the total number of cycles to failure, with the subsequent first creep stage lasting 10% of the creep life of the material. During each creep loading stage, specimens were loaded at a constant stress of 70 MPa, i.e., the same as the upper stress of the cyclic stress. This sequence of cyclic loading and creep loading continued until the material failure. After material failure, the fractography of the failed specimens was studied.

Table 4 presents the planned test of fatigue and creep loading stages in their sequential order. It also shows the planned structural analysis (SA) of the material following the loading stages. For example, after the first stage of the fatigue loading, the test was stopped, and portions of the specimens were cut out and prepared for further structural analysis. The purpose was to investigate the effect of fatigue-creep sequential loading on the material structure. Afterwards, a new test started with a new specimen that was subjected to fatigue stage 1, creep stage 1 and fatigue stage 2. Then, the test was stopped, and the specimen was taken for structural analysis. The sequence of the loading test was continued until the specimen failed as a test plan. Accordingly, the distribution of dislocations, the interface between the matrix and reinforcement, and crack initiation site were analyzed.

Table 4. A planned test of fatigue-creep sequential stages

| No. | Stages of test sequences |
|---|---|
| 1 | F   SA |
| 2 | F   C   F   SA |
| 3 | F   C   F   C   F   SA |
| 4 | F   C   F   C   F   C   F   SA |
| 5 | F   C   F   C   F   C   F   C   F   SA |
| 6 | F   C   F   C   F   C   F   C   F   C   F   SA |
| 7 | F   C   F   C   F   C   F   C   F   C   F   C   F   SA |
| 8 | F   C   F   C   F   C   F   C   F   C   F   C   F   C   F   SA |
| 9 | F   C   F   C   F   C   F   C   F   C   F   C   F   C   F   C   F   SA |
| 10 | F   C   F   C   F   C   F   C   F   C   F   C   F   C   F   C   F   C   F   SA |

Where; F is fatigue

C is creep

SA is structural analysis

## 6.6   Fatigue and stress relaxation sequential loading conditions

Similar to the fatigue creep loading sequence test, this experiment employs two sequential loading stages depicted in Figure 48: fatigue and stress relaxation. Stress relaxation loading stages (SRLS) replaced creep place in this case. Following each fatigue stage, the specimen undergoes stress relaxation. This involves applying an initial stress equivalent to the maximum stress from the fatigue stage and holding the specimen at the corresponding strain for a duration equal to the time used in the creep stages of the previous test. Table 5 presents the planned test of fatigue and stress relaxation sequential loading and structural analysis. In this case, stress relaxation loading stages

(SRLS) replaced the place of creep stages described in Section 6.5. After the sequential fatigue-relaxation tests, portions of the specimens were cut out and prepared for further structural analysis. The purpose was to investigate the effect of fatigue-relaxation sequential loading on the material structure. The analysis was carried out using SEM. Accordingly, the distribution of dislocations, the interface between the matrix and reinforcement, and the crack initiation site were analyzed.
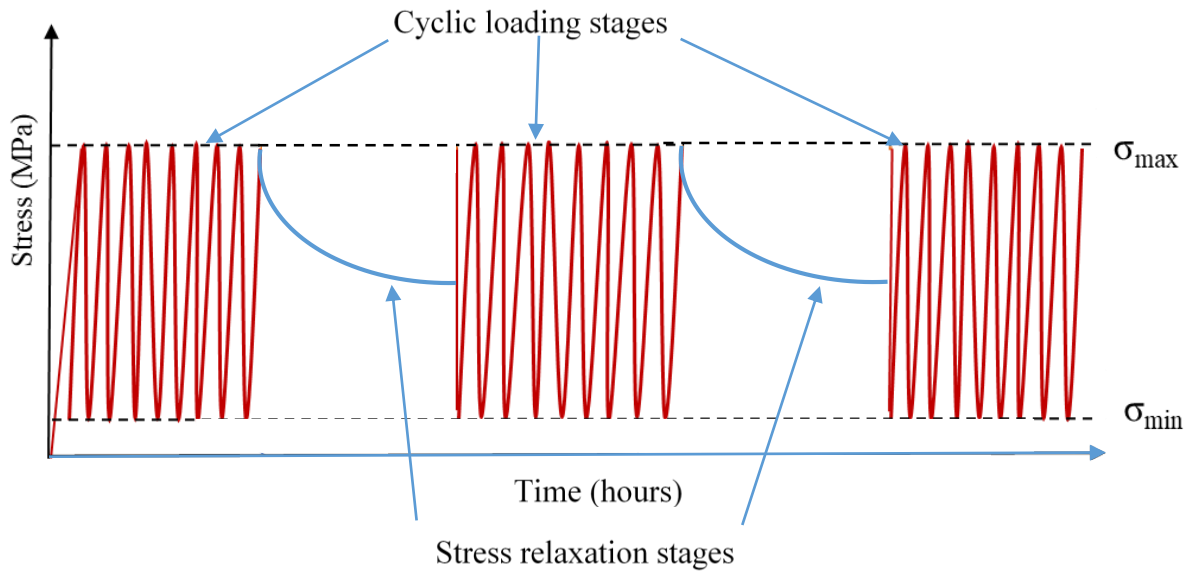


Figure 48. A sequence of relaxation and cyclic loading stages

Table 5. A planned test of fatigue-stress relaxation sequential stages

| No. | Stages of test sequences | | | | | | | | | | | | | | | | | | |
|---|---|---|---|---|---|---|---|---|---|---|---|---|---|---|---|---|---|---|---|
| 1 | F | SA | | | | | | | | | | | | | | | | | |
| 2 | F | R | F | SA | | | | | | | | | | | | | | | |
| 3 | F | R | F | R | F | SA | | | | | | | | | | | | | |
| 4 | F | R | F | R | F | R | F | SA | | | | | | | | | | | |
| 5 | F | R | F | R | F | R | F | R | F | SA | | | | | | | | | |
| 6 | F | R | F | R | F | R | F | R | F | R | F | SA | | | | | | | |
| 7 | F | R | F | R | F | R | F | R | F | R | F | R | F | SA | | | | | |
| 8 | F | R | F | R | F | R | F | R | F | R | F | R | F | R | F | SA | | | |
| 9 | F | R | F | R | F | R | F | R | F | R | F | R | F | R | F | R | F | SA | |
| 10 | F | R | F | R | F | R | F | R | F | R | F | R | F | R | F | R | F | R | F SA |

Where: F is fatigue
R is stress relaxation
SA is structural analysis

## 6.7 Results and discussion

### *6.7.1 Fatigue test results*

This section describes the results obtained from a complete cyclic test of the specimen to failure before sequential loading tests started. Figure 49 shows the stress-strain response of the material under cyclic loading. A continuous increase of maximum strain as the number of cycles increased was observed. In the initial stages, the maximum strain increases faster until it stabilizes. After stabilizing, the increment of maximum strain is almost constant. This phenomenon shows a cyclic material flow that increases the material's maximum strain (shift of hysteresis loops along the strain axis), as shown in Figure 50. The shift of hysteresis loops along the strain axis indicates a progressive material degradation over time. This progressive degradation led to the failure of the material.
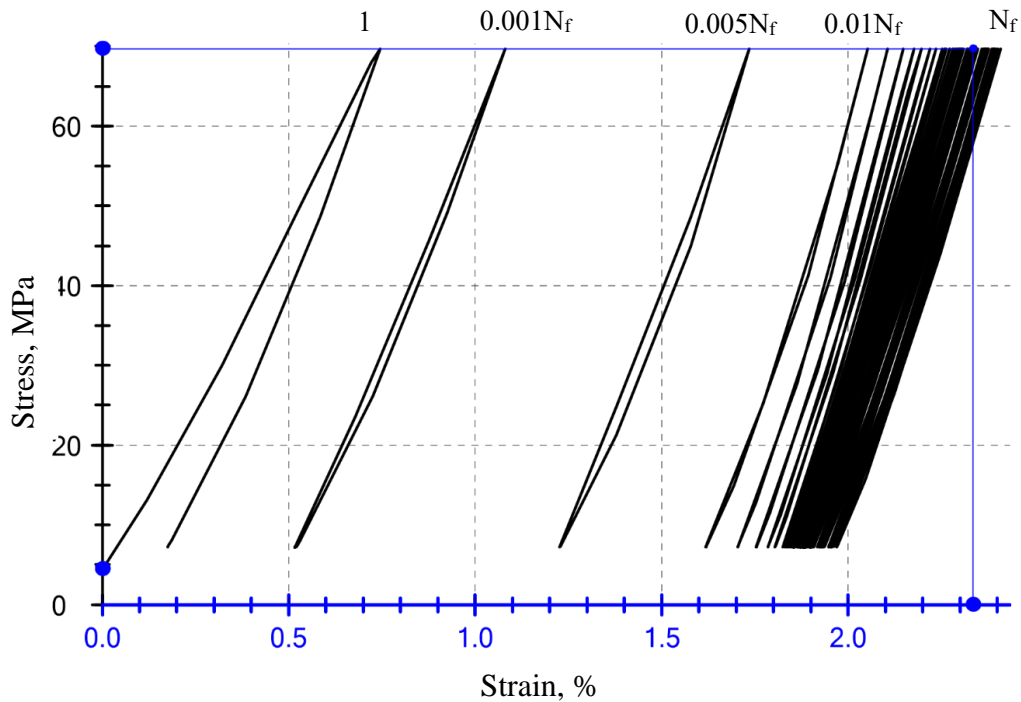


Figure 49. Stress strain responses under constant stress amplitude and temperature of 250°C
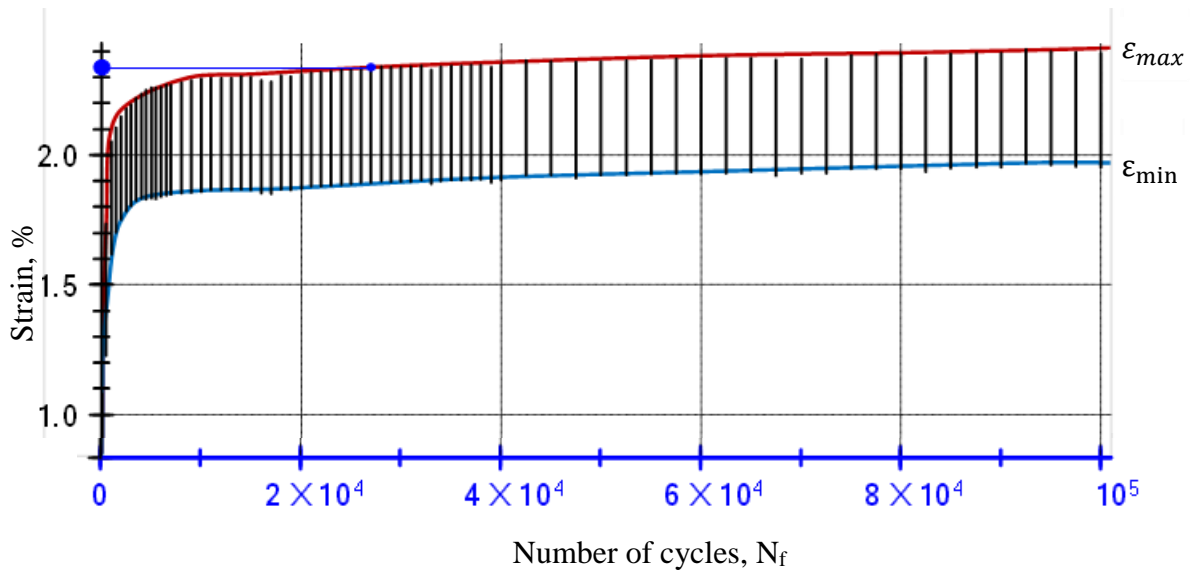
Figure 50. Increment of maximum strain under constant stress amplitude
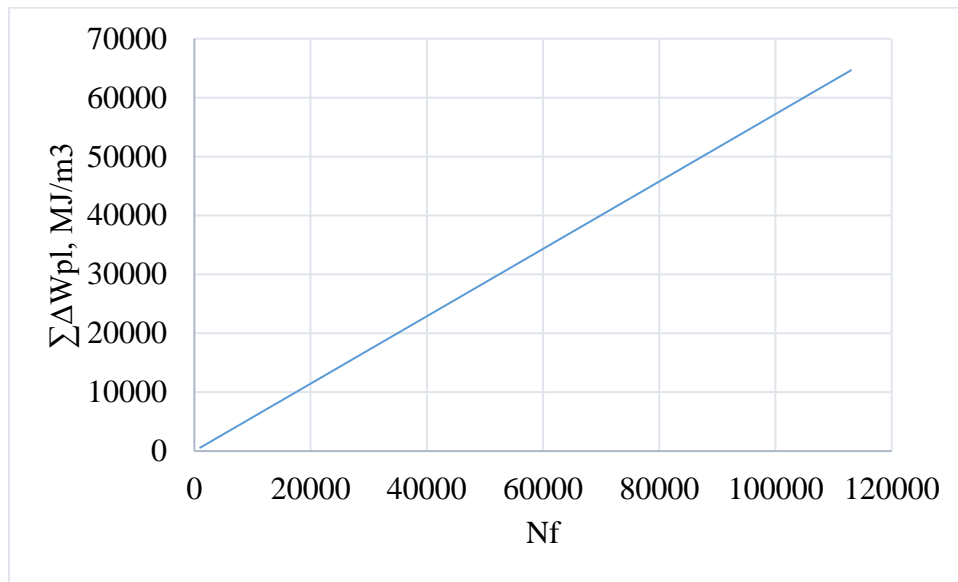


Figure 51. Accumulation of energy dissipated of the SiC reinforced Al12Si alloy at 250°C temperature

The energy density versus lifetime curve defines the relationship between the amount of energy stored in the material and the number of load cycles to failure. The values of the stored energy $\sum \Delta W_{pl}$ versus fatigue life $N_f$, (calculated based on Equation (11)) are shown in Figure 51. This curve indicates that energy density increases with the number of cycles. This means that as the accumulated energy increases, the material becomes more vulnerable to failure. In other words, higher energy density leads to faster material degradation and failure.

### 6.7.2 Creep test results

The strain versus time curves of the composite is shown in Figure 52. The curve shows time dependent deformation behaviour of the composite under constant stress. Typically, creep curve has three stages, primary, secondary, and tertiary stages [206,207]. However, the tested composite material showed only two stages: primary and secondary stages. The composite has not shown the tertiary stages, this could be because of the presence of hard and brittle $SiC_p$ reinforcement in the composite structure. After 120 hours of creep loading, the specimen was broken. The total elongation of the specimen until failure under the full creep loading was about 2.2%.
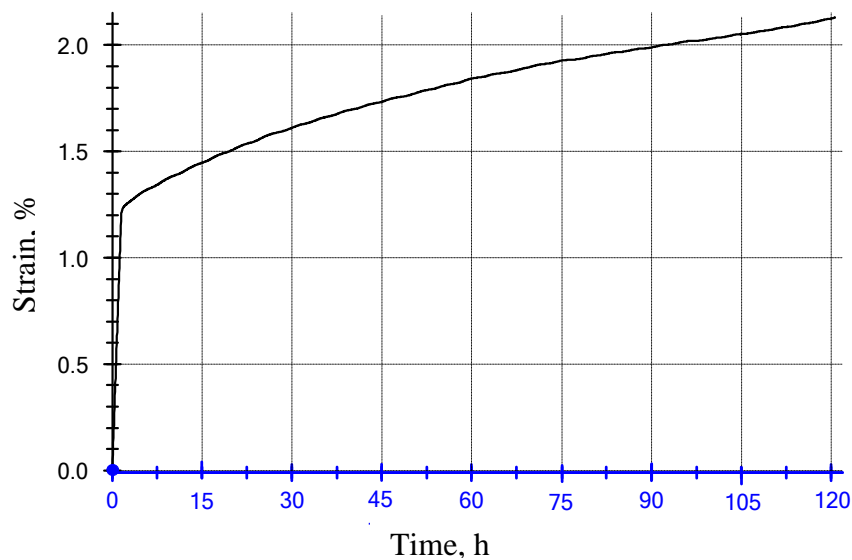


Figure 52. Creep curves of AlSi composite at 250°C temperature

### 6.7.3 Sequential loading test results

**A. Fatigue-creep sequential loading test results**

The combined effect of fatigue and creep loading leads to a significant decrease in the material's fatigue life. As described in Section 6.7.1, the number of cycles to failure under the full fatigue test was $1.0 \times 10^5$ cycles. However, under sequential fatigue-creep loading, the average fatigue life of three specimens dropped to $3.5 \times 10^4$ cycles. This indicates a decrease of approximately 65% in the number of cycles to failure compared to the full fatigue test described in Section 6.7.1. Table 4 presents the planned fatigue-creep sequential test; however, this combination of loading led the specimens to rupture during the fourth and fifth stages of fatigue during the sequence.

Figure 53 illustrates the number of cycles endured by one specimen until the fifth step during the fatigue-creep loading sequence. This specimen exhibited the longest life among the tested specimens. When subjected to the combined full fatigue creep loading sequence, this specific specimen experienced a decrease in fatigue life of approximately 57%. The final axial strain at the end of each loading stage of the specimen shown in Figure 54 are:

- Cyclic loading stages: 1.70%, 1.85%, 1.99%, 2.1%
- Creep loading stages: 1.82%, 1.95%, 2.05%, 2.2%

Therefore, the elongation under each fatigue loading stage is 1.7%, 0.03%, 0.04%, and 0.05%, while the elongation under each creep loading stage is about 0.12%, 0.1%, 0.06%, and 0.1%, respectively. The deformation in creep loading stages is greater in comparison to each cyclic loading stage with respect to axial strain, except during the initial stages of fatigue loading. This indicates that the deformation was mainly influenced by creep loading. In general, these results indicate that the material experiences more significant deformation during creep loading stages than during fatigue loading stages, especially when the material is subjected to a constant stress equal to the maximum level cyclic stress for an extended period. After the initial stages of cyclic loading, the material stabilizes and exhibits minimal deformation. This behavior indicates the material's ability to withstand cyclic loading without experiencing substantial deformation once it reaches stabilization. This stability in deformation could be due to the material's microstructure changes, which allow it to resist deformation under cyclic loading conditions.

The combination of fatigue and creep creates a synergistic effect that accelerates material deterioration through mechanisms such as crack propagation and grain boundary degradation, resulting in a reduced service life. The combination of fatigue and creep loads increases the damage accumulation more than what is observed in full fatigue tests. The sequential application of cyclic loads and sustained stresses during the creep phase causes microstructural changes such as microcrack formation, grain boundary sliding, and dislocation movements in the composite material, ultimately resulting in premature failure.
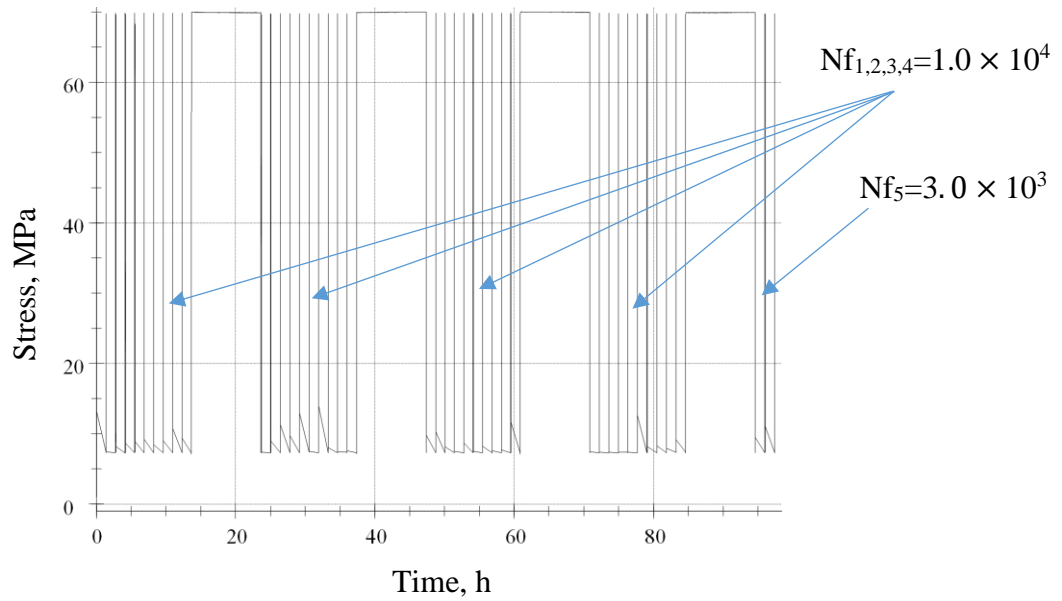
Figure 53. Fatigue-creep sequential loading

The arrows in the figure are labeled:

$Nf_{1,2,3,4}=1.0 \times 10^4$

$Nf_5=3.0 \times 10^3$
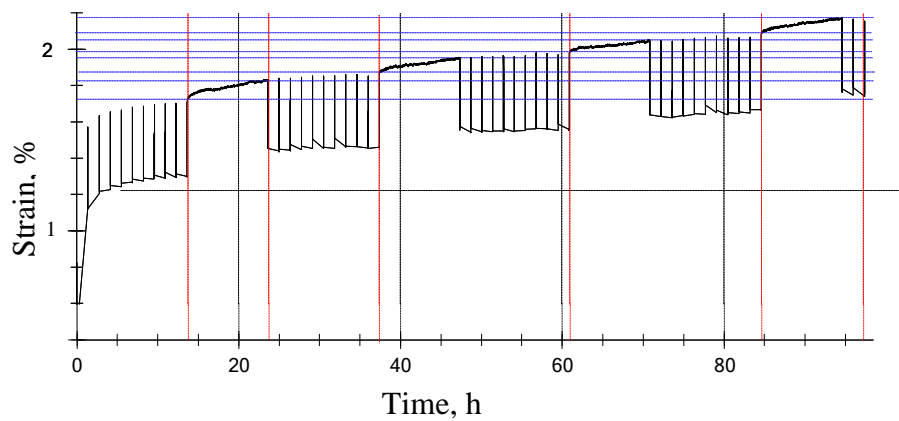


Figure 54. Strain increment under fatigue-creep sequential test

**B. Fatigue-stress relaxation sequential loading test results**

Similar to the fatigue-creep loading sequence, the combined effect of fatigue and stress relaxation loading greatly affects the material's fatigue life. As described in Section 6.7.1, a full fatigue test resulted in failure at 100,000 cycles. However, the number of cycles to failure decreased to about 30,000 cycles on average in the full fatigue-stress relaxation loading sequential test. This indicates a 60% reduction in the material's durability due to the combined effect of fatigue and stress relaxation loading. The reduced durability under the combined loading sequences could be due to the accelerated damage accumulation caused by stress relaxation. Table 5 presents the test plan of

83

fatigue-stress relaxation sequential loading. However, this combination of loading resulted in the specimens rupturing during the third stage of fatigue in the sequence.

Figure 55 illustrates the number of cycles endured by one specimen until the third step during the fatigue-creep loading sequence. Other tested specimens exhibited similar durability under the combined loading of fatigue and stress relaxation. Figure 56 shows the percentage of strain increment under fatigue-stress relaxation loading. The final axial strain at the end of each fatigue loading stage of the specimen is 1.85%, 1.95%, and 2.1%. Since the material was held at constant strain during the stress relaxation stages, the increment in axial strain of the material is observed only during the fatigue loading stages of this sequence.

The combination of fatigue and stress relaxation causes a synergistic effect that accelerates material degradation through microstructural changes like dislocation movement, rearrangement of grain boundaries, and microcrack nucleation. These changes ultimately lead to premature failure.
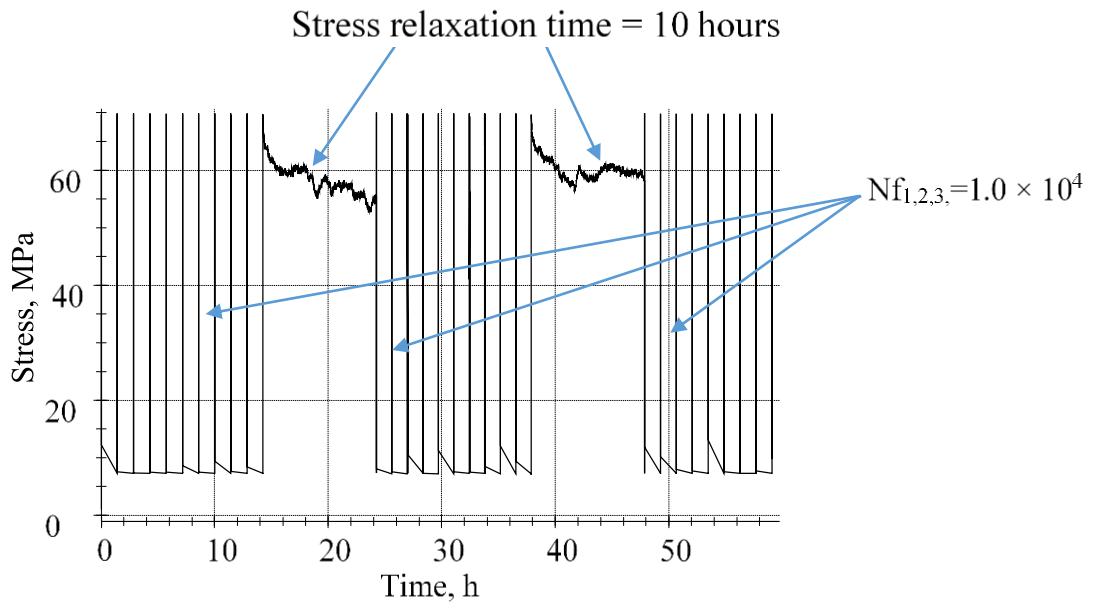


Figure 55. Fatigue-relaxation sequential test
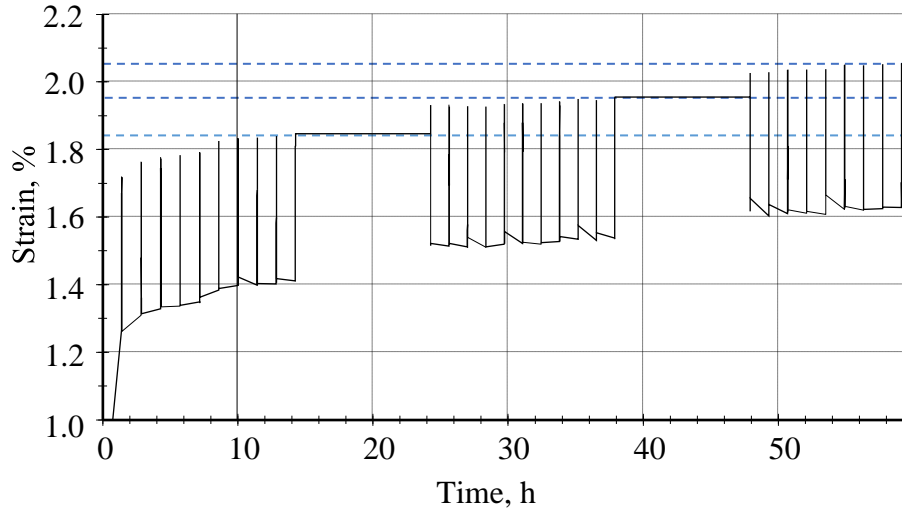
Figure 56. Strain increment under fatigue-stress relaxation sequential loading

### *6.7.4  The effect of loading sequence on the structure of the material*

**The influence of loading sequence on microstructure of material**

SEM was used to study the microstructural analysis of the loading sequence of SiC particle-reinforced AlSi composites. Two distinct loading sequences, fatigue-creep and fatigue-relaxation, were studied.

**Fatigue-Creep loading Sequence:**

After being exposed to the first stage of fatigue loading, the composite undergoes microstructural analysis. SEM analysis after the first stage of fatigue revealed microstructural damage such as interfacial debonding, microcracking, and crack initiation sites, as shown in Figure 57 a). The interfacial debonding between the SiC particles and the matrix, microcracking within the matrix, and crack initiation sites could be observed at the particle-matrix interface. After the first stage of creep and the second stage of fatigue are applied to the composite material, SEM again observed the microstructure, as shown in Figure 57 b). Following the interaction between the creep and fatigue stages, interfacial debonding between the SiC particles and matrix increased, along with an increase in the size of microcracks. This observation suggests that creep shortens the fatigue life, accelerates microstructural changes, and induces plastic deformation in the material.

**Fatigue-Relaxation Sequence:**

Here, the composite undergoes cyclic fatigue loading followed by periods of complete stress relaxation. SEM analysis was conducted after the specimen underwent the first fatigue stage, initial relaxation stage, and second fatigue stage. SEM analysis reveals the presence of secondary cracks and fatigue striations, indicating structural weaknesses within the matrix. Figure 58 a) and b) display the micrographs of the composite illustrating the effects of fatigue loading and fatigue-stress relaxation.
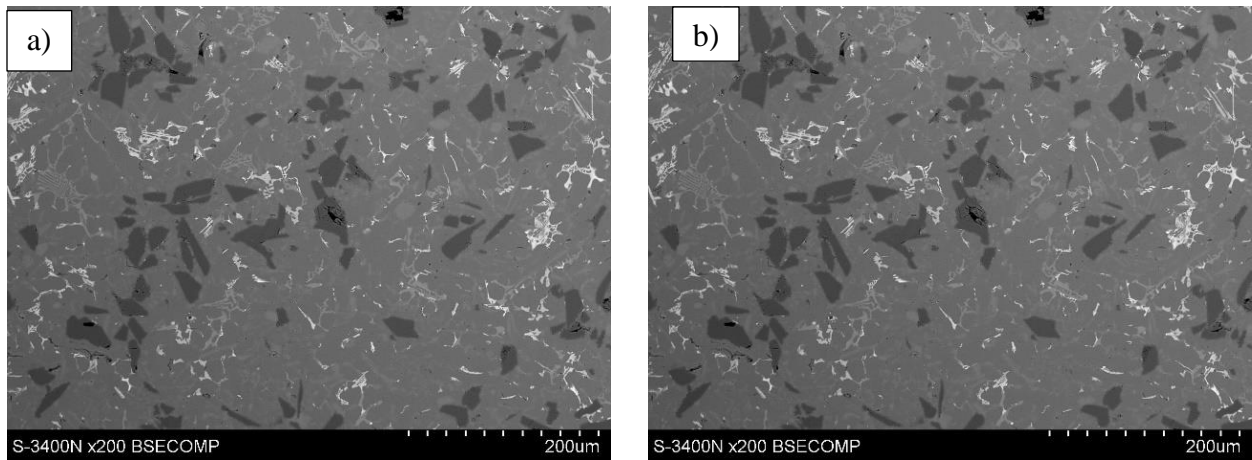


Figure 57. Micrograph of the composite a) first fatigue stage loading, b) first stage of fatigue and creep, and second stage of fatigue sequential loading
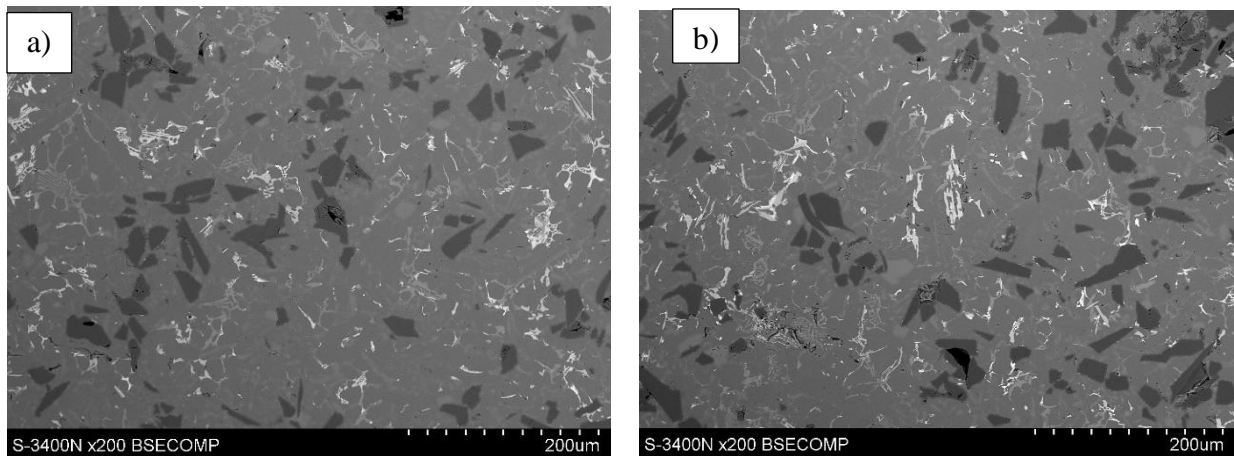


Figure 58. Micrograph of the composite after a) first fatigue stage loading, b) first stage of fatigue and relaxation, and second stage of fatigue sequential loading

**Fractography of specimens after sequential loading**

The fractography analysis of the failed specimens revealed the presence of fatigue cracks and creep cavities, indicating the failure mechanism of the material under the combined loading conditions. The distribution and size of the cracks and cavities shows the progression of damage leading to failure. For this study, the fracture surface of the Al-Si/SiC$_p$ composite were analyzed using SEM after failure due to fatigue, creep, fatigue-creep sequence and fatigue-relaxation sequence.

**A. Fracture surface analysis of the broken specimen after fatigue loading**

Fatigue fractures occur in the Al-Si/SiCP composite by the formation of microcracks, followed by debonding of the interface between the Al matrix and SiC$_p$ reinforcement. Figure 59 shows the SEM fracture surface of the Al-Si/SiCp composite after failure due to fatigue at an elevated temperature of 250°C. The fracture surface exhibits numerous shallow dimples, which are indicative of ductile failure, along with voids, and some cleavage planes suggesting brittle fracture. The formation of these shallow dimple structures can be attributed to the cracking of particles, the separation of SiCp from the Al matrix due to decohesion, and fractures within the matrix. The fracture of particles occurs when the interface between the SiC particle and the AlSi matrix is stronger than the strength of the particles [208]. While the fracture surface exhibits both ductile and brittle features, it predominantly indicates a ductile failure mechanism. As a result, the composite material becomes more susceptible to fatigue failure over time as the voids continue to grow and weaken the entire structure.

At elevated temperatures, it is assumed that the particle and matrix interfaces are easy to decohere due to the mismatch in thermal expansion coefficient between the particle and matrix [209]. The coefficients of thermal expansion for the SiC particle and Al-Si matrix are approximately $4.7 \times 10^{-6}$ K$^{-1}$ and $22 \times 10^{-6}$ K$^{-1}$ over a range of temperatures, respectively [210,211]. The fatigue crack propagated along the interface between the matrix and particles, resulting in further weakening of the material. Consequently, the fatigue failures in the composite material were primarily attributed to the debonding of the particle-matrix interfaces at elevated temperatures.
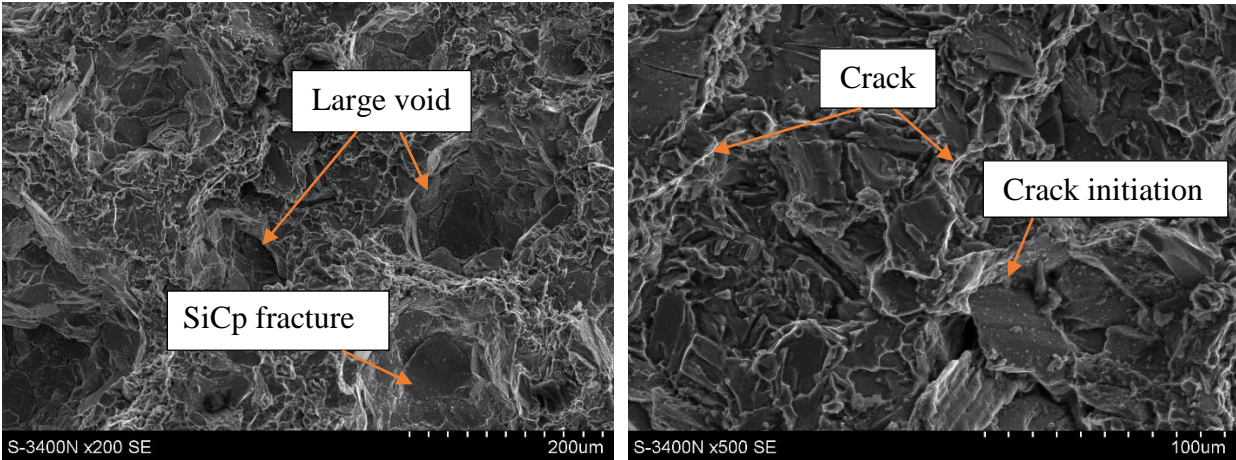
Figure 59. Fracture surface of the composite after fatigue loading

**B. Fracture surface analysis of the broken specimen after creep loading**

The fracture behaviour of Al-Si/SiCp composite samples was observed by SEM after being subjected to creep loading at 250°C. Figure 6060 shows the fractography of a sample after creep loading. Initially, the high temperature softens the Al-Si matrix. As a result, creep loading induces microstructural changes in the Al-Si matrix. These changes weaken the interface between the SiC particles and the matrix, thus accelerating the degradation of the composite. The initiation of cracks and debonding between the SiC particles and the Al-Si matrix is mainly due to the weakened interface between the matrix and the SiC particles.

SEM analysis reveals an intergranular fracture mode, indicating that the fracture path follows the weakened boundaries of the composite structure. The cavities and voids on the fracture surface, as shown in Figure 60, are likely due to the formation of microcracks around the SiC particles, which gradually contribute to crack propagation. These cavities indicate localized deformation and stress accumulation, specifically induced by the elastic load within the composite structure. However, these cavities are less pronounced under creep loading compared to the composite failure under fatigue loading. In addition to the intergranular fracture mode, the existence of transgranular cracking suggests a slightly brittle fracture mode. However, the presence of several dimples on the fracture surface indicates the ductile-dominated fracture behaviour of the composite under creep loading. This suggests that the composite has a combination of brittle and ductile properties, with ductile behaviour being dominant during the fracture process. The presence of dimples indicates that the material was capable of deforming and absorbing energy before finally

88
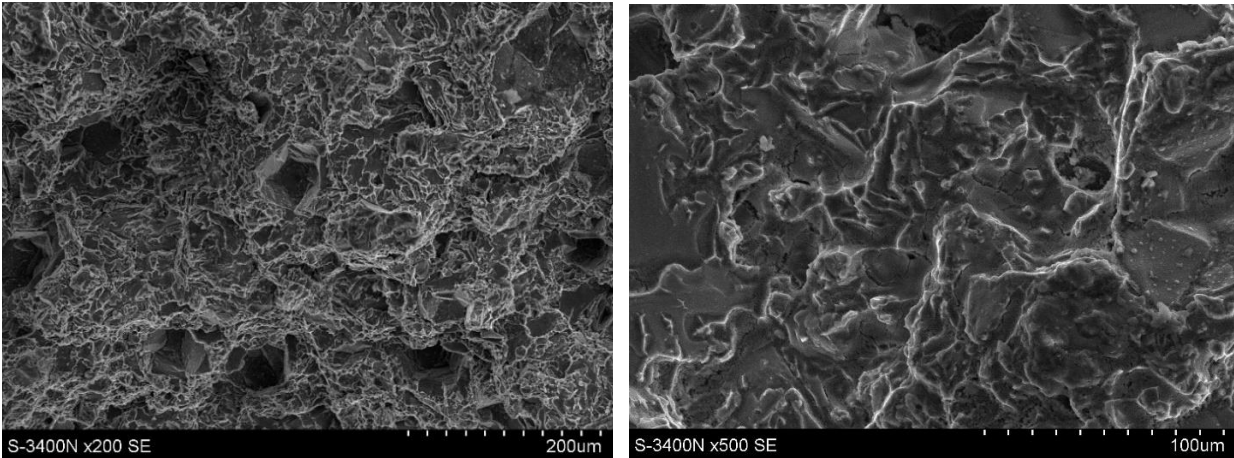
Figure 60. Fracture surface of the composite after creep loading

breaking, thus providing some level of resistance to fracture. SEM analysis reveals that the main cause of composite failure under creep loading is the degradation of the interface between the matrix and the reinforcing particles.

## C. Fracture surface analysis of the broken specimen after fatigue-creep loading sequence

Figure 61 shows a scanning electron microscope (SEM) image of the fracture surface of an Al-Si/SiCp composite specimen following failure caused by sequential fatigue and creep loading. The image reveals clear debonding along the interface between the SiC particles and the Al-Si matrix. It also revealed distinctive fatigue striations as well as extensive coalescence of microvoids in the fractography of the composite. The difference in fracture morphology was identified between the sample subjected to fatigue loading alone and that subjected to sequential fatigue and creep loading. This difference was particularly visible in the different crack propagation patterns and in the characteristics of the final fracture surfaces. Fatigue-creep loading led to a higher degree of intergranular fracture and a higher density of secondary cracks, indicating a more complex failure mechanism compared to pure fatigue loading.

The fracture from the fatigue-creep loading sequence shows more surface dimples and cracked SiC particles, due to the combined effects of fatigue and creep. However, with fatigue loading, interfacial cracks appear on the fracture surface, as shown in Figure 59. The dimples on the fracture surface are shallower under the fatigue-creep loading sequence compared to fatigue loading alone, mainly due to sustained stress and temperature exposure causing more creep deformation and cracking of SiC particles. This indicates that the combination of fatigue and creep loading leads to
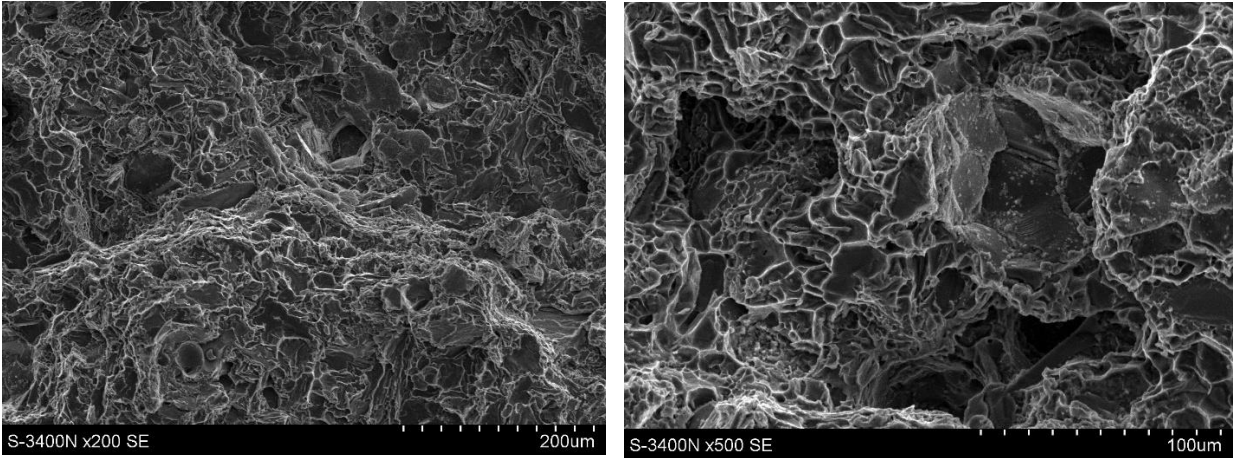
Figure 61. Fracture surface of the composite after fatigue-creep sequential loading

a more complex failure mechanism in the composite. The presence of shallow dimples and interfacial cracks suggests that the material undergoes both ductile and brittle fracture processes under different loading conditions, indicating complex fracture behaviour. The fracture mechanisms in Al-Si/SiCp material undergo significant changes with different loading conditions, characterized by a notable increase in ductile void coalescence observed on the fracture surface, specifically during fatigue and creep loading.

## D. Fracture surface analysis of the broken specimen after fatigue-relaxation loading sequence

Figure 62 shows the fractography of the Al-Si/SiCp composite sample after failure due to fatigue-stress relaxation sequence loading at 250°C. On the composite sample's fracture surface, dimples, minor cleavage planes, and tear ridges can be seen. These features show mix-mode fracture behavior, but ductile fracture is the main type of failure behavior for the composite. The fracture surface analysis revealed a combination of fatigue cracks and secondary cracks, including intergranular and transgranular cracks, around the SiCp particles. These cracks directly result from the fatigue-relaxation sequential loading, causing localized damage within the composite material. The fatigue cracks primarily occur around the SiCp particles, indicating that these regions experienced the highest stress concentrations during loading. The presence of localized plastic deformation and the formation of microcracks indicate that the material experienced significant stress concentrations and deformation during the loading sequence. The presence of fatigue cracks and debonding of SiC particles were clearly observed, signifying the active initiation and propagation of cracks within the material.

The relaxation periods after fatigue cycles could have exacerbated the debonding between the SiC particles and the Al-Si matrix, possibly due to cyclic loading-induced microstructural changes that impacted the interface strength. This suggests that stress relaxation may contribute to damage at the interface, regardless of its initial strength. The observations suggest that the material was experiencing progressive degradation due to cyclic loading. The weakening of the interface between the SiC particles and the matrix likely led to further crack initiation and growth, ultimately leading to the material's failure. The comparison highlights the significant role of stress relaxation in the fatigue behavior of the material, especially when compared to the composite's fracture surface under fatigue loading alone, as depicted in Figure 59.
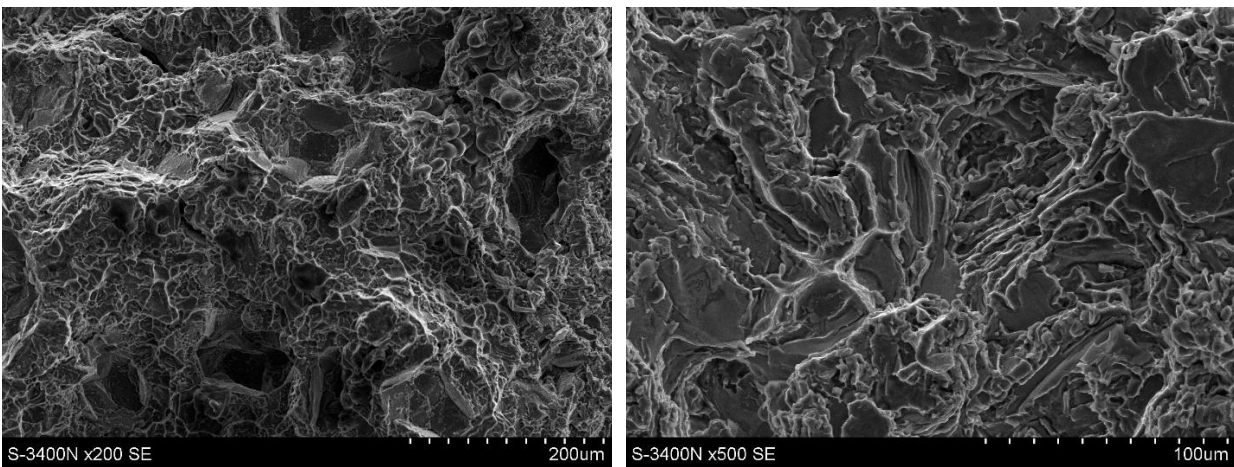


Figure 62. Fracture surface of the composite after fatigue-stress relaxation sequential loading

# 7. CONCLUSIONS AND RECOMMENDATIONS

## 7.1 Conclusions

This dissertation deals with the influence of combined stress relaxation, creep and fatigue on the final durability and structure of aluminium silicon composite reinforced with SiC particles. To achieve this, the study began with investigating the basic mechanical properties and microstructure of the unreinforced alloy (EN AC-Al Si12CuNiMg), followed by analysis of the composite material.

Light microscopy (LM) and scanning electron microscopy (SEM) were also used to perform microstructural analysis of the EN AC-Al Si12CuNiMg alloy. The analysis revealed a structural composition such as α-Al matrix, eutectic Si particles, and other intermetallic compounds. In the structure of the alloy, aluminium dendrite arms, which could be a result of non-equilibrium solidification conditions during casting, and micro-pores, which were likely due to shrinkage during solidification, were observed.

The monotonic uniaxial tensile test on the unreinforced alloy at various temperatures (room temperature, 150, 250, 300, and 350°C) was conducted. The aim was to evaluate the effect of temperature on the alloy's tensile properties, such as ultimate tensile strength, yield strength, Young's modulus, and ductility. The experimental data indicated a gradual decrease in ultimate tensile strength and yield strength with increasing temperatures up to 250°C. However, a significant drop in the tensile strength of the alloy was observed between 250 and 350°C. However, the Young's modulus of the alloy showed a different trend, initially increasing with temperature up to around 150°C then declining with further temperature increase.

Following the monotonic tensile test at various temperatures, the tensile fracture surface analysis was conducted using SEM. The fracture surface of specimens ruptured at room temperature exhibited intergranular fracture behaviour, cleavage facets, and dimples, indicating a semi-brittle fracture mode. However, the fracture surface of specimens ruptured at elevated temperatures, particularly 300 and 350°C, exhibited deeper dimples, fewer cleavage facets, and several microvoids, indicating a transition towards a more ductile fracture mode. This suggests that the EN AC-Al Si12CuNiMg alloy becomes less brittle and shows more plastic deformation at elevated temperatures.

Further study of the behaviour of EN AC-Al Si12CuNiMg alloy under stress relaxation and creep loading at various temperatures was conducted. The experimental tests were conducted at 150, 250, and 350°C temperature. A least squares method was used to fit stress relaxation and creep curves obtained from experimental tests with a standard linear solid model (SLSM). From the curve fit, the SLSM parameters were determined. The results showed that the model parameters vary with temperature. The fitted curves showed good agreement with the experimental result, indicating that the determined SLSM model parameters can define the alloy's stress relaxation and creep behaviour under various temperatures.

The stress relaxation test revealed a rapid drop in stress levels within the initial phase of the loading, with the most significant reduction occurring within 2 hours of loading, followed by a gradual decrease with time. This rapid stress relaxation of the initial phase could be a result of a rapid rearrangement of dislocation within the alloy's crystal structure at elevated temperatures. Additionally, the experimental result showed that the rate of stress relaxation increases with increasing temperature.

Like stress relaxation rates, creep rates showed a continuous increase with temperature. This indicates that the material undergoes continuous plastic deformation under sustained load at elevated temperatures. The initial rapid changes were attributed to the rearrangement of dislocations within the alloy's microstructure. As dislocations rearrange themselves, the stress relaxation and creep rates decrease, gradually reaching a steady state where the rates become almost constant.

Similar to unreinforced alloy, the mechanical properties and microstructure of an AlSi composite reinforced with SiC particles were investigated. The composite's microstructure and mechanical properties were then compared with those of the unreinforced alloy. The aim was to evaluate the potential enhancement by incorporating SiC particles as reinforcement.

Microstructural analysis performed using LM and SEM showed a uniform distribution of SiC particles within the aluminium matrix. In addition, SEM observation showed the strong interfacial bonding between the matrix and the reinforcement particles.

The tensile testing and harness measurement proved the enhancement of the mechanical properties of the composite except for ductility. The tensile tests were performed at various temperatures (room temperature, 150, 200, 250, 300, and 350°C). The composite material exhibited higher

ultimate tensile strength and yield strength compared to the unreinforced alloy at all test temperatures. This indicates that the composite can withstand higher loads before deformation than unreinforced alloy. Additionally, the composite displayed a higher Young's modulus, indicating higher stiffness of the composite. However, the composite exhibited lower ductility compared to the unreinforced alloy, indicating a lower ability to deform plastically before fracture than unreinforced alloy.

Hardness measurement further proved the enhancement of the hardness of the composite reinforced with SiC particles. A considerable improvement in the hardness of the composite by 20% compared to the unreinforced alloy was also observed. This increase in hardness could be due to the dispersion of the SiC particles within the matrix.

Similar to the unreinforced alloy, the composite tensile fracture surface was further investigated using SEM. Fractographic observation of the composite revealed smaller dimples and cleavage planes compared to unreinforced alloy, which indicate a lower degree of ductility. The decrease in ductility could be due to strong interfacial bonding between the matrix and reinforcement particles. The ductility increases as the temperature increases from room temperature to 150, 200, 250, 300, and 350°C. This indicates the weakening and breaking of the interfacial bonding between the reinforcement and matrix.

After proving the enhancement of the basic mechanical properties of the composite compared to unreinforced alloy, the further study of the combined effect of stress relaxation, creep, and fatigue sequential loading on the durability and structure of the composite was continued. SEM analysis was conducted to analyze the influence of individual loading and sequential loading on the microstructure of the composite.

The combined effect of fatigue and creep loading significantly decreases the material's fatigue life. The fatigue-creep loading sequence results in an average fatigue life of $3.5 \times 10^4$ cycles, a decrease of approximately 65% compared to the full fatigue test. This combination of loading leads to specimen rupture during the fourth and fifth stages of fatigue, indicating a significant deformation during the creep loading stages.

The combination of fatigue and creep loads accelerates material deterioration through mechanisms such as crack propagation and grain boundary degradation, resulting in a reduced service life. The sequential application of cyclic loads and sustained stresses during the creep phase causes

microstructural changes, leading to premature failure. Fractography analysis of the failed specimens revealed the presence of fatigue cracks and creep cavities, indicating the failure mechanism of the material under the combined loading conditions.

Fatigue fractures occur in the Al-Si/SiC$_P$ composite by the formation of microcracks, followed by debonding of the interface between the Al matrix and SiC$_p$ reinforcement. The fatigue fracture surface of the composite exhibits numerous shallow dimples, voids, and some cleavage planes, indicating semi-brittle fracture mode.

At elevated temperatures, it is assumed that the particle and matrix interfaces are easy to decohere due to the mismatch in thermal expansion coefficient between the particle and matrix. This results a further weakening of the material and enables the fatigue crack propagation along the interface between the matrix and particles.

The fracture behavior of Al-Si/SiCp composite samples was analyzed using scanning electron microscopy (SEM) after being subjected to creep loading at 250°C.

Fracture surface analysis of the specimen ruptured due to creep loading shows an intergranular fracture mode, with cavities and voids on the fracture surface likely due to the formation of microcracks around SiC particles. However, these cavities are less observed under creep loading compared to fatigue loading.

Fatigue-creep loading led to a higher degree of intergranular fracture and a higher density of secondary cracks, indicating a more complex failure mechanism compared to pure fatigue loading. The fractography of the specimen ruptured due to the fatigue creep loading sequence reveal more surface dimples and cracked SiC particles, which could be due to the combined effects of fatigue and creep loading. The presence of shallow dimples and interfacial cracks suggests that the material undergoes both ductile and brittle fracture processes under the combination of loading conditions.

Fatigue-stress relaxation sequential loading at 250°C resulted in a combination of primary and secondary cracks, including intergranular and transgranular cracks, around the SiCp particles. The presence of micro cracks and debonding of SiC particles was clearly observed, signifying the active initiation and propagation of cracks within the material. The relaxation periods following

the fatigue cycles might have worsened the debonding between the SiC particles and the aluminium-silicon matrix (Al-Si).

In general, the combined effect of stress relaxation, creep, and fatigue sequential loading significantly decreased the material durability. Under the fatigue-creep loading sequence, the material endured about 35% of its full fatigue life. Similarly, the material endured about 30% of its full fatigue life under the fatigue-stress relaxation loading sequence. This decrease in material durability could be related to the structural changes during the loading sequence.

## 7.2   Recommendations for future work

The primary focus of this thesis is to analyze the effects of combined relaxation, creep, and low-cycle fatigue on the durability and structure of Al-Si/SiCp composites. The study examined the behaviour of Al-Si/SiCp composite under combined loading conditions, fatigue-relaxation, and fatigue-creep sequence, which are commonly employed in engineering applications such as combustion engines. A specific stress level and temperature were chosen to investigate the impact of these combined loading conditions. Future work could consider the following:

- Investigate the combined relaxation, creep, and low-cycle fatigue behaviour of Al-Si/SiCp composites at various stress and temperature levels.
- Explore the influence of different amounts of SiC particles on the combined relaxation, creep, and low-cycle fatigue on the durability of the composite.
- Explore the influence of alternative reinforcement types that could enhance the durability of the composites under the combined effect of relaxation, creep, and low-cycle fatigue.
- Explore the impact of other environmental factors, such as corrosion, on the durability of the composite.

# REFERENCES

[1]     Callister WD. Materials science and engineering an introduction. John Wiley; 2007.

[2]     Carlisle R. Scientific American inventions and discoveries: all the milestones in ingenuity–from the discovery of fire to the invention of the microwave oven. Turner Publishing Company; 2008.

[3]     Sharma AK, Bhandari R, Aherwar A, Rimašauskienė R. Matrix materials used in composites: A comprehensive study. Materials Today: Proceedings 2020;21:1559–62.

[4]     Lakshmikanthan A, Angadi S, Malik V, Saxena KK, Prakash C, Dixit S, et al. Mechanical and tribological properties of aluminum-based metal-matrix composites. Materials 2022;15:6111.

[5]     Karadimas G, Salonitis K. Ceramic Matrix Composites for Aero Engine Applications—A Review. Applied Sciences 2023;13:3017. https://doi.org/10.3390/app13053017.

[6]     Gavalda Diaz O, Garcia Luna G, Liao Z, Axinte D. The new challenges of machining Ceramic Matrix Composites (CMCs): Review of surface integrity. International Journal of Machine Tools and Manufacture 2019;139:24–36. https://doi.org/10.1016/j.ijmachtools.2019.01.003.

[7]     Polymer Matrix Composites - an overview | ScienceDirect Topics n.d. https://www.sciencedirect.com/topics/materials-science/polymer-matrix-composites (accessed April 15, 2024).

[8]     Wang R-M, Zheng S-R, Zheng YG. Polymer matrix composites and technology. Elsevier; 2011.

[9]     Zhu S-P, Huang H-Z, Liu Y, Yuan R, He L. An efficient life prediction methodology for low cycle fatigue–creep based on ductility exhaustion theory. International Journal of Damage Mechanics 2013;22:556–71.

[10]    Pineau A, Antolovich SD. High temperature fatigue of nickel-base superalloys–a review with special emphasis on deformation modes and oxidation. Engineering Failure Analysis 2009;16:2668–97.

[11]    Verma V, Khvan A, Verma V, Khvan A. A Short Review on Al MMC with Reinforcement Addition Effect on Their Mechanical and Wear Behaviour. Advances in Composite Materials Development, IntechOpen; 2019. https://doi.org/10.5772/intechopen.83584.

[12]    Sharma DK, Mahant D, Upadhyay G. Manufacturing of metal matrix composites: A state of review. Materials Today: Proceedings 2020;26:506–19. https://doi.org/10.1016/j.matpr.2019.12.128.

[13]    Kumar Sharma A, Bhandari R, Aherwar A, Rimašauskienė R, Pinca-Bretotean C. A study of advancement in application opportunities of aluminum metal matrix composites. Materials Today: Proceedings 2020;26:2419–24. https://doi.org/10.1016/j.matpr.2020.02.516.

[14]    Mistry JM, Gohil PP. Research review of diversified reinforcement on aluminum metal matrix composites: fabrication processes and mechanical characterization. Science and Engineering of Composite Materials 2018;25:633–47. https://doi.org/10.1515/secm-2016-0278.

[15]    Kassner ME. Fundamentals of creep in metals and alloys. Butterworth-Heinemann; 2015.

[16]    Starke EA. Alloys: Aluminum. In: Bassani F, Liedl GL, Wyder P, editors. Encyclopedia of Condensed Matter Physics, Oxford: Elsevier; 2005, p. 18–24. https://doi.org/10.1016/B0-12-369401-9/00534-9.

[17] Birbilis N, Muster TH, Buchheit RG. Corrosion of Aluminum Alloys. Corrosion Mechanisms in Theory and Practice 2011:705–36.

[18] Bucci RJ. Selecting aluminum alloys to resist failure by fracture mechanisms. Engineering Fracture Mechanics 1979;12:407–41.

[19] Poznak A, Freiberg D, Sanders P. Chapter 10 - Automotive Wrought Aluminium Alloys. In: Lumley RN, editor. Fundamentals of Aluminium Metallurgy, Woodhead Publishing; 2018, p. 333–86. https://doi.org/10.1016/B978-0-08-102063-0.00010-2.

[20] Cayless RBC. Alloy and temper designation systems for aluminum and aluminum alloys 1990.

[21] Sun Y. The use of aluminum alloys in structures: Review and outlook. Structures, vol. 57, Elsevier; 2023, p. 105290.

[22] Mazzolani F. Aluminium alloy structures. CRC Press; 1994.

[23] Wang L, Makhlouf M, Apelian D. Aluminium die casting alloys: alloy composition, microstructure, and properties-performance relationships. International Materials Reviews 1995;40:221–38. https://doi.org/10.1179/imr.1995.40.6.221.

[24] CASTING MPOAA. The effect of sand casting process parameters on mechanical properties of aluminum alloy casting. Materials Science and Engineering (IJMMSE) 2012;2:32–41.

[25] Hu Z, Wan L, Lü S, Zhu P, Wu S. Research on the microstructure, fatigue and corrosion behavior of permanent mold and die cast aluminum alloy. Materials & Design 2014;55:353–60.

[26] Trejo E. Centrifugal casting of an aluminium alloy. PhD Thesis. University of Birmingham, 2011.

[27] Hamilton RW, See D, Butler S, Lee PD. Multiscale modeling for the prediction of casting defects in investment cast aluminum alloys. Materials Science and Engineering: A 2003;343:290–300.

[28] Campbell J. Castings. Elsevier; 2003.

[29] Otarawanna S, Dahle AK. Casting of aluminium alloys. Fundamentals of aluminium metallurgy, Elsevier; 2011, p. 141–54.

[30] Lampman S. Permanent mold casting of aluminum alloys 2018.

[31] Wei S, Lampman S. Centrifugal casting 2008.

[32] Alting L, Boothroyd G. Liquid Materials: Casting Processes. Manufacturing Engineering Processes, Second Edition, CRC Press; 2020, p. 301–42.

[33] Pattnaik S, Karunakar DB, Jha PK. Developments in investment casting process—A review. Journal of Materials Processing Technology 2012;212:2332–48.

[34] Horton RA. Investment casting 2008.

[35] Cheah CM, Chua CK, Lee CW, Feng C, Totong K. Rapid prototyping and tooling techniques: a review of applications for rapid investment casting. Int J Adv Manuf Technol 2005;25:308–20. https://doi.org/10.1007/s00170-003-1840-6.

[36] Di Sabatino M, Arnberg L. Castability of aluminium alloys. Trans Indian Inst Met 2009;62:321–5. https://doi.org/10.1007/s12666-009-0049-2.

[37] Robles Hernandez FC, Herrera Ramírez JM, Mackay R. Al-Si Alloys, Minor, Major, and Impurity Elements. Al-Si Alloys, Cham: Springer International Publishing; 2017, p. 1–15. https://doi.org/10.1007/978-3-319-58380-8_1.

[38] Robles Hernandez FC, Herrera Ramírez JM, Mackay R. Al-Si Alloys: Automotive, Aeronautical, and Aerospace Applications. Cham: Springer International Publishing; 2017. https://doi.org/10.1007/978-3-319-58380-8.

[39] Nwaeju CC, Edoziuno FO, Adediran AA, Tuaweri TJ, Saravana Kumar M. Grain characteristics and mechanical properties of as-cast Cu-10%Al alloy: Effects of alloying additions. Results in Engineering 2021;12:100295. https://doi.org/10.1016/j.rineng.2021.100295.

[40] Elgallad E, Samuel F, Samuel A, Doty H. Development of New Al-Cu Based Alloys Aimed at Improving the Machinability of Automotive Castings. Inter Metalcast 2009;3:29–41. https://doi.org/10.1007/BF03355446.

[41] Yamamoto K, Takahashi M, Kamikubo Y, Sugiura Y, Iwasawa S, Nakata T, et al. Influence of process conditions on microstructures and mechanical properties of T5-treated 357 aluminum alloys. Journal of Alloys and Compounds 2020;834:155133. https://doi.org/10.1016/j.jallcom.2020.155133.

[42] Çadırlı E, Kaya H, Büyük U, Üstün E, Gündüz M. Effect of Heat Treatment on the Microstructures and Mechanical Properties of Al–4Cu–1.5Mg Alloy. Inter Metalcast 2022;16:1020–33. https://doi.org/10.1007/s40962-021-00667-8.

[43] He C, Yu W, Li Y, Wang Z, Wu D, Xu G. Relationship between cooling rate, microstructure evolution, and performance improvement of an Al–Cu alloy prepared using different methods. Materials Research Express 2020;7:116501.

[44] Krupiński M, Labisz K, Rdzawski Z, Pawlyta M. Cooling rate and chemical composition influence on structure of Al-Si-Cu alloys. Journal of Achievements in Materials and Manufacturing Engineering 2011;45:13–22.

[45] Kammer C. Aluminum and Aluminum Alloys. In: Warlimont H, Martienssen W, editors. Springer Handbook of Materials Data, Cham: Springer International Publishing; 2018, p. 161–97. https://doi.org/10.1007/978-3-319-69743-7_6.

[46] LF M. ondolfo, Aluminium alloys: Structure and Properties. Éd: London, Butterworth &Co (Publishers) Ltd 1976.

[47] Kammer C. Aluminium-Taschenbuch. Aluminium-Verlag Düsseldorf; 1998.

[48] Flaig B. Isothermes und thermisch-mechanisches Ermüdungsverhalten von GK-AlSi10Mg wa, GK-AlSi12CuMgNi und GK-AlSi6Cu4. na; 1995.

[49] Djurdjevic M, Byczynski G, Schechowiak C, Stieler H, Pavlovic J. Quantification of the Impact of Strontium on the Solidification Path of the Aluminum-Silicon-Copper Alloys Using Thermal Analysis Technique. Practical Metallography 2009;46:137–52.

[50] Johnsson M. Grain refinement of aluminium studied by use of a thermal analytical technique. Thermochimica Acta 1995;256:107–21.

[51] Wang QG. Microstructural effects on the tensile and fracture behavior of aluminum casting alloys A356/357. Metallurgical and Materials Transactions A 2003;34:2887–99.

[52] Khomamizadeh F. Evaluation of quality index of A-356 aluminum alloy by microstructural analysis. Scientia Iranica 2004;11.

[53] Allison JE, Salzman R, Weber SJ, Boileau J. ALUMINUM, Div. 2-Effect of Porosity Size on Tensile Properties of a Cast 319-T7 Aluminum Alloy. Transactions of the American Foundry Society 2001;109:419–32.

[54] Boileau JM, Cloutier CA, Godlewski LA, Reeber-Symanski PA, Wolverton C, Allison JE. The Dimensional Stability of Cast 319 Aluminum: SAE International 2003.

[55] Tash M, Samuel FH, Mucciardi F, Doty HW. Effect of metallurgical parameters on the hardness and microstructural characterization of as-cast and heat-treated 356 and 319 aluminum alloys. Materials Science and Engineering: A 2007;443:185–201.

[56] Thirugnanam A, Sukumaran K, Pillai UTS, Raghukandan K, Pai BC. Effect of Mg on the fracture characteristics of cast Al–7Si–Mg alloys. Materials Science and Engineering: A 2007;445:405–14.

[57] Caceres CH, Davidson CJ, Griffiths JR, Wang QG. The effect of Mg on the microstructure and mechanical behavior of Al-Si-Mg casting alloys. Metallurgical and Materials Transactions A 1999;30:2611–8.

[58] Caceres CH, Davidson CJ, Griffiths JR, Hogan LM, Wang QG. Hypoeutectic Al-Si-Mg foundry alloys. Materials Forum, vol. 21, 1997, p. 27–43.

[59] Efzan ME, Kong HJ, Kok CK. Review: Effect of alloying element on Al-Si alloys. Advanced Materials Research 2013;845:355–9.

[60] Nam SW, Lee DH. The effect of Mn on the mechanical behavior of Al alloys. Metals and Materials 2000;6:13–6. https://doi.org/10.1007/BF03026339.

[61] Kliemt C. Thermo-mechanical fatigue of cast aluminium alloys for engine applications under severe conditions. PhD Thesis. Heriot-Watt University, 2012.

[62] Bolibruchová D, Podprocká R, Pastirčák R, Major-Gabryś K. The role of Mn in aluminium alloys with a higher iron content. Archives of Metallurgy and Materials 2018:1883–8.

[63] Rana RS, Purohit R, Das S. Reviews on the influences of alloying elements on the microstructure and mechanical properties of aluminum alloys and aluminum alloy composites. International Journal of Scientific and Research Publications 2012;2:1–7.

[64] Caceres CH, Djurdjevic MB, Stockwell TJ, Sokolowski JH. The effect of Cu content on the level of microporosity in Al-Si-Cu-Mg casting alloys. Scripta Materialia 1999;40:631–7.

[65] Handbook ASM. Metals Handbook Ninth Edition Volume 15 Casting. ASM International, USA 1988.

[66] Taylor JA. Iron-Containing Intermetallic Phases in Al-Si Based Casting Alloys. Procedia Materials Science 2012;1:19–33. https://doi.org/10.1016/j.mspro.2012.06.004.

[67] Mbuya TO, Odera BO, Ng'ang'a SP. Influence of iron on castability and properties of aluminium silicon alloys: literature review. International Journal of Cast Metals Research 2003;16:451–65. https://doi.org/10.1080/13640461.2003.11819622.

[68] Que Z, Wang Y, Fan Z. Formation of the Fe-Containing Intermetallic Compounds during Solidification of Al-5Mg-2Si-0.7Mn-1.1Fe Alloy. Metall Mater Trans A 2018;49:2173–81. https://doi.org/10.1007/s11661-018-4591-6.

[69] Taylor JA. The effect of iron in Al-Si casting alloys. 35th Australian foundry institute national conference, vol. 31, Australian Foundry Institute (AFI) Adelaide, South Australia; 2004, p. 148–57.

[70] Otte MO, McDonald SD, Taylor JA, St John DH, Schneider W. Controlling porosity-related casting rejects: understanding the role of iron in Al-Si alloys. Transactions of the American Foundrymen'S Society, Vol 107 1999;107:471–8.

[71] Ma Z, Samuel AM, Samuel FH, Doty HW, Valtierra S. A study of tensile properties in Al–Si–Cu and Al–Si–Mg alloys: Effect of β-iron intermetallics and porosity. Materials Science and Engineering: A 2008;490:36–51.

[72] Belov NA, Aksenov AA, Eskin DG. Iron in aluminium alloys: impurity and alloying element. CRC Press; 2002.

[73] Kori SA, Murty BS, Chakraborty M. Development of an efficient grain refiner for Al–7Si alloy. Materials Science and Engineering: A 2000;280:58–61.

[74] Committee AIH, Division AS for MHT. Heat treating. vol. 4. ASM international; 1991.

[75] Kaufman JG, Rooy EL. Aluminum alloy castings: properties, processes, and applications. Asm International; 2004.

[76] Pezda J. Effect of the T6 heat treatment on change of mechanical properties of the AlSi12CuNiMg alloy modified with strontium. Archives of Metallurgy and Materials 2015;60:627–32.

[77] Zhao H, Bai H, Wang J, Guan S. Preparation of Al–Ti–C–Sr master alloys and their refining efficiency on A356 alloy. Materials Characterization 2009;60:377–83.

[78] Chakrapani P, Suryakumari TSA. Mechanical properties of aluminium metal matrix composites-A review. Materials Today: Proceedings 2021;45:5960–4. https://doi.org/10.1016/j.matpr.2020.09.247.

[79] Mavhungu ST, Akinlabi ET, Onitiri MA, Varachia FM. Aluminum Matrix Composites for Industrial Use: Advances and Trends. Procedia Manufacturing 2017;7:178–82. https://doi.org/10.1016/j.promfg.2016.12.045.

[80] KARAOĞLU SY, KARAOĞLU S, İmgesu Ü. Aerospace industry and aluminum metal matrix composites. International Journal of Aviation Science and Technology 2021;2:73–81.

[81] Yılmaz T. Development of functionally graded aluminum matrix composite materials for defense industry applications. Master's Thesis. Middle East Technical University, 2019.

[82] Srinivasan V, Kunjiappan S, Palanisamy P. A brief review of carbon nanotube reinforced metal matrix composites for aerospace and defense applications. Int Nano Lett 2021;11:321–45. https://doi.org/10.1007/s40089-021-00328-y.

[83] Siengchin S. A review on lightweight materials for defence applications: Present and future developments. Defence Technology 2023;24:1–17. https://doi.org/10.1016/j.dt.2023.02.025.

[84] Maurya M, Kumar S, Bajpai V. Assessment of the mechanical properties of aluminium metal matrix composite: A review. Journal of Reinforced Plastics and Composites 2019;38:267–98.

[85] Leparoux M, Kollo L, Kwon H, Kallip K, Babu NK, AlOgab K, et al. Solid State Processing of Aluminum Matrix Composites Reinforced with Nanoparticulate Materials. Adv Eng Mater 2018;20:1800401. https://doi.org/10.1002/adem.201800401.

[86] Srivatsan TS, Ibrahim IA, Mohamed FA, Lavernia EJ. Processing techniques for particulate-reinforced metal aluminium matrix composites. J Mater Sci 1991;26:5965–78. https://doi.org/10.1007/BF01113872.

[87] Bhandare RG, Sonawane PM. Preparation of aluminium matrix composite by using stir casting method. International Journal of Engineering and Advanced Technology (IJEAT) 2013;3:61–5.

[88] Hashim J, Looney L, Hashmi MSJ. Metal matrix composites: production by the stir casting method. Journal of Materials Processing Technology 1999;92:1–7.

[89] Wu Y. Fabrication of metal matrix composite by semi-solid powder processing, 2011, p. IS--T 3083, 1082974. https://doi.org/10.2172/1082974.

[90] Kumar Sharma A, Bhandari R, Aherwar A, Pinca-Bretotean C. A study of fabrication methods of aluminum based composites focused on stir casting process. Materials Today: Proceedings 2020;27:1608–12. https://doi.org/10.1016/j.matpr.2020.03.316.

[91] Lee J. Elevated-temperature properties of ASTM A992 steel for structural-fire engineering analysis. PhD Thesis. 2012.

[92] Mishra S, Yadava M, Kulkarni KN, Gurao NP. Stress relaxation behavior of an aluminium magnesium silicon alloy in different temper condition. Mechanics of Materials 2018;125:80–93.

[93] Puspitasari P, Soepriyanto OR, Sasongko MIN, Dika JW. Mechanical and physical properties of aluminium-silicon (Al-Si) casting alloys reinforced by Zinc Oxide (ZnO). MATEC Web of Conferences, vol. 204, EDP Sciences; 2018, p. 05003.

[94] Butt MZ, Zubair M, Ul-Haq I. A comparative study of the stress relaxation in aged and un-aged high-purity aluminium polycrystals. Journal of Materials Science 2000;35:6139–44.

[95] Lyu F, Li Y, Shi Z, Huang X, Zeng Y, Lin J. Stress and temperature dependence of stress relaxation ageing behaviour of an Al–Zn–Mg alloy. Materials Science and Engineering: A 2020;773:138859.

[96] Hamasaki H, Morimitsu Y, Yoshida F. Stress relaxation of AA5182-O aluminum alloy sheet at warm temperature. Procedia Engineering 2017;207:2405–10.

[97] Butt MZ, Zubair M, Ul-Haq I. A comparative study of the stress relaxation in aged and un-aged high-purity aluminium polycrystals. Journal of Materials Science 2000;35:6139–44. https://doi.org/10.1023/A:1026752404893.

[98] Carreño-Morelli E, Urreta SE, Schaller R. Mechanical Spectroscopy of Thermal Stress Relaxation in Aluminium Alloys Reinforced with Short Alumina Fibres. Phys Stat Sol (a) 1998;167:61–9. https://doi.org/10.1002/(SICI)1521-396X(199805)167:1<61::AID-PSSA61>3.0.CO;2-M.

[99] Carreño-Morelli E, Urreta SE, Gabella L, Schaller R. Thermal stress relaxation in Al-Al2O3 (f) composites during thermal cycling. Le Journal de Physique IV 1996;6:C8-735.

[100] Vattur Sundaram M. Low Temperature Creep/Relaxation Behaviour of PM Steels under Static Load. Master's Thesis. 2014.

[101] Larson FR, Miller J. A time-temperature relationship for rupture and creep stresses. Transactions of the American Society of Mechanical Engineers 1952;74:765–71.

[102] Furillo FT, Purushothaman S, Tien JK. Understanding the larson-miller parameter. Scripta Metallurgica 1977;11.

[103] Pavlou DG. Creep life prediction under stepwise constant uniaxial stress and temperature conditions. Engineering Structures 2001;23:656–62.

[104] Zhao X, Niu X, Song Y, Sun Z. An investigation of the nonlinear creep damage accumulation of different materials: Application of a novel damage model. Fatigue Fract Eng Mat Struct 2022;45:530–45. https://doi.org/10.1111/ffe.13616.

[105] Batsoulas ND. Creep Damage Assessment and Lifetime Predictions for Metallic Materials under Variable Loading Conditions in Elevated Temperature Applications. Steel Research International 2009;80:152–9. https://doi.org/10.2374/SRI08SP086.

[106] Hu X, Ye W, Ma X, Song Y. A new creep damage assessment method for metallic material under variable load conditions at elevated temperature. Fatigue Fract Eng Mat Struct 2019;42:2725–37. https://doi.org/10.1111/ffe.13106.

[107] Yu W, Zhan L, Xu Y, Chen K, Yang Y, Xu L, et al. Temperature-dependent creep aging behavior of 2A14 aluminum alloy. Journal of Materials Research and Technology 2022;19:1343–54.

[108] Zhang S, Zhang Y, Chen M, Wang Y, Cui Q, Wu R, et al. Characterization of mechanical properties of aluminum cast alloy at elevated temperature. Applied Mathematics and Mechanics 2018;39:967–80.

[109] Golshan AMA, Aroo H, Azadi M. Sensitivity analysis for effects of heat treatment, stress, and temperature on AlSi12CuNiMg aluminum alloy behavior under force-controlled creep loading. Applied Physics A 2021;127:1–18.

[110] Zhan L, Wu X, Wang X, Yang Y, Liu G, Xu Y. Effect of process parameters on fatigue and fracture behavior of Al-Cu-Mg alloy after creep aging. Metals 2018;8:298.

[111] Ellyin F. Fatigue damage, crack growth and life prediction. Springer Science & Business Media; 2012.

[112] Santecchia E, Hamouda AMS, Musharavati F, Zalnezhad E, Cabibbo M, El Mehtedi M, et al. A review on fatigue life prediction methods for metals. Advances in Materials Science and Engineering 2016;2016.

[113] Mughrabi H. Dislocations in fatigue. Dislocations and Properties of Real Materials 1984:244–62.

[114] Basquin O. The experimental law of endurance tests. Proc. AsTM, vol. 10, 1969, p. 625.

[115] Haji ZN. LOW CYCLE FATIGUE BEHAVIOR OF ALUMINUM ALLOYS AA2024-T6 AND AA7020-T6. DIYALA JOURNAL OF ENGINEERING SCIENCES 2010;Engineering Sc. Conference.

[116] Minichmayr R, Riedler M, Winter G, Leitner H, Eichlseder W. Thermo-mechanical fatigue life assessment of aluminium components using the damage rate model of Sehitoglu. International Journal of Fatigue 2008;30:298–304.

[117] Azadi M. Effects of strain rate and mean strain on cyclic behavior of aluminum alloys under isothermal and thermo-mechanical fatigue loadings. International Journal of Fatigue 2013;47:148–53. https://doi.org/10.1016/j.ijfatigue.2012.08.005.

[118] Bharath V, Auradi V, Kumar GV, Nagaral M, Chavali M, Helal M, et al. Microstructural evolution, tensile failure, fatigue behavior and wear properties of Al2O3 reinforced Al2014 alloy T6 heat treated metal composites. Materials 2022;15:4244.

[119] Mamoon A, Al-Jaafari A. Fatigue behavior of aluminum sic nano composites material with different reinforcement ratio. IOP Conference Series: Materials Science and Engineering, vol. 870, IOP Publishing; 2020, p. 012159.

[120] Myriounis DP, Matikas TE, Hasan ST. Fatigue Behaviour of SiC Particulate-Reinforced A359 Aluminium Matrix Composites. Strain 2012;48:333–41. https://doi.org/10.1111/j.1475-1305.2011.00827.x.

[121] Kaynak C, Boylu S. Effects of SiC particulates on the fatigue behaviour of an Al-alloy matrix composite. Materials & Design 2006;27:776–82. https://doi.org/10.1016/j.matdes.2005.01.009.

[122] Hadianfard MJ, Mai Y-W. Low cycle fatigue behaviour of particulate reinforced metal matrix composites. Journal of Materials Science 2000;35:1715–23. https://doi.org/10.1023/A:1004720300774.

[123] Shang JK, Ritchie RO. Crack bridging by uncracked ligaments during fatigue-crack growth in SiC-reinforced aluminum-alloy composites. Metall Trans A 1989;20:897–908. https://doi.org/10.1007/BF02651656.

[124] Uygur I, Külekci MK. Low cycle fatigue properties of 2124/SiCp Al-alloy composites. Turkish Journal of Engineering and Environmental Sciences 2002.

[125] Bonnen JJ, Allison JE, Jones JW. Fatigue behavior of a 2XXX series aluminum alloy reinforced with 15 vol Pct SiCp. Metall Trans A 1991;22:1007–19. https://doi.org/10.1007/BF02661094.

[126] Hall JN, Jones JW, Sachdev AK. Particle size, volume fraction and matrix strength effects on fatigue behavior and particle fracture in 2124 aluminum-SiCp composites. Materials Science and Engineering: A 1994;183:69–80.

[127] McCullough RR, Jordon JB, Brammer AT, Manigandan K, Srivatsan TS, Allison PG, et al. A Fatigue Model for Discontinuous Particulate-Reinforced Aluminum Alloy Composite: Influence of Microstructure. J of Materi Eng and Perform 2014;23:65–76. https://doi.org/10.1007/s11665-013-0766-x.

[128] Zhu S-P, Yue P, Yu Z-Y, Wang Q. A combined high and low cycle fatigue model for life prediction of turbine blades. Materials 2017;10:698.

[129] Kumar N, Gautam G, Mohan A, Mohan S. High Temperature Tensile and Strain Hardening Behaviour of AA5052/9 vol.% ZrB2 insitu Composite. Materials Research 2018;21.

[130] Sahin H, Atik M, Tezer F, Temel S, Aydin O, Kesen O, et al. Prediction of Fracture Stress with Regard to Porosity in Cast A356 Alloy. Archives of Foundry Engineering 2021.

[131] Kahrıman F, Zeren M. Microstructural and Mechanical Characterization of Al-0.80 Mg-0.85 Si-0.3 Zr Alloy. Archives of Foundry Engineering 2017;17.

[132] Triyono T, Muhayat N, Supriyanto A, Lutiyatmi L. Effect of Degassing Treatment on the Interfacial Reaction of Molten Aluminum and Solid Steel. Archives of Foundry Engineering 2017.

[133] de Rosso E, dos Santos CA, Garcia A. Microstructure, Hardness, Tensile Strength, and Sliding Wear of Hypoeutectic Al–Si Cast Alloys with Small Cr Additions and Fe-Impurity Content. Advanced Engineering Materials 2021:2001552.

[134] Bia\lobrzeski A. Continuous sodium modification of nearly-eutectic aluminium alloys. Part I. Theoretical backgrounds of the process. Archives of Foundry Engineering 2007;7:53–6.

[135] Zamani M. Al-Si Cast alloys-microstructure and mechanical properties at ambient and elevated temperatures. PhD Thesis. Jönköping University, School of Engineering, 2017.

[136] Yağcı T, Cöcen Ü, Çulha O. Aluminum Alloy Development for Wheel Production by Low Pressure Die Casting with New Generation Computational Materials Engineering Approaches. Archives of Foundry Engineering 2021.

[137] Sajjadi SA, Ezatpour HR, Beygi H. Microstructure and mechanical properties of Al–Al2O3 micro and nano composites fabricated by stir casting. Materials Science and Engineering: A 2011;528:8765–71.

[138] Weijing LI, Shihai CUI, Jianmin HAN, Chao XU. Effect of Silicon on the casting properties of Al-5.0% Cu alloy. Rare Metals 2006;25:133–5.

[139] Caceres CH, Svensson IL, Taylor JA. Strength-ductility behaviour of Al-Si-Cu-Mg casting alloys in T6 temper. International Journal of Cast Metals Research 2003;15:531–43.

[140] Liao H, Sun Y, Sun G. Correlation between mechanical properties and amount of dendritic α-Al phase in as-cast near-eutectic Al–11.6% Si alloys modified with strontium. Materials Science and Engineering: A 2002;335:62–6.

[141] Bogdanoff T. Development of aluminium-silicon alloys with improved properties at elevated temperature 2017.

[142] Ebhota WS, Jen T-C. Intermetallics Formation and Their Effect on Mechanical Properties of Al-Si-X Alloys. IntechOpen; 2018. https://doi.org/10.5772/intechopen.73188.

[143] Warmuzek M. Aluminum-silicon casting alloys: an atlas of microfractographs. ASM international; 2004.

[144] Siddique S. Reliability of selective laser melted AlSi12 alloy for quasistatic and fatigue applications. Springer; 2019.

[145] Xu Z, Wang S, Wang H, Song H, Li S, Chen X. Effect of cooling rate on Microstructure and properties of twin-roll casting 6061 aluminum alloy sheet. Metals 2020;10:1168.

[146] Ou M, Zhang S, Song H, Liang Y. Effects of different cooling methods on microstructure and mechanical properties of TC4 alloy. Chinese Materials Conference, Springer; 2017, p. 539–47.

[147] Wang R, Lu W. Direct Electrolytic Al-Si Alloys (DEASA)–An Undercooled Alloy Self-Modified Structure and Mechanical Properties. Edited by Janis Kleperis and Vladimir Linkov 2012:107.

[148] Das K. Liquid Metal Processing: Application to Aluminium Alloy Production. JOM 2003;55:64.

[149] Lipiński T. Structure and mechanical properties of Al-12% Si alloy with fast cooling Al-12% Si. Archives of Foundry of Engineering 2008;8:51–4.

[150] Guo M, Sun M, Huang J, Pang S. A Comparative Study on the Microstructures and Mechanical Properties of Al-10Si-0.5 Mg Alloys Prepared under Different Conditions. Metals 2022;12:142.

[151] Mohamed AMA, Samuel FH. A review on the heat treatment of Al-Si-Cu/Mg casting alloys. Heat Treatment-Conventional and Novel Applications 2012:55–72.

[152] Çolak M. Modification of eutectic Al–Si alloys by Sr and CuSn5. Materials Research Express 2019;6:1065a2.

[153] Siemińska-Jankowska B, Pietrowski S. The effects of temperature on strength of the new piston aluminum materials. Journal of KONES Internal Combustion Engines 2003;10.

[154] Sirata GG, Wacławiak K, Dyzia M. Mechanical and Microstructural Characterization of Aluminium Alloy, EN AC-Al Si12CuNiMg. Archives of Foundry Engineering 2022;22.

[155] ASTM. Standard test methods for stress relaxation tests for materials and structures. E328-02, International, West Conshohocken, PA 2008.

[156] Plaseied A, Fatemi A. Deformation response and constitutive modeling of vinyl ester polymer including strain rate and temperature effects. Journal of Materials Science 2008;43:1191–9.

[157] Lin C-Y. Alternative form of standard linear solid model for characterizing stress relaxation and creep: Including a novel parameter for quantifying the ratio of fluids to solids of a viscoelastic solid. Frontiers in Materials 2020;7:11.

[158] Beddoes J, Mohammadi T. Comparison of stress relaxation and creep strain rates for the superalloy IN738LC. The Journal of Strain Analysis for Engineering Design 2010;45:587–92. https://doi.org/10.1177/030932471004500805.

[159] Zhan LH, Li YG, Huang MH, Lin JG. Comparative study of creep and stress relaxation behavior for 7055 aluminum alloy. Advanced Materials Research 2011;314:772–7.

[160] Zheng J-H, Jin Y, Xu L, Fan C, Song W, Chen Y. Comparative Study of Creep and Stress Relaxation Behaviour during Ageing of 7050 Aluminum Alloy. Metals 2023;13:778.

[161] Naumenko K, Altenbach H. Modeling high temperature materials behavior for structural analysis. Springer; 2016.

[162] Ma Z, Samuel AM, Doty HW, Samuel FH. On the Fractography of Impact-Tested Samples of Al-Si Alloys for Automotive Alloys. Fracture Mechanics—Properties, Patterns and Behaviours 2016.

[163] Skolianos S. Mechanical behavior of cast SiCp-reinforced Al-4.5% Cu-1.5% Mg alloy. Materials Science and Engineering: A 1996;210:76–82.

[164] Hochreiter E, Panzenböck M, Jeglitsch F. Fatigue properties of particle-reinforced metal-matrix composites. International Journal of Fatigue 1993;15:493–9.

[165] Vencl A, Bobic I, Arostegui S, Bobic B, Marinković A, Babić M. Structural, mechanical and tribological properties of A356 aluminium alloy reinforced with Al2O3, SiC and SiC+ graphite particles. Journal of Alloys and Compounds 2010;506:631–9.

[166] Sirata GG, Wac\lawiak K, Dyzia M. Mechanical and Microstructural Characterization of Aluminium Alloy, EN AC-Al Si12CuNiMg. Archives of Foundry Engineering 2022;22.

[167] Kurzawa A, Kaczmar JW. Bending Strength of EN AC-44200–Al2O3 Composites at Elevated Temperatures. Archives of Foundry Engineering 2017;17:103–8.

[168] Lijay KJ, Selvam JDR, Dinaharan I, Vijay SJ. Microstructure and mechanical properties characterization of AA6061/TiC aluminum matrix composites synthesized by in situ reaction of silicon carbide and potassium fluotitanate. Transactions of Nonferrous Metals Society of China 2016;26:1791–800.

[169] Lakshmipathy J, Kulendran B. Reciprocating wear behavior of 7075Al/SiC in comparison with 6061Al/Al2O3 composites. International Journal of Refractory Metals and Hard Materials 2014;46:137–44.

[170] Jayashree PK, Gowrishankar MC, Sharma S, Shetty R, Hiremath P, Shettar M. The effect of SiC content in aluminum-based metal matrix composites on the microstructure and mechanical properties of welded joints. Journal of Materials Research and Technology 2021;12:2325–39.

[171] Dolata-Grosz A, Dyzia M, Śleziona J, Wieczorek J. Composites applied for pistons. Archives of Foundry Engineering 2007;7:37–40.

[172] Moćko W, Kowalewski ZL. Mechanical properties of A359/SiCp metal matrix composites at wide range of strain rates. Applied Mechanics and Materials 2011;82:166–71.

[173] Dolata AJ, Dyzia M. Effect of Chemical Composition of the Matrix on AlSi/SiC p+ C p Composite Structure. Archives of Foundry Engineering 2014;14:135–8.

[174] Wysocki J, Grabian J, Przetakiewicz W. Continuous drive friction welding of cast AlSi/SiC (p) metal matrix composites. Archives of Foundry Engineering 2007;7:47–52.

[175] Li R, Pan Z, Zeng Q, Xiaoli Y. Influence of the Interface of Carbon Nanotube-Reinforced Aluminum Matrix Composites on the Mechanical Properties–a Review. Archives of Foundry Engineering 2022;22.

[176] Dolata AJ, Mróz M, Dyzia M, Jacek-Burek M. Scratch testing of AlSi12/SiCp composite layer with high share of reinforcing phase formed in the centrifugal casting process. Materials 2020;13:1685.

[177] Ozben T, Kilickap E, Çakır O. Investigation of mechanical and machinability properties of SiC particle reinforced Al-MMC. Journal of Materials Processing Technology 2008;198:220–5. https://doi.org/10.1016/j.jmatprotec.2007.06.082.

[178] Ozden S, Ekici R, Nair F. Investigation of impact behaviour of aluminium based SiC particle reinforced metal–matrix composites. Composites Part A: Applied Science and Manufacturing 2007;38:484–94. https://doi.org/10.1016/j.compositesa.2006.02.026.

[179] Shuvho MBA, Chowdhury MA, Kchaou M, Roy BK, Rahman A, Islam MA. Surface characterization and mechanical behavior of aluminum based metal matrix composite reinforced with nano Al2O3, SiC, TiO2 particles. Chemical Data Collections 2020;28:100442.

[180] Peng Z, Fuguo L. Effects of Particle Clustering on the Flow Behavior of SiC Particle Reinforced Al Metal Matrix Composites. Rare Metal Materials and Engineering 2010;39:1525–31. https://doi.org/10.1016/S1875-5372(10)60123-3.

[181] Pawar PB, Utpat AA. Development of aluminium based silicon carbide particulate metal matrix composite for spur gear. Procedia Materials Science 2014;6:1150–6.

[182] Kurzawa A, Kaczmar JW. Impact strength of composite materials based on EN AC-44200 matrix reinforced with Al2O3 particles. Archives of Foundry Engineering 2017;17:73–8.

[183] Azadi M, Bahmanabadi H, Gruen F, Winter G. Evaluation of tensile and low-cycle fatigue properties at elevated temperatures in piston aluminum-silicon alloys with and without nano-clay-particles and heat treatment. Materials Science and Engineering: A 2020;788:139497.

[184] Li Y, Yang Y, Wu Y, Wang L, Liu X. Quantitative comparison of three Ni-containing phases to the elevated-temperature properties of Al–Si piston alloys. Materials Science and Engineering: A 2010;527:7132–7.

[185] Dolata AJ, Dyzia M, Boczkal S. Structure of interface between matrix alloy and reinforcement particles in Al/SiCp+ Cgp hybrid composites. Materials Today: Proceedings 2016;3:235–9.

[186] Keshavamurthy R, Mageri S, Raj G, Naveenkumar B, Kadakol PM, Vasu K. Microstructure and Mechanical Properties of Al7075-TiB2 in-situ composite. Res J Mat Sci ISSN 2013;2320:6055.

[187] Moustafa SF. Wear and wear mechanisms of Al-22% Si/A12O3f composite. Wear 1995;185:189–95.

[188] Fayomi OSI, Babaremu KO, Akande IG. Impact of Al-Composites in the Manufacturing Industry: A Neccessity. International Journal of Civil Engineering and Technology 2019;10.

[189] Singh AK, Soni S, Rana RS. A Critical Review on Synthesis of Aluminum Metallic Composites through Stir Casting: Challenges and Opportunities. Adv Eng Mater 2020;22:2000322. https://doi.org/10.1002/adem.202000322.

[190] Ayar MS, George PM, Patel RR. Advanced research progresses in aluminium metal matrix composites: An overview. AIP Conference Proceedings, vol. 2317, AIP Publishing; 2021.

[191] Myriounis DP, Matikas TE, Hasan ST. Fatigue Behaviour of SiC Particulate-Reinforced A359 Aluminium Matrix Composites. Strain 2012;48:333–41. https://doi.org/10.1111/j.1475-1305.2011.00827.x.

[192] Ozdemir I, Toparli M, Onel K, Tsunekawa Y. Fracture and Failure of Al-SiCpComposites at Different Temperatures and Conditions. Journal of Composite Materials 2005;39:601–15. https://doi.org/10.1177/0021998305047102.

[193] Nair SV, Tien JK, Bates RC. SiC-reinforced aluminium metal matrix composites. International Metals Reviews 1985;30:275–90. https://doi.org/10.1179/imtr.1985.30.1.275.

[194] Pandey AB, Majumdar BS, Miracle DB. Deformation and fracture of a particle-reinforced aluminum alloy composite: Part I. Experiments. Metall Mater Trans A 2000;31:921–36. https://doi.org/10.1007/s11661-000-0035-0.

[195] Chawla KK. Composite materials: science and engineering. Springer Science & Business Media; 2012.

[196] Mroziński S, Lis Z, Egner H. Energy dissipated in fatigue and creep conditions. Materials 2021;14:4724.

[197] Manson SS, Halford GR. Re-examination of cumulative fatigue damage analysis—an engineering perspective. Engineering Fracture Mechanics 1986;25:539–71.

[198] Zarandi EP, Skallerud BH. Cyclic behavior and strain energy-based fatigue damage analysis of mooring chains high strength steel. Marine Structures 2020;70:102703.

[199] Ellyin F, Kujawski D. Plastic strain energy in fatigue failure 1984.

[200] Erber T, Guralnick SA, Michels SC. Hysteresis and fatigue. Annals of Physics 1993;224:157–92.

[201] Sucuoğlu H, Erberik A. Energy-based hysteresis and damage models for deteriorating systems. Earthq Engng Struct Dyn 2004;33:69–88. https://doi.org/10.1002/eqe.338.

[202] Ramberg W, Osgood WR. Description of stress-strain curves by three parameters 1943.

[203] Mroziński S. Energy-based method of fatigue damage cumulation. International Journal of Fatigue 2019;121:73–83.

[204] Egner W, Sulich P, Mroziński S, Egner H. Modelling thermo-mechanical cyclic behavior of P91 steel. International Journal of Plasticity 2020;135:102820.

[205] Sivaram AR, Krishnakumar K, Rajavel DR, Sabarish R. Experimental Investigation of Creep Behaviour of Aluminium Alloy (LM25) and Zirconium DI-Oxide (ZR02) Particulate MMC. Int J Mech Eng Technol 2015;6:126–38.

[206] Lee LS. Creep and time-dependent response of composites. Durability of Composites for Civil Structural Applications, Elsevier; 2007, p. 150–69.

[207] Samareh-Mousavi SS, Taheri-Behrooz F. A novel creep-fatigue stiffness degradation model for composite materials. Composite Structures 2020;237:111955.

[208] Lu YX, Lu YX, Meng XM, Meng XM, Lee CS, Li RKY, et al. Failure Mechanisms of a SiC Particles/2024Al Composite under Dynamic Loading. Phys Stat Sol (a) 1998;169:49–55. https://doi.org/10.1002/(SICI)1521-396X(199809)169:1<49::AID-PSSA49>3.0.CO;2-9.

[209] Uematsu Y, Tokaji K, Kawamura M. Fatigue behaviour of SiC-particulate-reinforced aluminium alloy composites with different particle sizes at elevated temperatures. Composites Science and Technology 2008;68:2785–91.

[210] Elomari S, Boukhili R, San Marchi C, Mortensen A, Lloyd D. Thermal expansion responses of pressure infiltrated SiC/Al metal-matrix composites. Journal of Materials Science 1997;32:2131–40.

[211] Sieminska B. Coefficient of thermal expansion as a component quality estimation of alloys on pistons of combustion engines. Journal of KONES 2009;16:575–83.

# ATTACHEMENT 1 DOCTORAL CANDIDATE'S CV

**Name**: Goftila Gudeta Sirata

**Email**: goftila.sirata@polsl.pl

## Education

**October 2019 – Present**

PhD Student in Materials Engineering, Silesian University of Technology, Poland.

**PhD thesis title:** Influence of combined relaxation, creeping and low-cycle fatigue on the final durability and structure of material

- **October 2017 – June 2019**

Master's of Science in Mechanical Engineering, Jimma University, Ethiopia.

**MSc.Thesis title**: Numerical Modelling of Fatigue Behaviour for Rail-Wheel Rolling Contact Problem

- **October 2010 – June 2015**

Bachelor of Science in Mechanical Engineering, Jimma University, Ethiopia.

- **February 2014-June 2014**

Internship at Homicho Ammunition Engineering Complex, Ethiopia.

## Employment

**July 2015 – October 2017**

Assistant lecturer, Jimma University, Ethiopia.

# ATTACHEMENT 2 ACADEMIC ACHIEVEMENTS

1. Sirata, G. G., Wacławiak, K., & Dyzia, M. (2022). Mechanical and Microstructural Characterization of Aluminium Alloy, EN AC-Al Si12CuNiMg. *Archives of Foundry Engineering*, 34-40.

2. Sirata, G. G., & Waclawiak, K. (2023, December). Material characterization of EN AC-Al Si12CuNiMg alloy in stress relaxation and creep conditions. In *Materials Science and Engineering Conference Series* (Vol. 1294, No. 1, p. 012025).

3. Sirata, G. G., Wacławiak, K., & Dolata, A.J. (2024). Microstructure and mechanical properties of the EN AC-AlSi12CuNiMg alloy and AlSi composite reinforced with SiC particles. *Archives of Foundry Engineering*

4. G.G.Sirata, K.Wacławiak, A.J.Dolata, M.Dyzia: Evaluation of the structure and mechanical properties of the AlSi12CuNiMg/10SiCp composite. BOOK OF ABSTRACTS, XXV Symposium "COMPOSITES - Theory and practice", 31.05-2.06 Brenna 2023, 83-84.